The logic of receptor-ligand interactions in the Notch signaling pathway

Thesis by

Lauren LeBon

In Partial Fulfillment of the Requirements

for the Degree of

Doctor of Philosophy

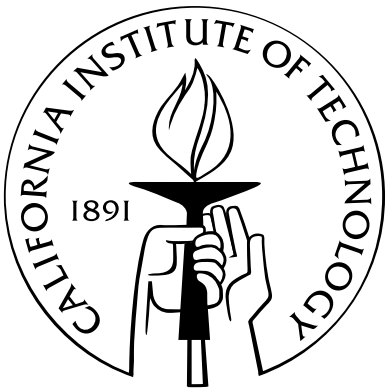

California Institute of Technology

Pasadena, California

2014

(Defended May 9, 2014)

To Mom, Dad, Lawrence, Katie, and Nick.

Acknowledgments

I must start with thanking my advisor, Michael Elowitz. His sheer enthusiasm and uncanny knack for finding cool scientific questions have made life in the Labowitz a constant adventure. Michael gives his team the freedom to follow whatever ideas we find exciting. He then teaches us the skills and gives us the opportunities to convey our excitement to the scientific community. I have learned so much from him, and from the excellent group he has put together, about every aspect of the scientific process.

David Sprinzak has been an outstanding mentor from my very first days on the Notch project. Every method I've used in this thesis, from experiments to modeling, I've learned through his patient guidance. He has taught me to think like scientist, and as a PI, I know he will continue to inspire many more students in the future.

The entire Elowitz lab has been a source of advice, technical know-how, and inspiration. I owe a special thanks to the Delta Force, including Amit Lakhanpal, Sandy Nandagopal, Leah Santat, and Jordi Garcia-Ojalvo, for being great collaborators. Leah, along with Michelle Fontes, Tara Orr, and James Linton kept the lab up and running. Chiraj Dalal and Long Cai took me on as an unexperienced rotation student and patiently taught me the basics of molecular biology. Jonathan Young, Joe Levine, Fred Tan, James Locke, Shaunak Sen, Georg Seelig, Sidney Cox, and Avigdor Eldar welcomed me into the lab. The lab has grown since, and I found new friends and colleagues in Yaron Antebi, John Yong, Zakary Singer, Pulin Li, Hao-Yuan Kueh, Emily Capra, Adam Rosenthal, Lacramoira Bintu, Julia Tischler, Stephanie Culler, Mary Dunlop, Ophelia Venturelli, Pierre Neveu, Fangyuan Ding, Mark Budde, Joe Markson, Jin Park, Yihan Lin, and Yutao Qi. I am grateful to have been a part of such a talented, hardworking, and cooperative team.

I'd like to thank Hamed Jafar-Nejad and his postdoc Tom Lee for designing and conducting the beautiful experiments (in Chapter 4) to test out our crazy cell culture ideas in real live flies, and for providing careful and insightful comments on this work.

My thesis committee has provided constructive advice for my project, as well as encouragement for my future endeavors. I thank David Anderson, Lea Goentoro, Bruce Hay, and Gerry Weinmaster for sharing with me their valuable time and expertise.

I thank the Caltech Computation and Neural Systems Department. Shin Shimojo and Pietro

Perona helped me to find my bearings at Caltech. Tanya Owen provided much assistance over the years. My CNS classmates Ronnie Bryan, Chess Stetson, Sina Tootoonian, Dan Wilhelm, and Peter Weir helped me through the first year and quals, and have been great friends since.

I send out my love and gratitude to my friends in the Caltech community and beyond who have been there for me over the years. There are far too many of them to list (I tried), but I am so grateful for the coffee breaks, camping trips, bike rides, dance parties, and countless other good times we've spent together. I feel lucky to have so many wildly brilliant people in my life.

My parents, Susan and Lawrence, have always fostered my curiosity, even if they weren't quite sure where it would lead. Along the way they have given me every opportunity to follow my inspiration without worrying about the "how." I realize now what a rare gift this is, and I will always be grateful. My brother, Lawrence, and my sister, Katie, have always kept my spirits high, taking the time from their busy lives to send me a funny message or words of encouragement. Thank you!

One of my heroes, Jacques Monod, once said "It is restlessness, anxiety, dissatisfaction, agony of mind that nourish science." Over the years, Nicolas Lacasse has put up with all of this, and much more, from this young investigator. I am so grateful to have such a patient, gracious and loving partner by my side. Thank you so much, Nick.

Abstract

The Notch signaling pathway enables neighboring cells to coordinate developmental fates in diverse processes such as angiogenesis, neuronal differentiation, and immune system development. Although key components and interactions in the Notch pathway are known, it remains unclear how they work together to determine a cell's signaling state, defined as its quantitative ability to send and receive signals using particular Notch receptors and ligands. Recent work suggests that several aspects of the system can lead to complex signaling behaviors: First, receptors and ligands interact in two distinct ways, inhibiting each other in the same cell (in *cis*) while productively interacting between cells (in *trans*) to signal. The ability of a cell to send or receive signals depends strongly on both types of interactions. Second, mammals have multiple types of receptors and ligands, which interact with different strengths, and are frequently co-expressed in natural systems. Third, the three mammalian Fringe proteins can modify receptor-ligand interaction strengths in distinct and ligand-specific ways. Consequently, cells can exhibit non-intuitive signaling states even with relatively few components.

In order to understand what signaling states occur in natural processes, and what types of signaling behaviors they enable, this thesis puts forward a quantitative and predictive model of how the Notch signaling state is determined by the expression levels of receptors, ligands, and Fringe proteins. To specify the parameters of the model, we constructed a set of cell lines that allow control of ligand and Fringe expression level, and readout of the resulting Notch activity. We subjected these cell lines to an assay to quantitatively assess the levels of Notch ligands and receptors on the surface of individual cells. We further analyzed the dependence of these interactions on the level and type of Fringe expression. We developed a mathematical modeling framework that uses these data to predict the signaling states of individual cells from component expression levels. These methods allow us to reconstitute and analyze a diverse set of Notch signaling configurations from the bottom up, and provide a comprehensive view of the signaling repertoire of this major signaling pathway.

Contents

List of Figures

Preface

All animals begin as a single-celled embryo that divides into hundreds or, in the case of humans, trillions of cells. As this teeming mass expands, the cells must negotiate among themselves to make a series of decisions, each one crucial for the proper construction of the body. These decisions begin with the initial establishment of the major axes of the organism and continue, over many developmental steps and cell divisions later, with the assembly of tissues and organs. All of these processes are carried out by an astonishingly small set of signaling pathways—families of interacting molecules that send and receive information from one cell to another, and convert these signals into lasting changes in gene expression.

Each signaling pathway is highly conserved, meaning that we see analogues of the signaling molecules in simple organisms like the *C. elegans* nematode still being used to pattern the vastly more complex human body. Not only are the signaling molecules themselves conserved, but the specific ways in which they interact—the circuits that they form—can be traced throughout evolution. But evolution has also expanded the functional range of each pathway as new challenges arise. For example, the Notch pathway, the subject of this thesis, has been co-opted to help connect neurons in the mammalian brain. What are the key features of each signaling pathway that make them so useful and so versatile? What makes each signaling pathway suitable for a given task?

With these questions in mind, our research group set out to understand and build patterning circuits using components from the Notch pathway. During the course of this project, we deepened our understanding of a key feature that enables the Notch pathway to carry out its many roles during development. In this thesis, I explore how this feature expands the functional repertoire of the Notch signaling pathway, making it more evident why it is so prevalent and so useful in animal development.

Chapter 1

Introduction

In the April 1917 edition of *The American Naturalist*, pioneering geneticist Thomas Hunt Morgan described a bizarre new strain of the fruit fly *Drosophila melanogaster* called *Notch*. John Dexter had first observed the strain in 1913 at his laboratory in Olivet, Michigan, and gave the mutant flies their name because they displayed deformed, notched wings.

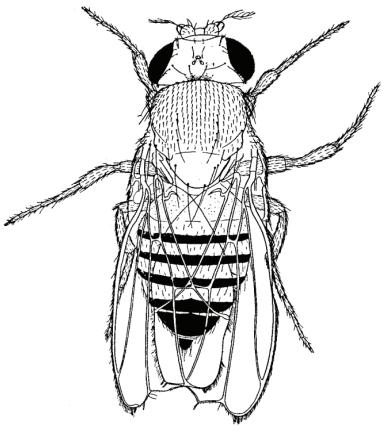

Figure 1.1: *Notch* mutant female. Image from T.H. Morgan, *The Theory of the Gene*, 1926 [43].

The *Notch* mutation showed an unusual pattern of inheritance. Half of the male offspring born to female *Notch* mutants died, while the other half survived. Morgan determined that the flies that died had inherited a mutated copy of the *Notch* gene, demonstrating its necessity for proper development [41]. Because the male offspring of a *Notch* mother died, but females did not, this implied the gene was linked to the X chromosome. Morgan's colleague Calvin Bridges confirmed this prediction in 1916 in their laboratory at Columbia University [43, 44].

However, the female offspring were not all normal: half of the female offspring displayed the notched wing phenotype. Morgan's group showed that these flies possessed one mutated copy and one normal copy of the *Notch* gene [41]. *Notch* therefore belonged to the class of rare haploinsufficient genes—so named because half of a functional pair of alleles is insufficient to generate the normal

phenotype [23].

Since Morgan's initial characterization of *Notch* mutations, the *Notch* gene has been identified not only in fruit flies, but also in the genomes of worms, sea urchins, and mammals, including humans [2, 24]. *Notch* not only plays a role in building fly wings, but in constructing nearly every tissue found in every metazoan species.

1.1 The Notch signaling pathway mediates short-range communication

One hundred years after its discovery, we now know that the *Notch* gene encodes for a receptor that enables communication between neighboring cells. The Notch receptor resides on a cell's surface and listens for signaling molecules, or ligands, produced by other cells. The ligands the Notch receptors are listening for belong to the class of DSL ligands, abbreviated for Delta, Serrate (in flies, known as Jagged in vertebrates), and Lag-2 (in *C. elegans*). When a Notch receptor and a DSL ligand bind, a signal is generated that ultimately results in changes in the gene expression of the cell. Together, the Notch receptors, DSL ligands, and related components that enable signaling are called the **Notch signaling pathway**, one member of a small set of major signaling pathways that coordinate animal development [2, 46].

The Notch signaling pathway is unique among the major developmental signaling pathways, in part because the DSL ligands are not secreted into the extracellular space, where they can diffuse away and affect cells located many cell diameters away, but are instead anchored to the membrane of the cell that produced them [34]. Consequently, only cells that come into direct physical contact can bring the ligand and receptor close enough to bind and transmit a Notch signal. Signaling that occurs only between adjacent cells is referred to as *juxtacrine*.

As the primary juxtacrine developmental signaling pathway, Notch is deployed to perform the fine-detail work of development, such as drawing sharp boundaries between different tissue compartments, casting an evenly-spaced checkerboard pattern of gene expression over a field of cells, or flipping a switch that drives the daughters of a dividing stem cell towards different fates [2, 5, 23, 34].

1.2 Notch signal is transmitted through *trans*-activation

Communication through Notch begins when a receptor binds to a DSL ligand on a neighboring cell, as shown in Figure 1.3. The bound Notch receptor undergoes two proteolytic reactions. The final γ-secretase-dependent reaction cuts the Notch receptor in two, separating the extracellular domain and intracellular domain [23, 31]. The extracellular domain of Notch, still bound to the DSL ligand, is endocytosed into the signal sending cell and presumably degraded. Meanwhile, the Notch

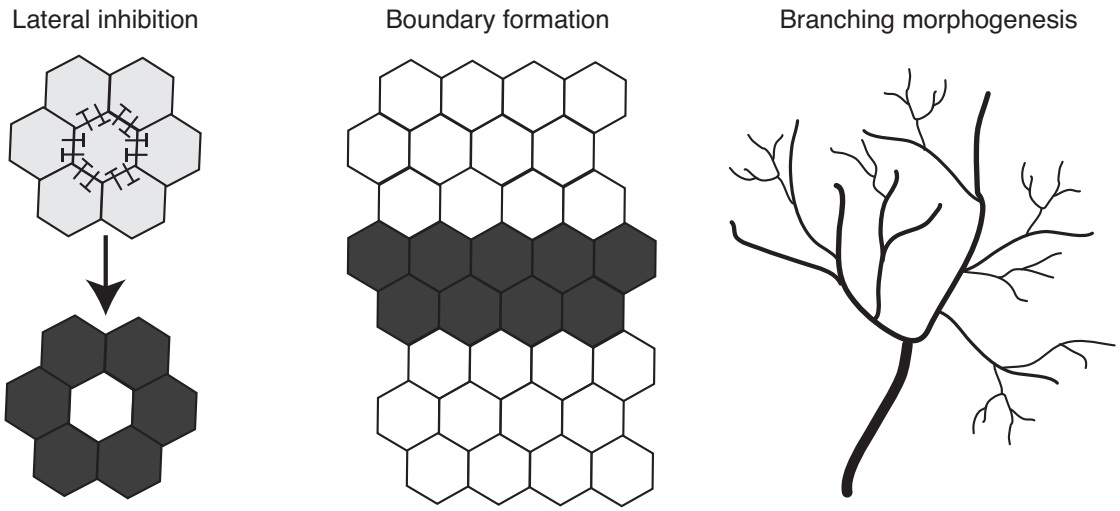

Figure 1.2: Notch signaling coordinates finely detailed patterning. Notch is used in many patterning processes that make sharp delineations between neighboring cells. (A) In lateral inhibition patterning, cells send Notch signals to one another, and reception of Notch signal leads to a decrease in the ability to send signal. Small fluctuations in signaling can destabilize an initially homogenous population of cells to adopt distinct heterogeneous fates, with one cell sending (white cell, below) and the surrounding neighbors receiving (black cells). One example is found in a fly eye, where cells in an ommatidium inhibit one another from expressing the same type of photoreceptor. (B) Notch is also used to form sharp boundaries between populations of cells. For example, a sharp stripe of Notch signaling separates the developing fly wing into two halves, and also defines the borders of the veins on the wing. (C) Notch is also used to coordinate the sprouting of new branches in fractal-like structures such as blood and lymphatic vessels [4]. Disruption of Notch signaling leads to over-branching.

intracellular domain (NICD) travels from the membrane to the nucleus, where it interacts with the CSL-Mastermind complex (RBPj-κ in vertebrates) to initiate transcription of target genes [2, 31]. This signal generation process is called ***trans*-activation**.

Notch *trans*-activation is remarkable because the receptor itself acts as a transcription factor; that is, the NICD is an essential component of the transcription machinery to activate target genes. This direct process contrasts with many other signaling pathways, where often an activated receptor hands off its message to a complex cascade of second messengers before affecting gene expression [46]. For example, in the Wingless (Wnt) signaling pathway, an activated Frizzled receptor affects transcription through the second messenger β-catenin. When the Frizzled receptor binds a Wnt ligand, the bound complex prevents the constitutive degradation of β-catenin. As β-catenin accumulates, it can enter the nucleus and affect gene expression [35]. This molecular relay race amplifies or transforms the signal, before it has a chance to act on the genome.

It seems, then, that Notch has traded the capability to compute on its signal in exchange for fast and faithful reporting on what is being heard at the cell surface.

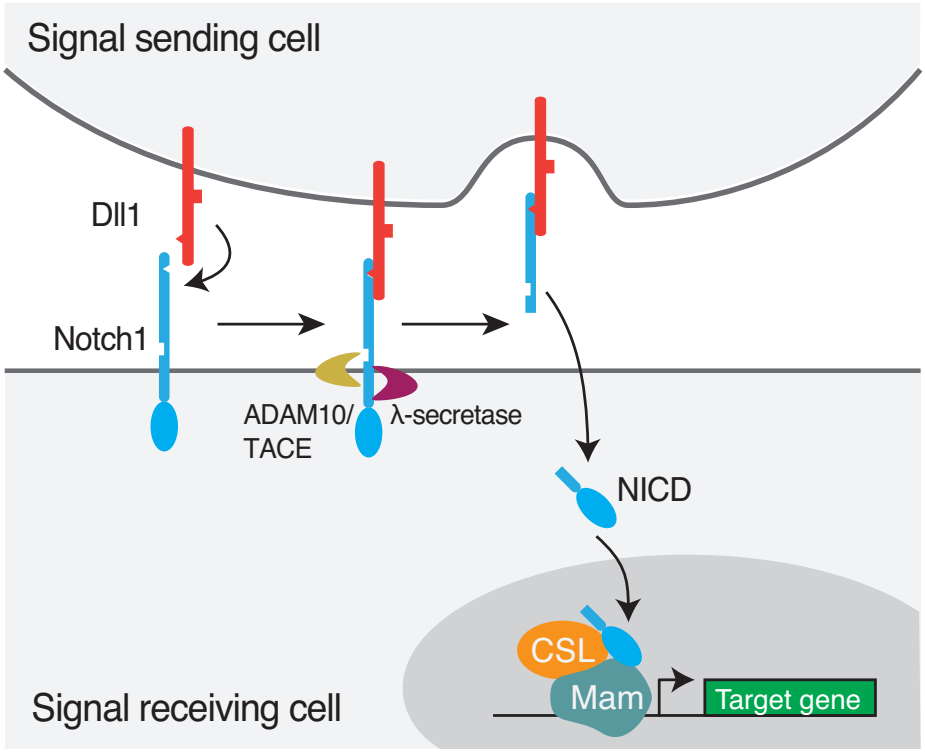

Figure 1.3: *trans*-activation of Notch. When a DSL ligand (here, Dll1) and Notch receptor (here, Notch1) bind, endocytosis of the ligands into the neighboring cell exposes the cleavage site of the receptor. Two proteolytic reactions at this site (S2 proteolysis, carried out by ADAM12 or TACE and S3 cleavage, carried out by γ-secretase) cut the Notch receptor in two. The intracellular domain of Notch (NICD) travels to the nucleus where it interacts with the CSL-Mastermind (CSL and Mam) complex to initiate transcription of target genes. Design of the diagram is based on Figure 1 from [5].

1.3 The strength of Notch *trans*-activation is the key determinant of cellular decision making

The direct nature of Notch *trans*-activation may be an important feature of the pathway, because the quantity of *trans*-activation felt by a cell seems to be the critical factor in its choice between different cell fates.

We illustrate this idea with an example from immunology. The decision for a common lymphoid progenitor (CLP) cell to commit to the B-cell or T-cell fate is governed by the dosage of Notch signaling. This dependence was shown in experiments where CLP cells were seeded on plates coated with increasing concentrations of the DSL ligand Dll1. When low levels of Dll1 were presented to the cells, leading to low levels of Notch activity, all cells chose the B-cell fate. As Dll1 levels, and in turn Notch activity, were increased, the percentage of cells adopting the B-cell fate diminished, while the percentage of cells choosing the T-cell fate increased [9, 14]. In this example and others, the dose of Notch signaling determines the developmental fate of the cell.

One way to modulate the strength of Notch signaling is by using different receptors and ligands for *trans*-activation. The collection of DSL receptors and ligands are depicted in Figure 1.4. In flies, there is a single Notch receptor and two DSL ligands, Delta and Serrate. In vertebrates, the collection of Notch pathway components has expanded to include four receptors (Notch 1-4), five DSL ligands (Delta-like-1, 3, and 4 and Jagged 1 and 2). Different ligand-receptor pairs have different interaction strengths in *trans*, leading to different developmental outcomes.

To illustrate, we turn to an example related to the one above. In this study, CLP cells were co-cultured with cells expressing Dll1 or Jag1 ligands. While cell-bound Dll1 ligands could drive the CLP cells towards the T-cell fate, cell-bound Jag1 ligands could not. Together with the results from the plate-bound ligand experiment, this suggests that Dll1 ligands elicit a higher dose of Notch signaling (through Notch1, the receptor used in this context) than Jag1 ligands [30]. These experiments demonstrate the different quantitative abilities of Dll1 and Jag1 to induce Notch1 activity.

To date, there is no evidence that different DSL ligands produce qualitatively different signals through a Notch receptor; that is, no matter which DSL ligand binds a Notch receptor, the same NICD is generated. Instead, the different functional consequences of signaling with different DSL ligands reside only in how much NICD they can generate. This means that receptors and ligands that interact strongly in *trans* (through a high affinity or high efficiency interaction) could generate more NICD than receptors and ligands that interact more weakly, leading to different developmental consequences.

Given the close dependence of signaling outcomes on the Notch signal strength, it is not surprising to find that organisms show an unusual sensitivity to changing the expression levels of Notch pathway

components. This phenomenon was evident in Morgan's discovery of *Notch* haploinsufficiency [2,24]. Further, *Notch* is one of the few genes in *Drosophila* that show both haploid and triploid phenotypes [24]. Even in mammalian systems, changing the dosage of Notch pathway components can lead to severe abnormalities. For example, mice lacking one copy of Dll4 show embryonic lethality due to spinal and vascular abnormalities. In humans, changing the dosage of pathway components is associated with many illnesses. Haploinsufficiency of Notch2 or Jag1 results in the disease Alagille syndrome, while mutations of one copy of Notch1 can lead to aortic disease [24]. Aberrant Notch signaling seems to play a causal role in many leukemias and solid tumors [24].

Here, we have tried to convey the importance of Notch signaling strength in cellular decision-making, and how this leads to sensitivity in the levels of pathway components. In the following sections, we consider two more important determinants of signaling strength: *cis*-inhibition and Fringe modification.

1.4 A second role for DSL ligands: *cis*-inhibition

DSL ligands also play a second role in the Notch pathway—in addition to *trans*-activating Notch receptors in neighboring cells, they can inhibit Notch receptors in the same cell. This interaction is termed ***cis*-inhibition** [15].

The first clues to the existence of *cis*-inhibition came about when investigating the synergy between Notch and Delta mutations in flies. Flies missing one copy of Notch ($Notch^{+/-}$ mutants) showed Morgan's wing notching and other phenotypes. One would think that a fly already missing a copy of Notch would show even more severe abnormalities if a copy of Delta was removed, as Notch signaling would be decreased even further. But surprisingly, a joint $Notch^{+/-}$ $Delta^{+/-}$ fly showed a suppression of the Notch (and Delta) haploinsufficient phenotypes, resulting in a normal looking fly [11, 13, 48]. These findings suggest that high levels of Delta relative to Notch can have an inhibitory effect on Notch signaling, and highlighted the importance of the ratio of receptor to ligand expression to Notch signaling processes in *Drosophila* [15].

cis-inhibition was first demonstrated in overexpression studies, where high levels of ectopic ligand expression prevented normal activation of Notch target genes. For example, in the *Drosophila* wing imaginal disc, a sharp stripe of Notch signaling divides the disc into dorsal and ventral halves, but overexpression of ligands in a patch of cells within this stripe interrupts the signaling in this region [10, 15, 38].

Subsequent studies have shown that *cis*-inhibition is not just an overexpression artifact, but is operative at physiological levels of receptor and ligand and plays a functional role in some signaling processes. For example, in the *Drosophila* eye, each of the eight cells within in an ommotidium expresses a different type of photoreceptor. The choice to express an R7 photoreceptor relies on Notch

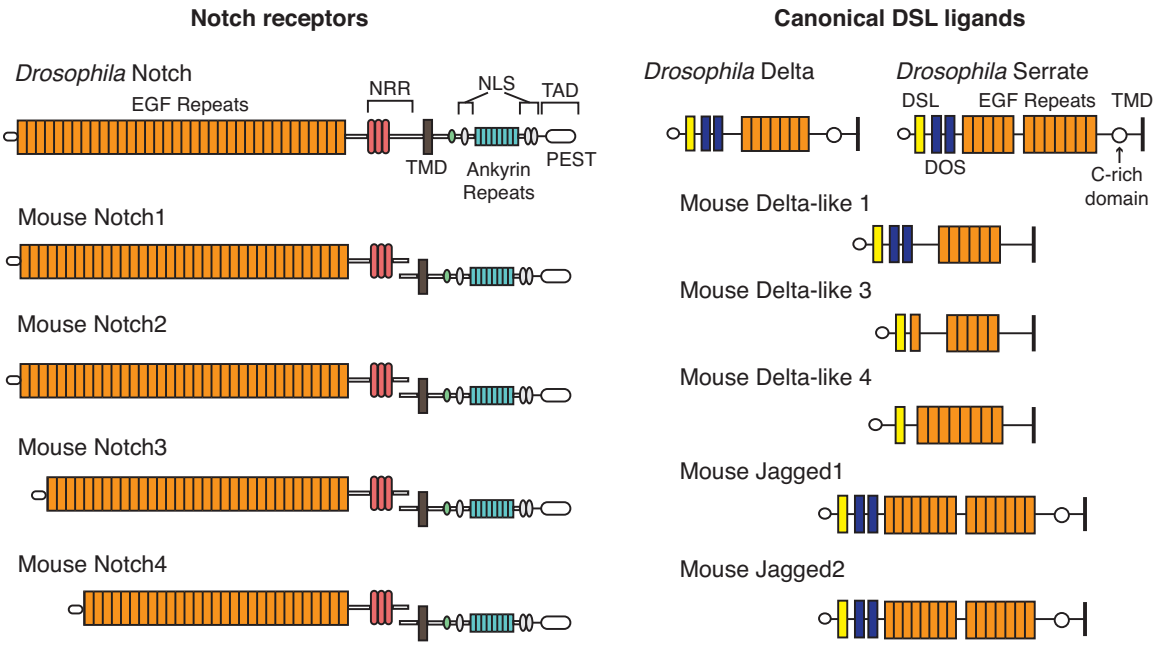

Figure 1.4: Receptors and ligands of the Notch pathway. A. In *Drosophila*, there is a single Notch ligand. The extracellular domain consists of 36 EGF-like repeats, followed by a negative regulatory region (NRR). The transmembrane domain (TMD) is the site of S1, S2, and S3 proteolysis that results in *trans*-activation. The Notch ICD consists of nuclear localization sequences (NLS), the Ankyrin repeats, a TAD domain, and the destabilizing PEST sequence. Duplications have resulted in four vertebrate Notch receptors, Notch 1-4, that vary in the number of EGF repeats. These receptors are cleaved at site S1 in the TMD; thus Notch exists as a heterodimer on the cell surface. B. In *Drosophila*, there are two DSL ligands, Delta and Serrate. Delta contains a DSL domain that is required for signaling, a DOS domain, and EGF repeats. Serrate has additional EGF repeats and a C-rich domain. In mammals, the Delta-like ligands are homologs of *Drosophila* Delta. Dll3 is highly divergent and lacks the DSL and DOS domains, and is unable to *trans*-activate Notch receptors, though it can *cis*-inhibit them [33]. The two vertebrate Jagged ligands are homologs of *Drosophila* Serrate. There are also several non-canonical ligands whose structure diverges from the DSL/DOS/EGF structure, and whose functions are less well established [17]. Design of the diagram is based on Figure 1 from [31].

signaling from cells expressing R1 and R6 photoreceptors. Loss-of-function experiments revealed that when R1 cells lose Delta expression, they suddenly become competent to receive a Notch signal, leading to adoption of the R7 fate. This suggests that R1 cells are normally *cis*-inhibited by Delta, leading to low Notch activity. In the corresponding gain-of-function experiment, R7 cells overexpressing Delta can no longer receive a Notch signal and adopt the R1/R6 cell fate, showing that the R7 cells *can* experience *cis*-inhibition; but, physiological Delta levels are low enough to permit R7 to receive a signal. Together, these experiments show that Delta expressed at physiological levels can regulate and block Notch signaling [15, 40].

While the examples thus far describe the inhibition of the receptor by the ligands, there has also been evidence of inhibition of the ligands by the receptor. For example, again in the *Drosophila* wing, cells mutant for Notch showed higher levels of the DSL ligand Serrate on their surfaces, and ectopic signaling in the adjacent normal cells [15, 19]. It is unclear whether the receptor-ligand and ligand-receptor mechanisms are distinct processes, and whether they occur in all Notch signaling contexts beyond the ones described and referenced here.

There have also been recent insights into the mechanism of *cis*-inhibition. Though the full-length crystal structures for the Notch receptors and DSL ligands are not solved, structural studies examining the portion of the proteins required for binding as well as for both the ability to *trans*-activate and *cis*-inhibit [7]. These authors solved the crystal structures of a fragment of human Notch1, consisting of EGF repeats 11-13 that had previously been shown to be essential for interactions with DSL ligands, and Jagged1, consisting of EGF repeat 3 in the highly conserved DSL region that is required for *trans*-activation. Analysis of these structures revealed that these fragments could form two distinct, anti-parallel complexes that correspond to the *cis* and *trans* ligand binding conformation.

This study raises the question of whether *cis*-ligands prevent activation simply by blocking the site for ligand binding in *trans*. However, one study showed that *cis* ligands also block the ligand-independent activation of Notch by the calcium chelator EDTA, which destabilizes the receptor and exposes the proteolytic cleavage site, suggesting that *cis* ligands are not just disrupting the binding of ligands in *trans* but also processes downstream of this step [15]. Further, different mutations in the ligands can selectively block *trans*, but not *cis*, interactions [7], and *cis*, but not *trans*, interactions [20], suggesting that the binding of ligands in both conformations must involve some distinct surfaces.

1.5 Integrating *cis* and *trans* interactions into a single model of Notch signaling

Given the two seemingly contradictory roles of the DSL ligands in Notch signaling, it was unclear how ligands in *cis* and in *trans* together could affect Notch activity. To this end, our lab used an in vitro experimental approach to determine how the two opposing actions of DSL ligands jointly determine Notch activity [51] (See also Appendix).

We constructed cell lines that allowed both readout of Notch activity and control of *cis* and *trans* ligand presented to the cells (Figure 1.5, A). To visualize Notch activity, we built "receiver" cell lines expressing Notch1 receptor and a fluorescent reporter for Notch signaling. To control the levels of *trans* ligand felt by the receiver cells, we adsorbed varying concentrations of Dll1 ligand to the cell culture plates. To control *cis* ligand expression, we incorporated Dll1, driven by an inducible promoter, into our receiver cell line. This genetic construct allows Dll1 expression to be controlled with a small molecule, doxycycline. (For a thorough description of the cell line construction and experimental methods, see Chapter 2).

We varied the levels of *cis* and *trans* ligand felt by our receiver cells and tracked the Notch activity by watching the response, measured by the fluorescence from the Notch activity reporter, in time-lapse movies. From these experiments, we made three key observations:

1. The response of our receiver cells to varying levels of plate-bound *trans* Dll1 was graded. We measured a very modest cooperativity in the relationship between *trans*-Dll1 concentration and Notch activity (Figure 1.5, B).

2. The response of our receiver cells to varying levels of *cis*-Dll1 was very sharp—in other words, receiver cells switched from a state where they were inhibited from receiving a Notch signal to a state where they were no longer inhibited from receiving a Notch signal over a very short range of *cis*-Dll1 concentrations (Figure 1.5, C).

3. Third, we observed that this sharp threshold in *cis*-Dll1 concentration did not depend on how much *trans*-Dll1 was adsorbed to the plate. Adding more *trans*-Dll1 on the plate could not out-compete *cis*-Dll1 from binding to receptors in the receiver cells (Figure 1.5, D).

We explored several simple mathematical models that described the receptor-ligand interactions and determined that the only model that can capture all three of these observations requires that the *cis* interaction between Notch receptor and Delta ligand in the same cell is mutually inhibitory. That is, when Notch receptor and Dll1 in the same cell bind one another, both are irreversibly prevented from participating in *trans* signaling. This could occur through degradation, irreversible sequestration, or some other mechanism. Specifying the *cis* interaction as mutually inhibitory can

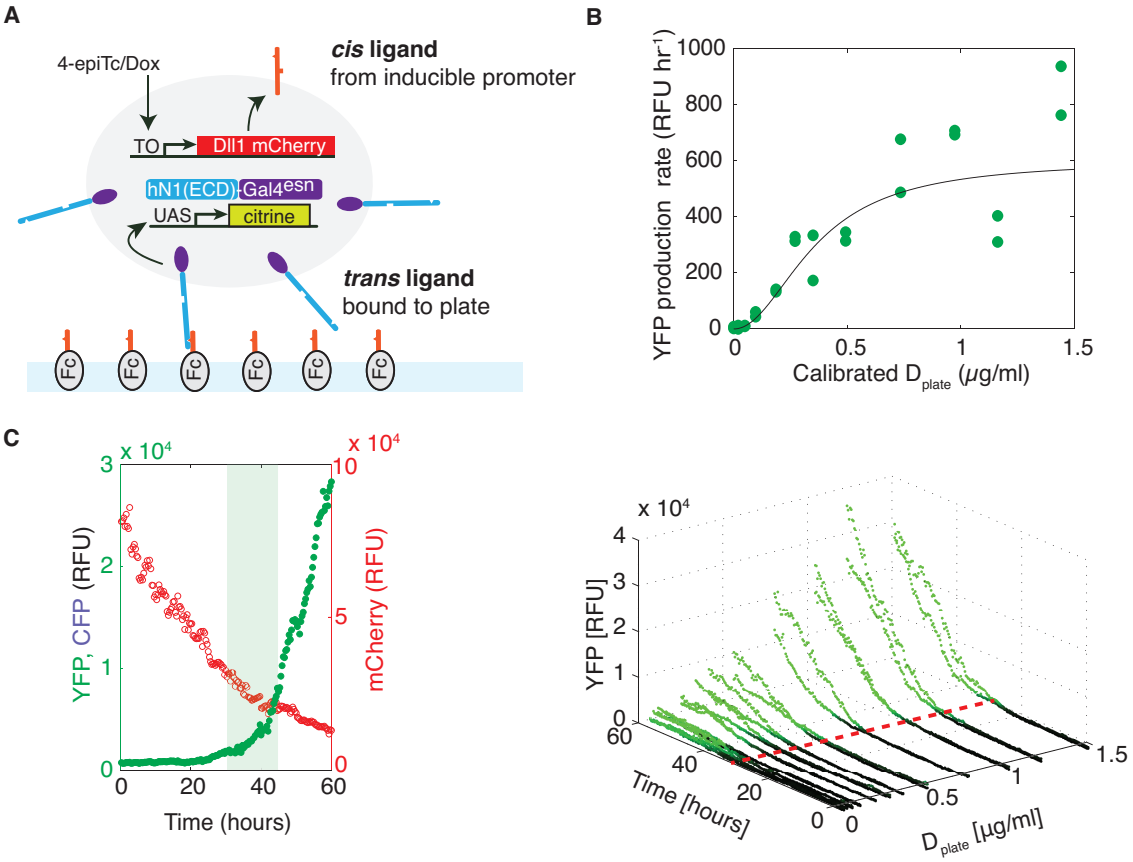

Figure 1.5: Investigating how *cis* and *trans* activities of DSL ligands combine to affect Notch activity (A) The experimental approach that allows us to integrate the effects of *cis* and *trans* ligand expression on Notch activity. Notch 1 was expressed from a constitutive promoter (hN1ΔICD-Gal4^{esn}) and Notch activity was visualized by a fluorescent reporter driven by the UAS promoter, which activates upon binding Gal4^{esn}. *trans*-Dll1 was controlled by adsorbing varying concentrations of Dll1 (D_{plate}). *cis*-Dll1 was controlled with an inducible promoter. (B) The response of the Notch receiver cells to increasing concentrations of *trans* D_{plate} showed a graded profile. (C) The response of Notch receiver cells to *cis*-Dll1 was sharp. The plot shows the fluorescence of cells in A in a time-lapse movie. The red open circles show the ligand-mCherry level in the cells, here decreasing over time. The green filled circles show the reporter fluorescence in the cells over time. The green shaded region shows that reporter cells activated very sharply despite a small change in *cis*-Dll1 levels. The response was even sharper in single cells. (D) The threshold (red dotted line) where receiver cells move from a inhibited (black) to uninhibited (green) state does not depend on the level of *trans*-Dll1.

account for the sharp threshold in *cis*-Dll1 concentration that transitions the receiver cell from an inhibited to uninhibited state, and for the fixed threshold as *trans*-Dll1 concentration is varied.

1.6 Mutually inhibitory *cis* interactions enforce exclusive sending or receiving signaling states

The finding that the *cis* interaction is mutually inhibitory has important consequences for Notch signaling [50, 51]. To illustrate, consider a cell expressing a single type of ligand, such as Delta, and a single type of Notch receptor (Figure 1.6). Consequently, if the cell produces more Delta than Notch, *cis* interactions consume all available Notches, but leave an excess of free Delta. The cell is thus able to send, but not receive, signals. On the other hand, if a cell produces more Notch than Delta, *cis* interactions consume all of the Delta, leaving an excess of free Notch, and enables the cell to receive, but not send. In this simple example, cells can only assume one of two possible signaling states: sending or receiving.

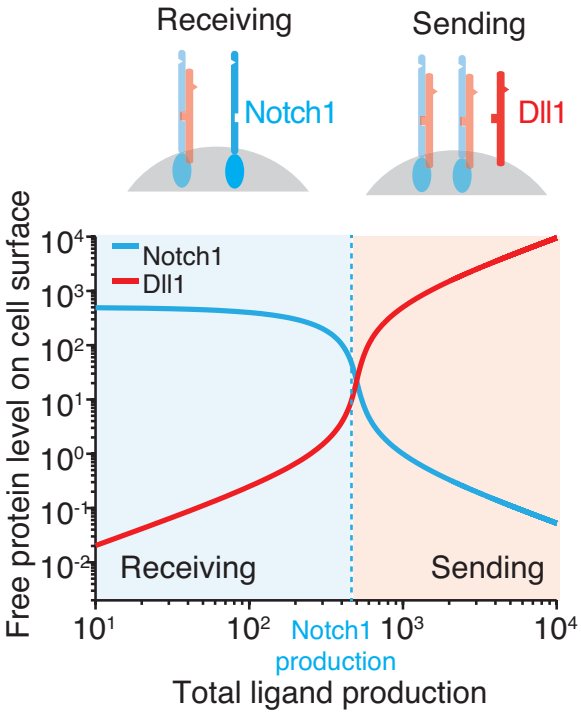

Figure 1.6: *cis* interactions between Notch receptors (here, Notch1) and ligands (here, Dll1) force cells into mutually exclusive signaling states. On the left, Notch1 levels exceed Dll1 levels. *cis* interactions deplete all of the Dll1, but leave an excess of Notch1, allowing the cell to receive signal. Moving to the right, as Dll1 levels increase, they begin to exceed Notch1 levels. Now, *cis* interactions deplete all of the Notch1, leaving only Dll1 remaining. Now, the cell can send, but not receive signal. The blue dotted line denotes where Notch1 and Dll1 production rates are equal.

If we take two cells expressing Notch and Delta, it is clear that signaling between the cells can

only occur in one direction, between a cell in a sending state and a cell in a receiving state. This example demonstrates that the relative levels of receptor and ligand expression in individual cells determines the strength and the directionality of Notch signaling. This sensitivity to the ratio of ligands to receptors is reflected in the many examples where developmental processes are interrupted by changes in the dosage of Notch pathway components, as well as the example of the restoration of the normal phenotype when both Notch and Delta dosages are halved [11, 13, 48].

1.7 Fringe proteins modulate Notch receptor-ligand interactions

The Notch pathway also includes various components that regulate the interactions between receptors and ligands. One of the most important and widely used modifiers of Notch activity is **Fringe**. Fringe encodes for a glycosyltransferase enzyme residing in the Golgi body that attaches an UDP-N-acetylglucosamine (GlcNAc) to fucose residues on the EGF repeats of Notch receptors [42, 52]. These sugar modifications alter the responsiveness of the Notch receptor to different DSL ligands in *trans*.

In *Drosophila*, Fringe increases *trans*-activation of Notch from Delta and inhibits *trans*-activation from Serrate. This effect is achieved by modulating the binding affinity between the receptor and the ligands [6, 56].

In vertebrates, the picture is, unsurprisingly, more complicated. To start, there are three Fringe variants, Lunatic Fringe (Lfng), Manic Fringe (Mfng) and Radical Fringe (Rfng). Each Fringe variant affects *trans*-activation, although whether this effect is mediated through binding affinities is unclear [52, 57]. Lfng and Mfng increase Dll1-Notch1 *trans* activation, while decreasing Jag1-Notch1 *trans* activation, similar to the pattern observed with *Drosophila* Fringe [26, 57]. On the other hand, Rfng increases Notch1 *trans*-activation from both Dll1 and Jag1 ligands [57].

Fringe is often expressed in complex patterns and directs the spatial layout of Notch activity. In the fly, Fringe is used to draw a sharp stripe of Notch signaling at a boundary between two compartments of cells, such as specifying the dorsal and ventral surfaces of the wing and establishing the segments of the legs [29]. In mammals, Lfng is required for proper development of the spinal cord. Loss of Lfng activity leads to disrupted somitogenesis and acute skeletal defects. Lfng is used to pattern the spinal cord into distinct segments to direct the differentiation and growth of neurons [36]. Mfng and Rfng are not required for survival, but there are subtle defects in some tissues when their activity is lost and can exacerbate illnesses related to defective Notch signaling, such as Alagille syndrome [52].

There are many outstanding puzzles regarding how Fringe enzymes affect Notch signaling. The first is if and whether Fringe affect *cis* interactions. If so, understanding how Fringe proteins influence

cis interactions could have important consequences for the sending and receiving abilities of cells. The second is how Fringes cooperate to impact Notch activity—are their effects additive, or does one Fringe dominate over the other? The methods described in this thesis aims to address these questions.

1.8 We can uncover the full repertoire of Notch signaling states through an analysis of receptor-ligand interactions

Our work on Notch1-Dll1 *cis* interactions describes the signaling states for a simple one-ligand one-receptor case. Now, a natural question arises: How general is this mechanism? Are only two sending and receiving signaling states possible that involve many Notch pathway components, including multiple Notch receptors, DSL ligands, and Fringe enzymes, or could more complicated behaviors become possible? To answer these questions, we need to determine a cell's signaling state given its expression of Notch pathway components.

The **signaling state** of a cell is defined here as its quantitative ability to send, and to receive signal through each ligand and receptor. For example, a cell capable of receiving signal through Delta-like-1 but not Jagged-1 (Lfng-modified) is in a different signaling state from one that can receive signal from either ligand. Knowing the signaling states of interacting cells is necessary to understand the strength and directionality of signaling between them. Even in relatively simple cases with a few components, it can be difficult to determine signaling states. However, many mammalian developmental systems (Figure 1.7) use combinations of several ligands, receptors, and Fringes, enabling a large number of possible *cis* and *trans* interactions:

- **Angiogenesis** Notch signaling is used to control the branching of new blood vessels [47]. When oxygen-deprived tissues secrete the diffusible molecule VEGF-A, blood vessel endothelial cells bind the VEGF-A signal and induce Dll4 expression. High Dll4 levels specify a single tip cell, a cell that will form a new vessel branch. The Dll4-high tip cell sends strong Notch signals to its neighbors, inhibiting them from also adopting the tip cell fate. Notch1, Jag1, and Fringe proteins are also involved in this complicated lateral inhibition process. A highly analogous Notch-dependent mechanism is used in other branching morphogenesis mechanisms during development, such as the patterning of the lymphatic vessels.

- **Regulation of adult stem cell populations** In adult mice and humans, stem cells residing in intestinal crypts continuously replenish the intestinal tissue as it is sloughed away. During this process, proliferation and differentiation of stem cells must be tightly balanced in order to both maintain the stem cell population as well as provide newly differentiated cells as needed. Notch signaling plays an important role in both of these processes: Loss of Notch signaling

leads to an overproduction of differentiated secretory cells, while ectopic Notch signaling leads to increased stem cell proliferation and inhibition of differentiation. These cells express Notch1 and Notch2, and the ligands Dll1 and Dll4 are important in these decisions. Jag1 and Dll3 may also play a role in the differentiation process [45].

- **Neuronal subtype specification** In the developing spinal cord, differentiation of the sensory and motor neuron subtypes occurs in spatially distinct domains. These domains are patterned by stripes of Notch pathway components, including Lfng, Dll1, Jag1 and Notch1 [36].

To determine the signaling state for a cell expressing an arbitrary combination of Notch pathway components, we need to know: (1) the relative expression levels of ligands, receptors, and Fringe proteins in each cell; (2) the interaction strengths, in *cis* and in *trans*, for each ligand-receptor pair; (3) how the Fringe proteins acting individually and in concert modulate these interaction strengths. Measurements of (1) are increasingly possible in biomedically important in vivo systems using single-cell techniques, but this data will remain difficult to interpret without (2) and (3), which we will measure here.

What new signaling states become available when new components are introduced? The answers to these questions are crucial, as Notch signaling processes that involve complicated spatial expression of multiple components are the rule and not the exception in mammals.

1.9 A guiding example: the dorsoventral boundary in the *Drosophila* wing imaginal disc

We can find clues to what signaling states are possible in more complicated Notch signaling contexts by looking to the simplest example of Notch signaling involving multiple ligands and Fringe expression; in fact, it is the very instance of Notch signaling first uncovered by Morgan.

The wing notching seen in Morgan's mutant fruit flies arises from defects in a Notch-dependent boundary formation process in the developing wing. The wing begins as a large sheet of cells, called the imaginal disc, that expands and eventually folds to form the dorsal and ventral surfaces of the wing. The structure that binds the edges of the dorsal and ventral surfaces together is called the wing margin. This stripe of specialized cells is defined early in larval development by Notch signaling.

While all cells in the wing disc express Notch and Delta, the dorsal cells also express Serrate and Fringe [12]. The paradox that arises is that at the interface between dorsal cells and ventral cells, both sets of cells receive a signal across the boundary. Mis-expression experiments where patches of cells are induced to ectopically express ligands, reveals that all of the cells on either side of the dorsoventral boundary in the disc can in principle receive a signal [10]. Thus, it appears that in the wing imaginal disc, cells violate the exclusive send/receive rule, and can both send a signal and

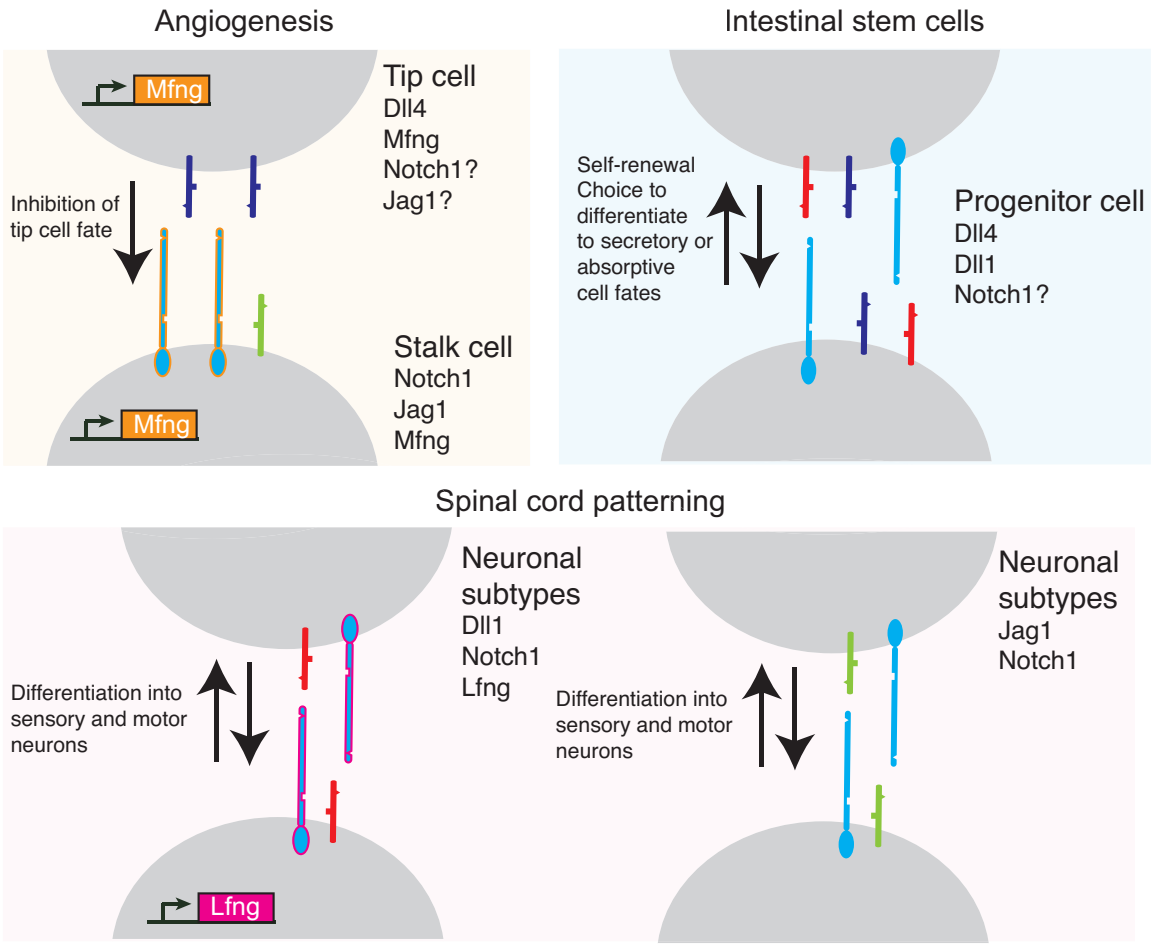

Figure 1.7: Mammalian developmental systems using multiple Notch components. Angiogenesis, intestinal stem cell differentiation, and neuronal subtype differentiation all rely on complex configuration of Notch receptors, ligands, and Fringe proteins.

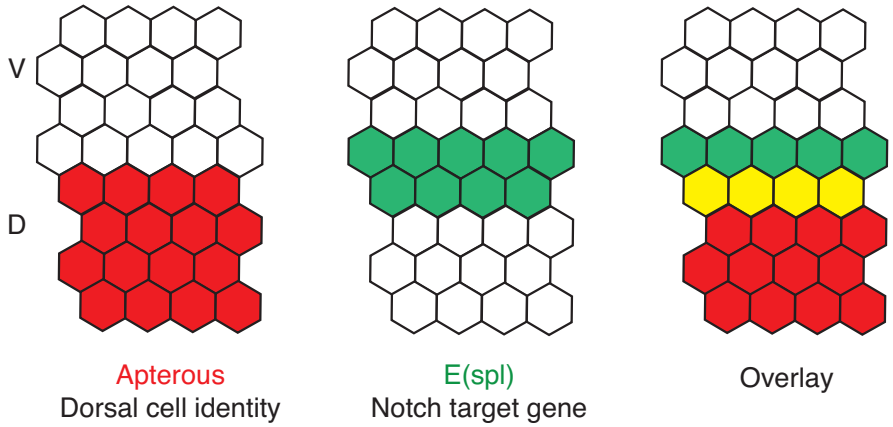

Figure 1.8: Simultaneous sending and receiving between dorsal and ventral cells at the dorsoventral boundary of the fly wing. Schematic of experimental results from Figure 4 of [12]. Antibody staining for Enhancer of split, a Notch target gene, marks cells that received a Notch signal in green. Antibody staining with anti-β-galactosidase marks cells expressing the dorsal identity marker Apterous in an *apterous-lacZ* fly strain, in red. In the overlay, the yellow cells show dorsal cells that received signal, while green cells mark the ventral cells that received signal.

receive a Notch signal simultaneously. How is this dual send/receive state achieved?

Measurements of the *cis* and *trans* interactions and particularly how they change after Fringe modification could provide insight into how the Notch pathway can achieve a signaling state that permits simultaneous receiving and sending.

1.10 Overview

In this thesis, we will establish a framework for making the measurements needed to characterize the full repertoire of Notch signaling states.

In Chapter 2, we will present a simple mathematical model that captures the *cis* and *trans* interactions for a single Notch receptor and ligand. This model can give us insight into the physical quantities that we must measure to find receptor-ligand interaction strengths. Next, we describe an experimental approach for finding these physical quantities. We build the Notch pathway from the bottom up in mammalian cells, allowing us to isolate individual ligand-receptor pairs. Then, we describe microscopy-based techniques for quantification of the *cis* and *trans* interaction strengths for each isolated pair.

In Chapter 3, we apply the methods described in Chapter 2 and present the results for two ligand-receptor pairs, Notch1-Dll1 and Notch1-Jag1, and the effects of each of the three Fringes on their *cis* and *trans* interactions. We demonstrate for the first time that Fringe modulates Notch-ligand *cis* interactions.

In Chapter 4, we will discuss the implications of these results for developmental processes. We

present data from our colleagues that corroborate our finding that Fringe modulates *cis* interactions, this time in an *in vivo* context. Using *Drosophila* developmental mutants, they show that Fringe modulates Serrate and Delta *cis*-inhibition differently consistent with our cell culture findings from Chapter 3. We discuss how these findings and our results from Chapter 3 expand the set of possible signaling states. We return to the wing dorsoventral boundary example from 1.9 and explain how the new signaling state enabled by Fringe modulation of *cis* interactions could explain this signaling process. Finally, we discuss outstanding questions and future directions for this work.

Together, the experimental approach and data presented in this thesis show that the logic of receptor-ligand interactions of the Notch signaling pathway lead to a constrained set of signaling states that enforce the specificity and directionality of Notch signaling.

Chapter 2

Theory and methods for measuring Notch-ligand *trans* and *cis* interactions

In this chapter, we describe a plan for measuring the interactions between Notch receptors and ligands in adjacent cells (*trans*-activation) and within the same cell (*cis*-inhibition). These measurements are essential for determining the Notch signaling states among cells expressing an arbitrary set of Notch pathway components. These methods are general and can be used to investigate the interactions for any Notch receptor-ligand pair, and to measure how these interactions change upon introduction of Notch pathway modifiers, such as Fringe proteins.

We begin by introducing a simple mathematical model that provides a conceptual motivation for the different experimental methods. This model originally appeared in our paper [51] and is included in the Appendix. These materials provide additional details and variations on the model. Next, we give an overview of each method. Each methods section is followed by a "Detailed methods" section for interested readers that contains comprehensive information about protocols and reagents.

2.1 A simple mathematical model gives a physical interpretation of interaction strengths

To gain an understanding of what *cis* and *trans* interactions represent in physical terms, we turn to a simple model that captures the basic interactions among receptors and ligands from [51]. This model considers two reactions that describe the interactions between a single type of receptor and a single type of ligand:

$$N_i + D_j \rightleftharpoons [N_i D_j] \rightarrow S_i \qquad \textit{trans}\text{-activation}, \tag{2.1a}$$

$$N_i + D_i \rightleftharpoons [N_i D_i] \rightarrow \emptyset \qquad \textit{cis}\text{-inhibition}. \tag{2.1b}$$

Equation 2.1a describes *trans*-activation, where Notch receptors in cell i (N_i) and DSL ligands in a neighboring cell j (D_j) associate and dissociate, and where a bound complex $[N_iD_j]$ generates an NICD (S_i, for 'signal').

Equation 2.1b describes mutual *cis*-inhibition, where receptors in cell i (N_i) and ligands in the same cell i (D_i) associate and dissociate , and where a bound complex $[N_iD_i]$ is inactivated.

These two reactions can be rewritten as a set of ordinary differential equations:

$$\frac{dN_i}{dt} = \beta_N - \gamma_N N_i - (k_D^+ N_i < D_j > -k_D^-[N_iD_j]) - (k_C^+ N_i D_i - k_C^-[N_iD_i]), \tag{2.2a}$$

$$\frac{dD_i}{dt} = \beta_D - \gamma_D D_i - (k_D^+ < N_j > D_i - k_D^-[N_jD_i]) - (k_C^+ N_i D_i - k_C^-[N_iD_i]), \tag{2.2b}$$

$$\frac{d[N_iD_j]}{dt} = k_D^+ N_i < D_j > -k_D^-[N_iD_j] - k_S[N_iD_j], \tag{2.2c}$$

$$\frac{d[N_iD_i]}{dt} = k_C^+ N_i D_i - k_C^-[N_iD_i] - k_I[N_iD_i], \tag{2.2d}$$

$$\frac{dS}{dt} = k_S[N_iD_j] - \gamma_S S_i. \tag{2.2e}$$

β_N describes the production rate of active Notch receptor, and γ_N describes the rate of degradation of active Notch receptor in Equation 2.2a. Likewise, β_D describes the production rate of active DSL ligand, and γ_D describes the rate of degradation of active DSL ligand in Equation 2.2b.

Notch receptors and Delta ligands in neighboring cells can associate and dissociate in *trans* with a rate $k_D^{\pm}$, and a bound complex $[N_iD_j]$ generates an NICD (S_i) with activation rate k_S. These processes affect the time evolution of Notch receptors, DSL ligands, *trans* complexes, and NICD (S_i), corresponding to Equations 2.2a, b, c, and e. $< D_j >$ and $< N_j >$ are the average concentrations of D_j and N_j felt by cell i in *trans*. This signal undergoes a spontaneous decay with rate γ_S.

Notch receptors and DSL ligands in the same cell can associate and dissociate in *cis* with a rate with a rate $k_C^{\pm}$. A bound complex $[N_iD_i]$ is inactivated with a rate k_I. These processes affect the time evolution of Notch receptors, DSL ligands, and *cis* complexes, corresponding to Equations 2.2a, b, and d respectively.

First, we want to know what the *trans* interaction strength represents in physical terms. We are able to isolate and measure *trans*-activation in the absence of *cis*-ligands, as well as to precisely control the level of ligand presentation in *trans*. We will describe these methods in detail in the coming sections (Section 2.3). Thus, we can simplify the above equations by removing the *cis* interaction terms, as well as by replacing the term $< D_j >$ with D_{trans}, the precise quantity of *trans*-ligand.

Next, we assume that the generation of the NICD is very fast compared to the other reactions, allowing us to assume that the bound complex $[N_iD_{trans}]$ achieves a quasi-steady state ($[N_iD_{trans}] \approx 0$). Using this assumption, we derive the following relationship:

$$S_{steady\ state} = \frac{1}{\gamma_S} \frac{\beta_N D_{trans}}{\frac{k_D^- + k_S}{k_S k_D^+}\gamma_n + D_{trans}}. \tag{2.3}$$

This equation shows a Michaelis-Menten relationship between the level of ligand presented to the receiver cells, D_{trans}, and Notch activity. The half-maximal activity occurs when the D_{trans} concentration is proportional to $\frac{k_D^- + k_S}{k_S k_D^+}$. This value is k_t, the *trans* interaction strength.

Next, we use the model to understand what the *cis* interaction strength represents in physical terms. Again, our experimental approach allows us to simplify the equations in 2.2. We are able to isolate the effects of *cis* interactions independent of *trans* interactions (Section 2.4). Thus, we can ignore the terms describing the *trans* interaction strength. Here, we assume that the inactivation of the $[N_i D_i]$ *cis*-complex occurs much faster than the other reactions, allowing us to again apply the quasi steady-state assumption, ($[N_i D_i] \approx 0$). We arrive at the following expression:

$$N_{steady\ state} = \frac{\frac{\beta_N}{\gamma_N}}{1 + \frac{D_{steady\ state}}{k_C \gamma_N}}. \tag{2.4}$$

where k_C^{-1} is defined as $\frac{k_c^+ k_I}{k_C^- + k_I}$. The physical meaning of this expression is that available Notch receptor is a decreasing function of *cis*-Delta concentration. When there is no *cis*-Delta expression steady state receptor levels equal the production divided by the degradation rate. However, as *cis*-Delta increases, the level of available Notch drops. The value where Delta depletes Notch receptor to one half its maximal value in the absence of *cis*-Delta is $k_c \gamma_N$, which is proportional to the *cis* interaction strength.

In summary, we must measure two quantities that represent the *trans*-activation and *cis*-inhibition strengths for each ligand-receptor pair. For the *trans*-activation, we must measure the ligand level that elicits a half-maximal level of Notch activity in pure Notch receiver cells. For *cis*-inhibition, we must measure the available Notch levels on cells as a function of *cis*-ligand expression, and the ligand expression level that depletes half of the total surface Notch will be our *cis*-inhibition strength. The following sections will describe how to find these values experimentally.

2.2 Building the Notch pathway from the bottom up

Measuring *cis* and *trans* interaction strengths for individual ligand-receptor pairs enables us to generate predictions about how combinatorial sets of Notch pathway components should behave. However, these individual measurements would be difficult or impossible to achieve in animal systems, where these components are expressed simultaneously and dynamically in single cells. Thus, our experimental approach is to isolate ligand-receptor pairs and to study their interactions *in vitro*, by building a synthetic Notch pathway from the bottom up.

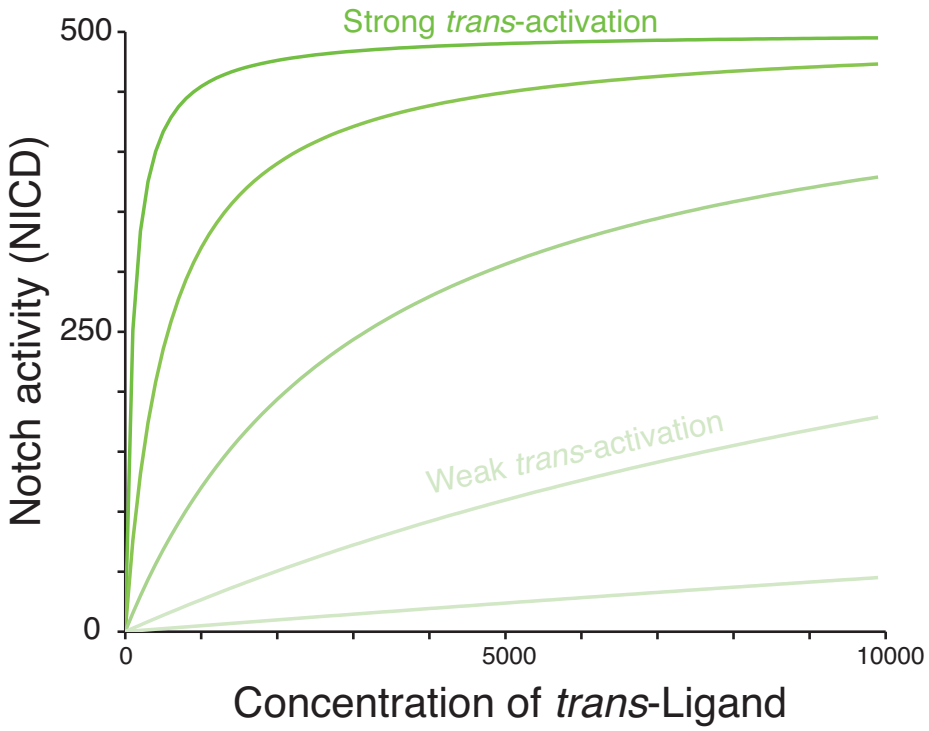

Figure 2.1: Plot of Equation 2.3 of single-cell Notch activity with increasing *trans*-ligand. As the concentration of *trans*-ligand is increased the signal (NICD) generated increases sharply when the receptor-ligand *trans*-interaction is strong (dark green curves) or graded when the *trans*-interaction is weak (light green curve). Parameters used to generate the curves are $\beta_N = 500$, $\gamma_N = 1$, $\gamma_S = 1$, $D_{trans} = 1$ to 10000, and $k_{trans} = 10^2$ (strong) to 10^5 (weak).

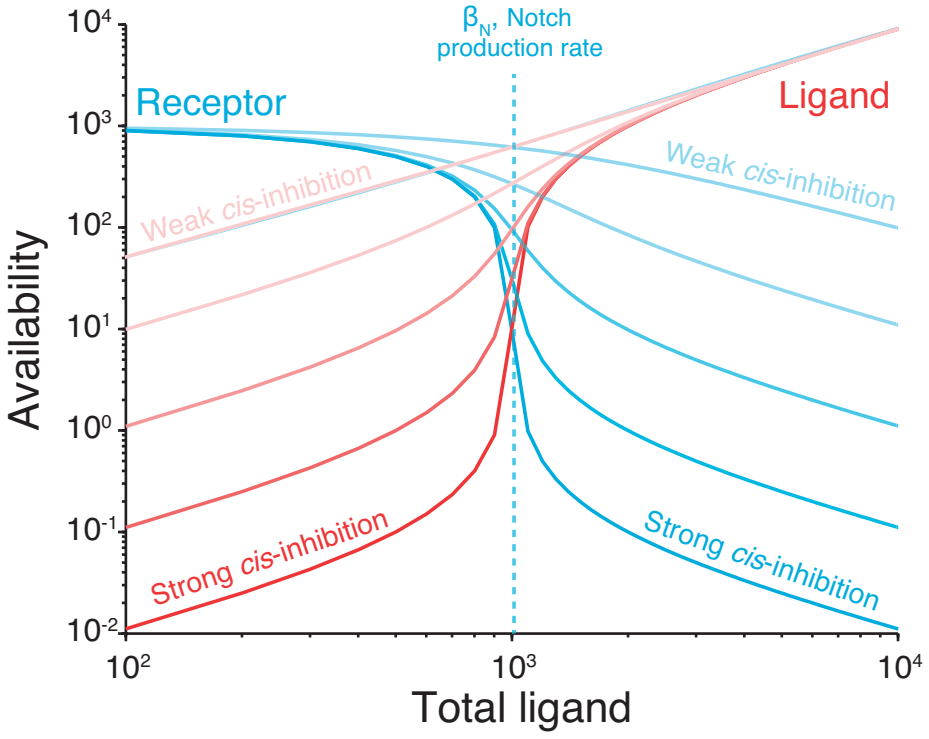

Figure 2.2: Plot of Equation 2.4 of single-cell receptor and ligand availability of a cell with constitutive Notch receptor expression and increasing ligand expression at varying *cis*-inhibition strengths. The blue curves show Notch receptors available on the surface for signaling. As ligand expression increases, the receptor availability falls off sharply, for strong *cis*-inhibition (dark blue curves), or gradually, for weak *cis*-inhibition (light blue curves). The red curves show the ligand available for signaling. At high *cis*-inhibition, Notch keeps available ligands low until total ligand levels exceed Notch levels, then shoots up sharply (dark red curves). At low *cis*-inhibition, ligand availability tracks ligand expression, unaffected by Notch levels (light red curves). Parameters used to generate the curves are $\beta_N = 1000$, $\gamma_N = 1$, $\gamma_S = 1$, $\beta_D = 10^2$ to 10^4, $k_{cis} = 10^{-1}$ (strong) to 10^3 (weak).

As a foundation for our bottom up construction of the Notch pathway, we chose CHO-K1 (Chinese Hamster Ovary), a standard laboratory cell line. CHO-K1 exhibits no detectable endogenous Notch activity under our growth conditions, and transcriptome analysis revealed no detectable expression of Notch receptors or ligands. Nevertheless, CHO-K1 cells express all essential components, such as the CSL (RBPJ-κ), proteins necessary to support Notch signaling. CHO-K1 also supports high transfection efficiencies, facilitating rapid cell line construction. The recently available public genome sequence of CHO and our own transcriptome analysis provide data for design of qPCR primers, shRNA, and other tools [25]. Finally, CHO-K1 have been used in several *in vitro* studies investigating Notch signaling and Fringe modification, and the findings from these studies have been consistent with *in vivo* findings [27].

2.2.1 Engineered cell lines allow control and readout of ligand expression and Notch activity in individual cells

To build the Notch pathway from the bottom up, we need a set of components that allow us to control and visualize Notch signaling. The components list is shown in Figure.2.3.

The first component is the Notch receptor. We constructed a 'diverted' variant of the Notch1 receptor, hN1(ΔICD)-Gal4^{esn}, based on an original design by Struhl [53]. This chimeric receptor has the ICD replaced with a minimal variant of the yeast transcriptional activator Gal4, here denoted Gal4^{esn}, to avoid activation of possible endogeneous Notch targets in CHO-K1 cells.

To monitor Notch activity, we built a second component where the UAS promoter drives expression of a Histone 2B (H2B)-3x-YFP (three citrine fluorescent proteins fused in tandem). When the diverted Notch receptor is *trans*-activated, the Gal4^{esn} binds to the UAS target promoter, and generates green, nuclear-localized fluorescence.

The third component for a synthetic Notch signaling pathway is a DSL ligand. We constructed chimeric ligand-Cerulean fluorescent protein or ligand-mCherry fluorescent protein fusion genes under control of a tetracycline-inducible (TO) promoter. Expression of the fluorescent ligand can be tuned by adding an inducer, such as doxycycline (dox, high affinity inducer), or 4-epitetracycline (4-epiTc, low affinity inducer). The TO promoter is a minimal CMV promoter that contains binding sites for the Tet repressor [22]. In the absence of 4-epiTc, the Tet repressor, expressed constitutively in our CHO-K1 cells, binds to the TO operator sites, blocking the transcriptional machinery for reading the DNA. When the Dox/4-epiTc is added, the drug binds to the TetR, freeing the TO operator and allowing the transcriptional machinery to proceed.

Together, these genetic engineering methods allow us to express single ligand-receptor pairs in the Notch pathway, as well as control over the level of the ligand expression. They also enable us to visualize the magnitude of Notch activity with a fluorescent reporter. We can also add additional

ligands and receptors, and Fringe proteins, building up more complex configurations of components.

2.2.2 Detailed methods for cell line construction

CHO-K1 cells were maintained as described in [51]. Briefly, cells were maintained in Alpha-MEM Earle's Salts media (Irvine Scientific) supplemented with 10% Tet-system approved FBS (Clontech) and an L-glutamine, penicillin and streptomycin additive (Gibco), and stored in an incubator at 37°C at 5% CO_2.

Genetic constructs, including siRNA constructs, were introduced into CHO-K1 cells using Lipofectamine 2000 reagent according to the manufacturers' protocol (Life Technologies), or FugeneHD reagent (Promega). Selection was performed using 400μg/mL Zeocin (Life Technologies), 10μg/mL Blasticidin (InvivoGen), 600μg/mL Geneticin (Life Technologies), 500μg/mL Hygromycin (InvivoGen) and/or 3μg/mL Puromycin (Life Technologies). Single clones were obtained using FACS sorting or limiting dilution. Single clones were chosen based on fluorescence or quantitative PCR for non-fluorescent constructs.

Quantitative PCR was used to measure gene expression of non-fluorescent components. RNA was isolated with the Qiagen RNAeasy kit according to the manufacturers protocol. cDNA was synthesized from 1μg of RNA using the iScript cDNA synthesis kit (Bio-Rad). For real-time PCR reactions, SsoFast Probes Supermix (Bio-Rad) was combined with 2μL of cDNA. Each reaction was performed in triplicate. In parallel, three real-time PCR reactions were performed to measure β-actin levels in the sample, allowing us to compute a Δ-Δ CT value for the gene of interest in our cell lines. Reactions were performed on a Bio-Rad CFX Real-Time PCR Detection System. Probe sets included the following:

β-actin

Primer 1: 5' – ACTGGGACGATATGGAGAAG –3'

Primer 2: 5' – GGTCATCTTTTCACGGTTGG –3'

Probe: 5'– HEX ACCACACCTTCTACAACGAGCTGC – BlkFQ-3',

Lfng

Primer 1: 5'-GAAGTTCTGTCCCCTCGC–3'

Primer 2: 5'-GATCCAGGTCTCGAACAGC–3'

Probe: 5'–FAM ACTTTCTGGTGGTCTTGACGGCG–BlkFQ-3',

Mfng

Primer 1: 5'–ACCACTCAAGTTTGTCCCAG–3'

Primer 2: 5'–GATGAAGATGTCGCCTAGCTG–3'

Probe: 5'–FAM TGAACCAACGGAACCCAGGACC–BlkFQ–3',

Rfng

Primer 1: 5'–TCATTGCAGTCAAGACCACTC–3'

Primer 2: 5'–CGGTGAAAATGAACGTCTGC–3'

Probe: 5'–FAM CTCGTGAGATCCAGGTACGCAGC–BlkFQ–3'.

2.3 Methods to measure and compare ligand-receptor *trans* interaction strengths

From our model in Section 2.1, we must measure the level of Notch activity in response to increasing levels of *trans*-ligand, and find the ligand level that elicits half-maximal Notch activity. To do this, we build Notch "receiver" cells, that express the diverted versions of our Notch receptor and activity reporter (See Figure 2.3) to measure activity stimulated by two different methods of *trans*-ligand presentation.

The first method is to present *trans*-ligands immobilized on cell culture plates. We seeded our receiver cell line on plates coated with varying concentrations of ligand-Fc fusion protein, which consists of a fragment of the DSL ligand fused to the Fc epitope (Figure 2.4A). The advantage of this method is that allows us to precisely control the quantity of ligand presented to the cells, and also provides a uniform level of ligand to all reporter cells in a large population of receiver cells, allowing us to quantify variability in their response. The disadvantage to this method is that the ligand presentation is artificial, and may not accurately reflect *trans*-activation with ligands expressed on the cell surface. This is especially a concern given the important role of a"pulling force" generated by the endocytosis of the DSL ligand-Notch ECD complex into the signal-sending cell during *trans*-activation [37].

Thus, we used a second, more natural method of ligand presentation in parallel. We used ligand-expressing "sender" cells, expressing our inducible ligand constructs, to present cell-based ligands to our receiver cells (Figure 2.4B). We co-cultured sender and receiver cells and measured the response of the activity reporter in the the receivers. The advantage to this method is that it is potentially more similar to endogenous ligand presentation. The disadvantage is that CHO-K1 cells are highly mobile, even at confluence, and the fluctuations of cell contacts leads to a highly variable response in the receiver cells. However, using a high ratio of sender cells to receiver cells and plating the cells at a high density can mitigate this variability.

With the results of these two assays, we can converge at a characterization of the *trans*-activation strength between each receptor-ligand pair that is both precise and physiologically relevant.

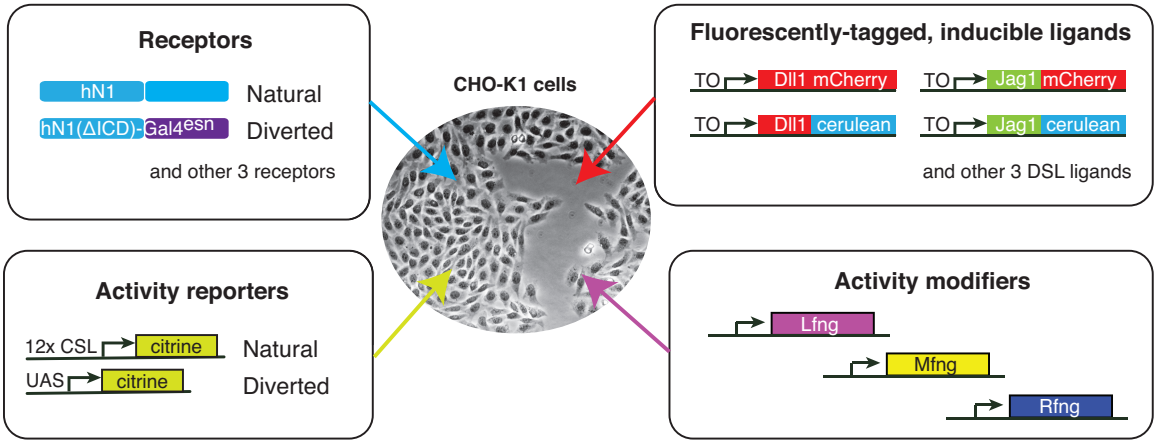

Figure 2.3: Components list for engineering the Notch pathway from the bottom up. Our CHO-K1 cell line expresses very low (if any) levels of Notch receptors and ligands. To this base cell line, we can add combintions of the following components. We can add one (or combinations) of the four Notch receptors in a natural or diverted (ICD replaced with a transcriptional activator) form. We can add reporters to generate fluorescence upon binding of NICD (12xCSL, 'Natural' reporter) or transcriptional activator (for example, a Notch-Gal4 paired with a UAS sequence, 'Diverted' reporter) to the promoter. We can also add DSL ligands fused to fluorescent proteins and under control of small-molecule inducible promoters. Finally, we can add activity modifiers, such as the Fringe proteins, under constitutive or inducible promoters.

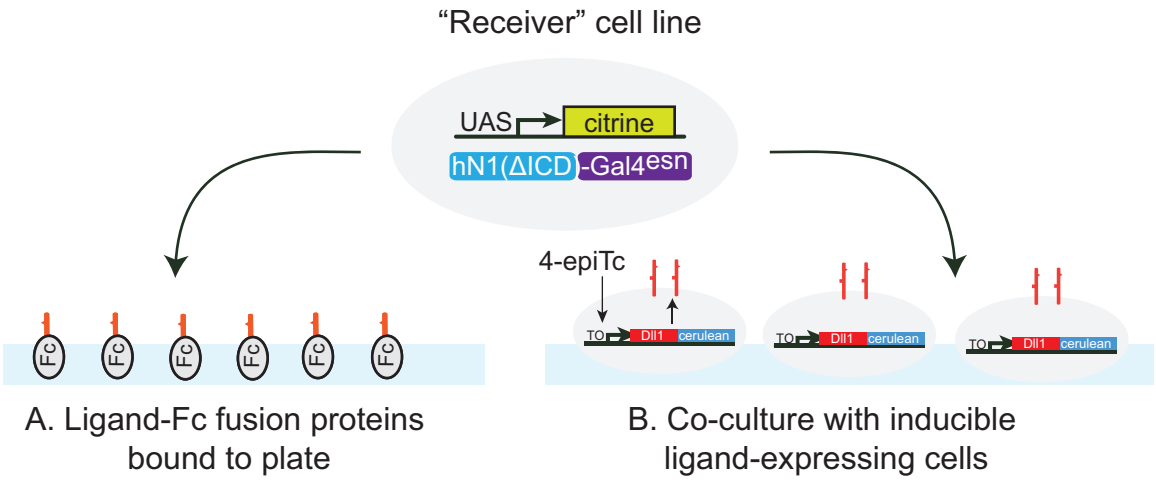

Figure 2.4: Two methods for measuring *trans*-activation. We plate "receiver" cells on plates coated with immobilized ligand-Fc fusion proteins. B. We also use "sender" cell lines expressing ligands under inducible control in a co-culture with receiver cells to evaluate the *trans*-activation capabilities of different ligands.

2.3.1 Detailed methods for *trans*-activation assays

For the plate-bound ligand method, we incubated cell culture plates with a fixed concentration (usually 1μg/mL unless noted otherwise) ligand-Fc fusion protein in PBS for 1 hour at 4°C. We washed the plates with PBS, and then added cell culture media and plated receiver cells. We assayed the cells, after 24-48 hours, by flow cytometry (See 2.4.2 for flow cytometry details).

In order to fairly compare the *trans*-activation capabilities of different ligands, we needed to calibrate the level of ligand bound to the plates. To do this, we incubated the plates as described above, and then applied an anti-Fc HRP-conjugated antibody to the plate (Figure 2.5). We detected the activity of the bound HRP-conjugated antibodies by adding a TMB substrate (Thermo Scientific 1-Step Turbo TMB-ELISA Substrate Solution). We measured the HRP chemiluminescence from the plates to determine the level of bound ligand using a plate reader (Wallac 1420, Perkin-Elmer). From this procedure, we determined that both the Dll1 and Jag1 ligands bound with similar efficiencies to the plate.

For the co-culture method, we mixed sender and receiver cells at a ratio of 90:10 and plated cells at very high density (90% confluence) to maximize cell contacts. We measured the cells after 48-72 hours to evaluate activation by flow cytometry.

We calibrated the level of ligands on the cell surface of each of our sender cell lines using the ligand availability assay described in the following sections. Briefly, this method allows us to tag ligands localized on the cell surface using soluble Notch receptor fragments conjugated to Fc epitopes, then label the bound Notch-Fc epitope with fluorescent reagents. Using this method, we were able to normalize our results to account for the differing levels of ligands on the cell surface (Figure 2.9E).

2.4 Availability assay to measure and compare ligand-receptor *cis*-interaction strengths

We recall from Section 2.1 that the quantity relevant for determining the strength of the *cis*-interaction is the amount of *cis*-ligand needed to deplete available surface Notch receptor levels to one-half their maximum value. Thus, our experimental method must be able to quantify the Notch receptors available on the cell surface as a function of *cis*-ligand expression.

To this end, we developed an immunostaining-based "availability" assay to label available Notch receptors on the surface of our cells as we vary the level of *cis*-ligand with 4-epiTc (based on [49]). To detect available Notch receptors on the cell surface, we incubated our test cell lines with soluble Dll1 fragments chimeric with the Fc epitope tag (Dll1$^{\text{ext}}$-Fc). We found that this reagent only binds to Notch receptors free to participate in *trans*-signaling, and does not label *cis* complexes that might be localized at the cell surface (Figure 2.6).

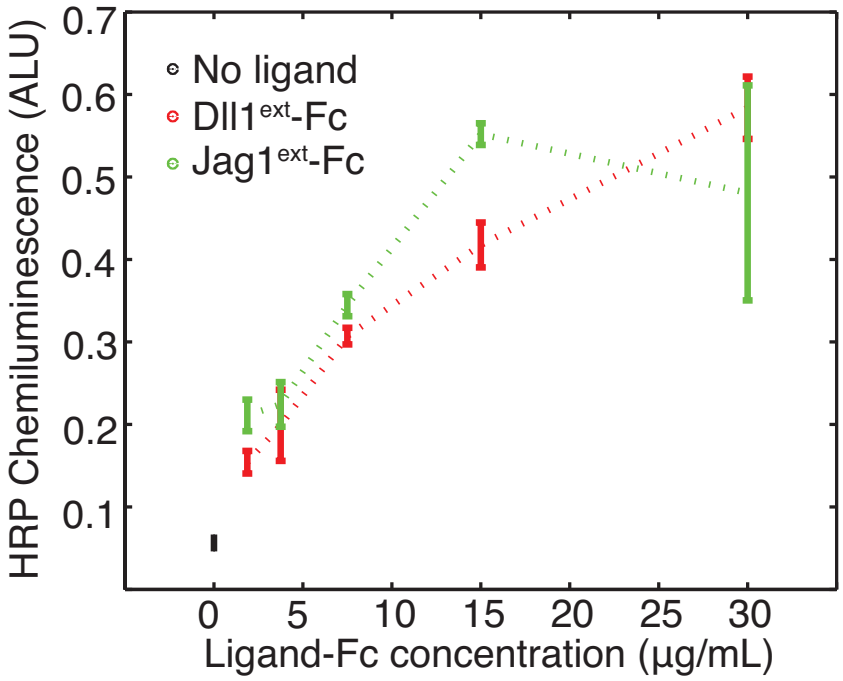

Figure 2.5: Calibration of plate-bound ligands. We coated plates with varying concentrations of Dll1^{ext}-Fc or Jag1-^{ext}-Fc protein, and then used anti-Fc HRP-conjugated antibodies to detect the amount of plate-bound ligand. We found that the Dll1 and Jag1 proteins bind to the plates with equal efficiencies, allowing for a direct comparison between the two ligands at the same incubation concentration.

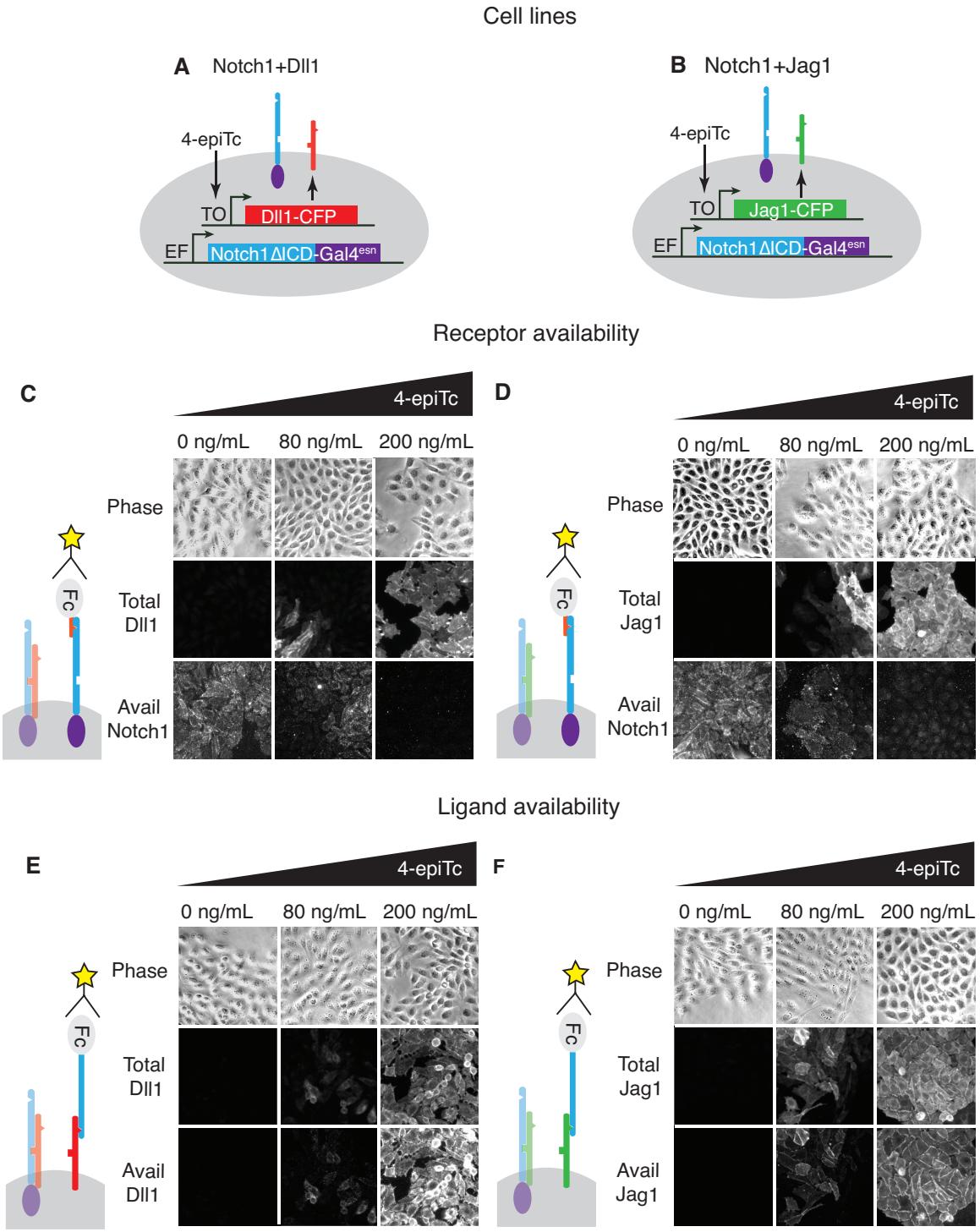

Figure 2.6: Availability assay for measuring *cis* interactions. (A-B) Stable CHO-K1 cell lines constitutively express a Notch1-Gal4 chimeric receptor and a tetracycline-inducible Dll1 (A) or Jag1 (B) ligand fused to cerulean fluorescent protein. (C-D) In the receptor availability assay, soluble Dll1^{ext}-Fc binds to free Notch receptor on the surface of live cells. After fixation, bound Dll1^{ext}-Fc is labeled with anti-Fc fluorescent reagents. Increasing ligand-Cerulean expression reduces receptor availability, as shown in these snapshots, consistent with *cis*-inhibition (C, D, bottom panels). (E-F) The ligand availability assay works similarly, except soluble N1^{ext}-Fc fragments bind free ligands on the cell surface. Increasing ligand-Cerulean expression (E, F, middle panels), leads to increased ligand availability (E, F bottom panels). The surface ligand availability shows good spatial correlation with the total cellular ligand staining. Note that cells were plated at high cell density for illustration purposes. For quantitative analysis, cells were dissociated and plated at low density before staining (Figure 2.9).

We performed the converse ligand availability experiment by incubating the same cells with soluble Notch1 fragments chimeric with Fc, $N1^{ext}$-Fc (Figure 2.6). We found that this procedure labels only ligands that are available to participate in *trans*-activation.

After the initial incubation with soluble receptor-Fc or ligand-Fc fragments, we washed away the unbound protein and fixed and permeabilized the cells. We then blocked the cells and then labeled the bound Fc fusion proteins with fluorescent anti-Fc secondary reagents. In parallel, we incubated the cells with a cytoplasmic blue stain for automatic segmentation of cell bodies. We then imaged the cells on the microscope and analyzed the single-cell fluorescence using a MATLAB routine.

2.4.1 Validation of availability assay

To validate the Notch availability assay, we performed the assay on cells expressing hN1(ΔICD)-$Gal4^{esn}$ and observed high levels of availability fluorescence. Meanwhile, the Notch availability assay performed on CHO-K1 cells lacking ectopic Notch expression showed minimal fluorescence (Figure 2.8A). To see if receptor availability corresponds to receiving ability, we seeded receiver cells on plates coated with $Dll1^{ext}$-Fc. We observed a strong response from the reporter (compare $\pm$ D_{plate}). When we knocked down receptor expression using siRNA against the extracellular domain of Notch1, receiving ability decreased (Figure 2.8A). In parallel we also observed a coincident decrease in Notch1 availability in receiver cells with and without siRNA against Notch1 (Figure 2.8B).

Cells expressing inducible ligand only showed increased ligand availability as ligand expression was induced with 4-epiTc (Figure 2.8C). We induced TO-Dll1-cerulean and TO-Jag1-cerulean cell lines with increasing concentrations of 4-epiTc and then stained each sample with ligand availability reagents. We found that ligand availability increased with ligand induction (Figure 2.8C). We also induced the cells with varying concentrations of 4-epiTc and co-cultured them with receiver cell lines. From this experiment, we found that inducible ligand cells could *trans*-activate receiver cells in a dose-dependent fashion (Figure 2.8D). Because ligand availability also increased with induction, ligand availability and sending ability are correlated.

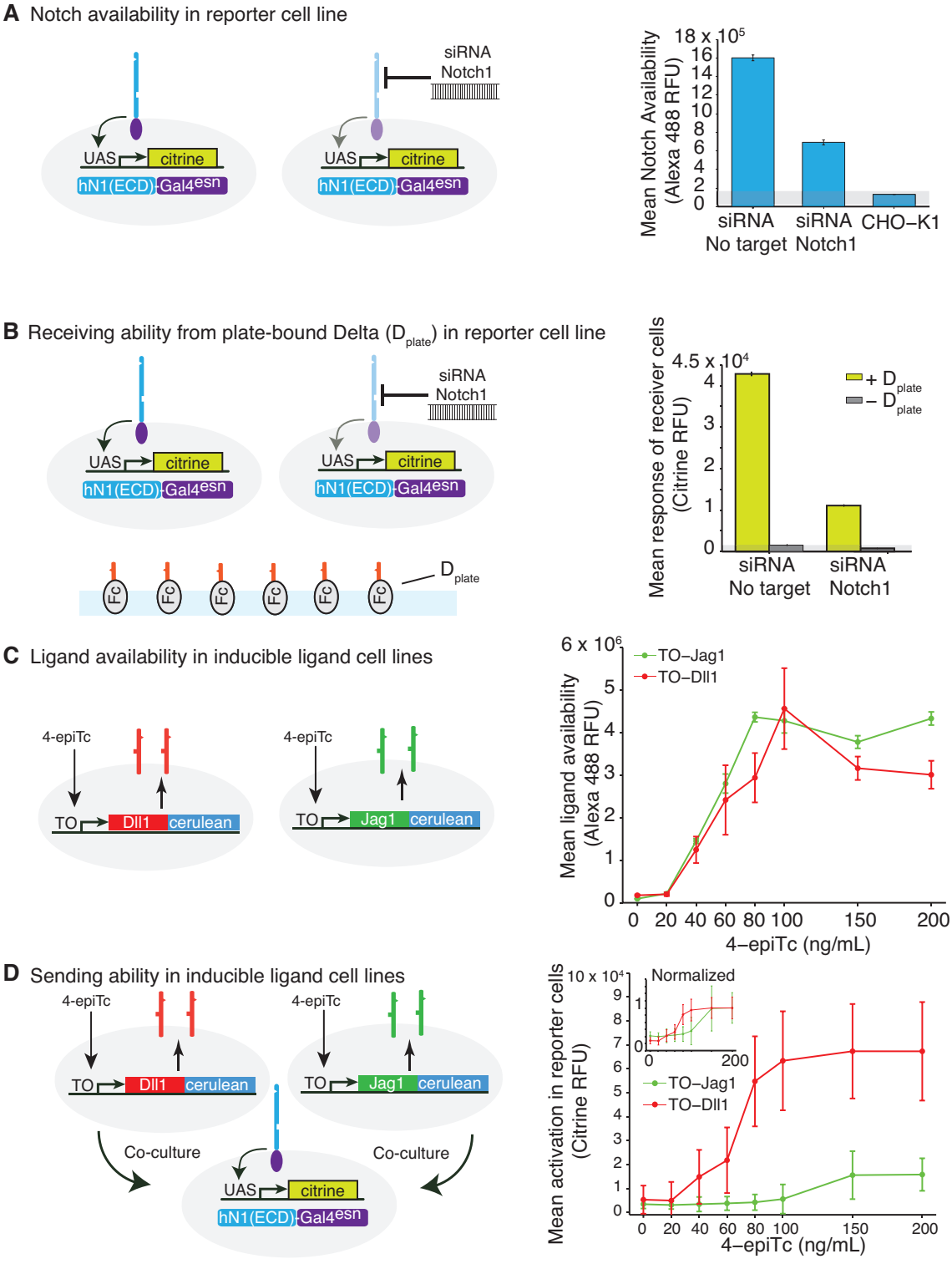
A Notch availability in reporter cell line
siRNA
Notch1
UAS
citrine
hN1(ECD)-Gal4esn
Mean Notch Availability (Alexa 488 RFU)
18 x 10^5
siRNA No target
siRNA Notch1
CHO–K1
B Receiving ability from plate-bound Delta (D_plate) in reporter cell line
D_plate
Fc
Mean response of receiver cells (Citrine RFU)
4.5 x 10^4
+ D_plate
– D_plate
C Ligand availability in inducible ligand cell lines
4-epiTc
TO
Dll1
cerulean
Jag1
Mean ligand availability (Alexa 488 RFU)
6 x 10^6
TO–Jag1
TO–Dll1
4–epiTc (ng/mL)
D Sending ability in inducible ligand cell lines
Co-culture
Mean activation in reporter cells (Citrine RFU)
10 x 10^4
Normalized

Figure 2.7

Figure 2.7 *(previous page)*: (A) To validate the Notch availability assay, we tested cells expressing hN1(ICD)-Gal4^{esn} and observed high levels of availability fluorescence, while CHO-K1 cells lacking ectopic Notch expression showed minimal availability fluorescence (Anti-IgG Alexa 488). Bars show mean Notch1 availability, and error bars show standard error of the mean (SEM). (B) To show that receptor availability corresponds to receiving ability, we seeded the receiver cell line expressing a diverted Notch receptor (hN1(ICD)-Gal4^{esn}) and a fluorescent reporter for Notch signaling (UAS-H2B-citrine) on plates coated with Dll1 ligands. We observed a strong response from the reporter (compare ±Dplate). When we knocked down receptor expression using siRNA against the extracellular domain of Notch1, receiving ability decreased, coinciding with the decrease in Notch1 availability from A. Bars show mean reporter fluorescence, error bars are SEM. (C) Inducible ligand cells show increased ligand availability as ligand expression is induced with 4-epiTc. The TO-Dll1-cerulean and TO-Jag1-cerulean cell lines were incubated with increasing concentrations of 4epi-Tc and stained with ligand availability reagents. Points show the mean availability at each induction level, error bars show the SEM. (D) Inducible ligand cells from C are able to *trans*-activate Notch receiver cells in a dose-dependent fashion as ligand induction is induced with 4epi-Tc. Because ligand availability also increases with induction, ligand availability and sending ability are correlated. In the inset, the same data normalized to the maximal activation elicited by each ligand. In all panels, cells were analyzed by flow cytometry.

2.4.2 Detailed methods for availability assay

For both availability assays, test cells were plated in 24-well plates (BD Falcon) at 25% confluence and treated with one of eight concentrations of 4-epiTc ranging from 0 to 200 ng/mL. In siRNA transfection experiments, silencing constructs were delivered after 24 hours of induction. After 48 hours of induction, cells from all 4-epiTc induction conditions were trypsinized, pooled into a single tube, and replated in triplicate at low (5-10% confluent) density. CHO-K1 and hN1(Δ ICD)-Gal4^{esn} cell lines were also plated as staining controls.

After 4-6 hours, test cells were blocked for 30 minutes at 37°C in blocking buffer (PBS with 2% FBS and 100 μg/mL $CaCl_2$). Next, cells were incubated with 10 μg/mL soluble Mouse Recombinant Dll1^{ext}-Fc chimera (receptor availability) or Mouse Recombinant Notch1^{ext}-Fc chimera (ligand availability), both from R & D Systems (5267-TK and 5026-DL, respectively) diluted in binding buffer (PBS with 2% Sigma Bovine serum albumin and 100 μg/mL $CaCl_2$), for 1 hour at 4°C. After incubation, cells were washed three times with binding buffer and fixed with 4% methanol-free formaldehyde (Polysciences Inc.). Cells were washed three times with binding buffer and permeabilized with .5% Triton X-100 (Thermo Scientific) and washed three more times.

Next, cells were blocked with blocking buffer for 30 minutes at room temperature and then incubated for 1 hour at room temperature with the following fluorescent secondary reagents: 1:500 dilution of anti-mouse IgG conjugated to Alexa 488 (Life Technologies) to stain cell-bound recombinant protein-Fc, 1:500 dilution of anti-GFP conjugated to Alexa 594 (Life Technologies) to visualize the ligand-CFP expressed by the cells, and a 1:10 dilution of HCS Cell Mask Blue (Life Technologies) to label the cells cytoplasm for automatic segmentation. All reagents were diluted in binding buffer. Finally, cells were washed three times with binding buffer and mounted in 70% glycerol for

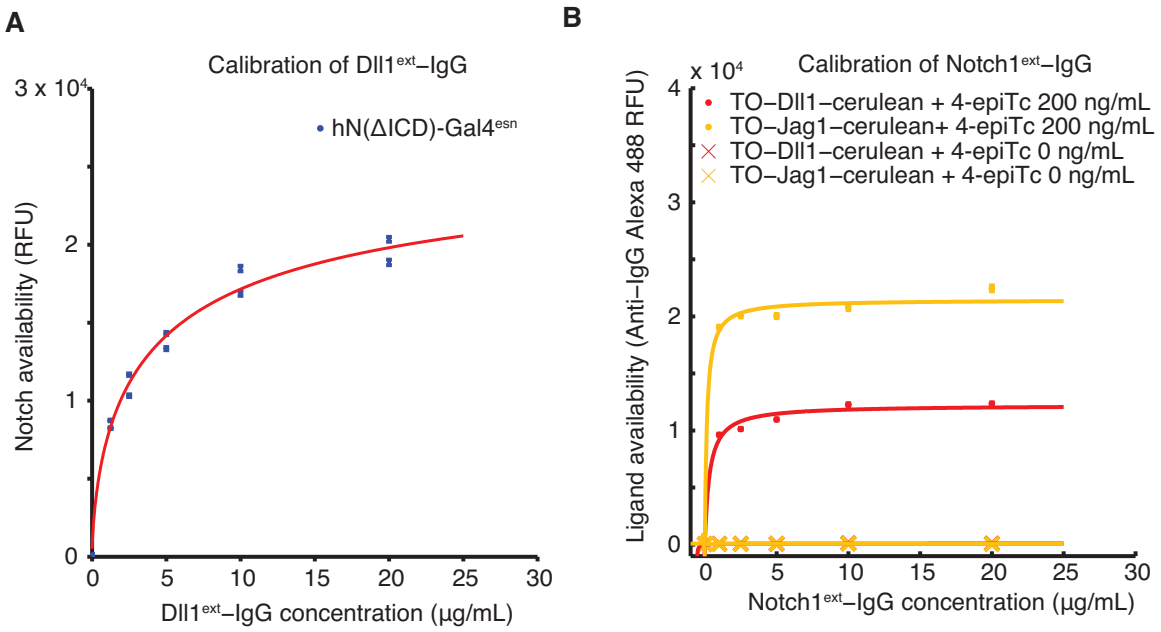

Figure 2.8: Calibration of availability assay reagents. (A) Pure receiver cell line expressing hN(ΔICD)-Gal4^{esn} was incubated with increasing concentrations of Dll1^{ext}-Fc followed by fluorescent anti-Fc reagents. Blue points are the results of two replicates. Data were fit (red line) to $N_{avail} = \frac{aD}{(D+K)}$, where D is the concentration of Dll1^{ext}-Fc, with $a = 2.1 \times 10^4 \pm .17 \times 10^4$, and $K = 2.27 \pm 0.6\mu$g/mL (red line). (B) Similarly, the working concentration of N1^{ext}-Fc was determined by incubating cells expressing fully induced TO-Jag1-cerulean (orange) and TO-Dll1-cerulean (red) with varying concentrations of N1^{ext}-Fc, and staining with secondary reagents. Data were fit (red and orange lines) to $L_{avail} = \frac{aL}{(L+K)}$. For the TO-Jag1-cerulean data, $a = 2.1 \times 10^4 \pm .14 \times 10^4$, and $K = .14 \pm 0.16\mu$g/mL (orange line). For the TO-Jag1-cerulean data, $a = 1.2 \times 10^4 \pm .11 \times 10^4$, and $K = .33 \pm 0.26\mu$g/mL (red line). Availability saturated at relatively low concentrations of the N1^{ext}-Fc ($<1\mu$g/mL), while un-induced cell lines showed no availability signal. Concentrations of secondary reagents were not limiting. The working concentration of both N1^{ext}-Fc and Dll1^{ext}-Fc reagents was set at a saturating level (10μg/mL) based on these measurements.

microscopy analysis.

Images were acquired with a CoolSnap HQ2 camera on a Nikon inverted TI-E microscope using a 20x long working distance objective. Metamorph 7.5 (Molecular Devices) controlled the microscope, camera, stage (ASI Instruments) and brightfield and epifluorescence shutters (Sutter Instruments) and collected the images. Fluorescent illumination was generated by the Sola LED light source (Lumencor) and filtered through the Chroma filter sets SpGold, SpRed, and SpGreen. Brightfield illumination was generated by a halogen bulb.

In experiments with gene silencing, siRNA against Notch1-ECD was delivered to cells using Lipofectamine 2000 reagent. Three dicer-substrate (dsiRNA from Integrated DNA Technologies) oligonucleotide duplexes against Notch1-ECD were pooled and 20 pmol of the mix were added to each well. IDT Universal Negative Control duplex was also transfected alongside each sample as a control. We used the following Notch1-ECD dsiRNA sequences:

NECD Antisense 1

5'–rCrArG rCrGrA rGrCrA rCrUrC rArUrC rCrArC rGrUrC rCrUrG rGrCrU–3'
5'–rCrCrA rGrGrA rCrGrU rGrGrA rUrGrA rGrUrG rCrUrC rGrCT G–3',

NECD Antisense 2

5'–rArCrA rCrCrA rGrUrG rCrArC rArArG rGrUrU rCrUrG rGrCrA rGrUrU-3'
5'–rCrUrG rCrCrA rGrArA rCrCrU rUrGrU rGrCrA rCrUrG rGrUG T-3',

NECD Antisense 3

5'–rUrUrG rArUrC rUrCrG rCrArG rUrUrG rGrGrU rCrCrU rGrUrG rGrUrC–3'm
5'–rCrCrA rCrArG rGrArC rCrCrA rArCrU rGrCrG rArGrA rUrCA A–3'.

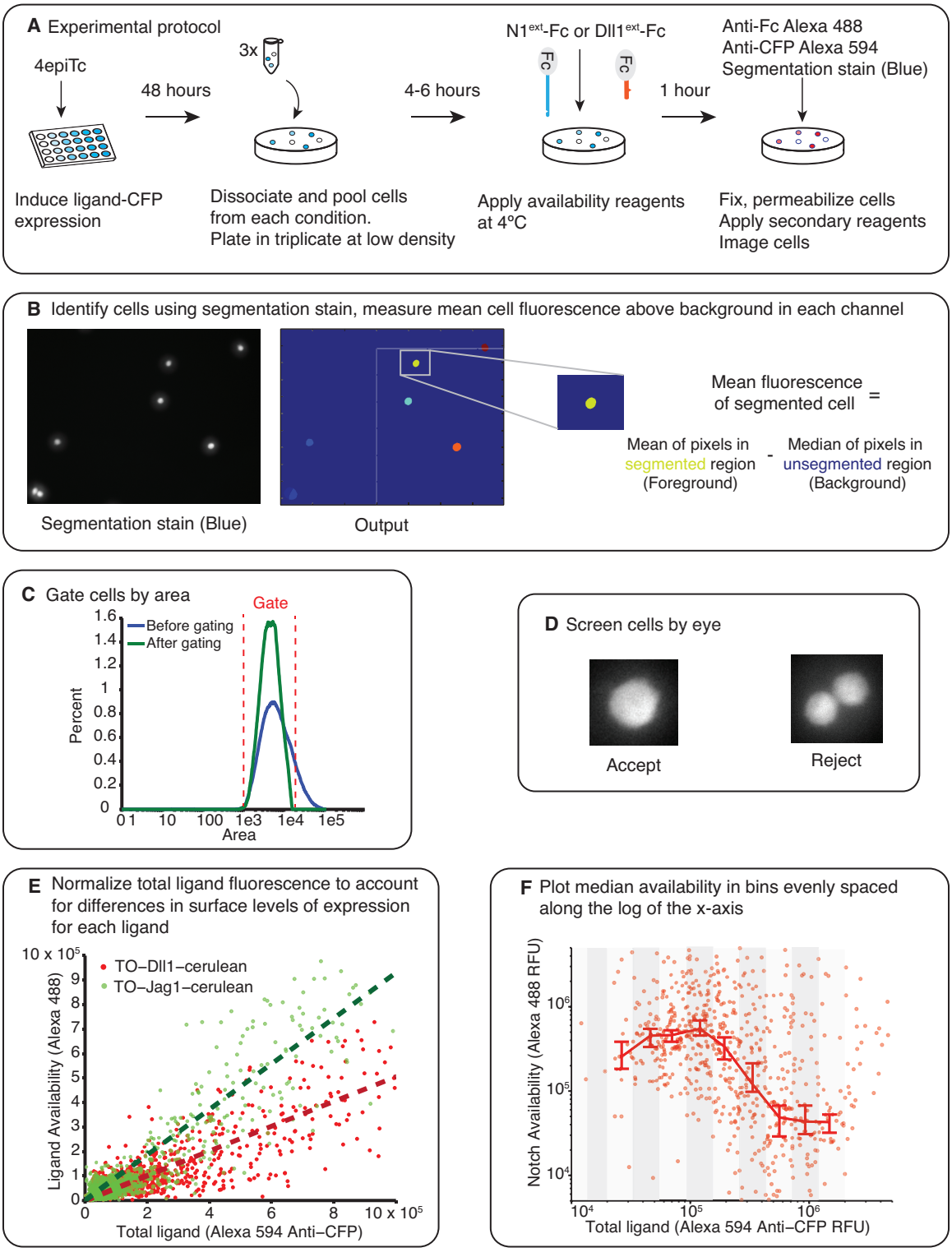
A Experimental protocol
4epiTc
48 hours
3x
4-6 hours
N1ext-Fc or Dll1ext-Fc
Fc
Fc
1 hour
Anti-Fc Alexa 488
Anti-CFP Alexa 594
Segmentation stain (Blue)
Induce ligand-CFP expression
Dissociate and pool cells from each condition.
Plate in triplicate at low density
Apply availability reagents at 4°C
Fix, permeabilize cells
Apply secondary reagents
Image cells
B Identify cells using segmentation stain, measure mean cell fluorescence above background in each channel
Mean fluorescence of segmented cell =
Mean of pixels in segmented region (Foreground)
-
Median of pixels in unsegmented region (Background)
Segmentation stain (Blue)
Output
C Gate cells by area
Gate
Before gating
After gating
Percent
Area
D Screen cells by eye
Accept
Reject
E Normalize total ligand fluorescence to account for differences in surface levels of expression for each ligand
TO–Dll1–cerulean
TO–Jag1–cerulean
Ligand Availability (Alexa 488)
Total ligand (Alexa 594 Anti–CFP)
F Plot median availability in bins evenly spaced along the log of the x-axis
Notch Availability (Alexa 488 RFU)
Total ligand (Alexa 594 Anti–CFP RFU)

Figure 2.9

Figure 2.9 *(previous page)*: Protocol and data analysis pipeline for availability assay. (A) Test cells were induced for 48 hours with varying concentrations of 4-epiTc. On the day of the experiment, the cells are dissociated with trypsin, split at low density and allowed to reattach to the cell culture plates. Cells are blocked with 2% FBS in PBS for 30 minutes at 37°C and then incubated with 10 μg/mL Dll1^{ext}-Fc (for receptor availability) or N1^{ext}-Fc (for ligand availability) for 1 hour at 4°C. Next, cells are washed, fixed, and permeabilized. To visualize the bound reagents, we incubated the cells with anti-Fc antibody conjugated to Alexa 488 dye. We also added anti-CFP conjugated to Alexa 594 to visualize the ligand expression. Finally, we added a blue cytoplasmic stain to identify individual cells. (B) After staining we imaged the cells on the microscope. The images are analyzed using a custom MATLAB script to identify the cells and take the mean of the total fluorescence within each cell for each fluorescence channel. At this stage we subtract a background fluorescence value from each cell, defined as the median of the background (unsegmented) pixels in the neighborhood of the cell. (C) Next, we impose a gate on the cell area to filter out doublets and segmentation errors. (D) Then, all cells are screened by eye so that only single, isolated cells are included in the final analysis. (E) Next, we normalize the total ligand (x-axis) to account for differences in the surface expression of each ligand. In the plot in F, the same CFP fluorescence level results in different surface availability measurements for a cell line expressing only Jag1 compared to a cell line expressing only Dll1, with Jag1 showing higher surface expression. To adjust for this difference in efficiency of surface expression between the different ligands, we fit the total ligand vs. ligand availability data from cells expressing ligand only with a linear fit. We use this fit to normalize the data for each ligand accordingly, allowing for comparison between different cell lines expressing different ligands. After this correction is applied, we refer to the total ligand as the"Effective total ligand." (F) The single cell data from each replicate is pooled and then divided into evenly spaced bins along the log of the x (total ligand)-axis and the median availability level for each bin is plotted. We use a Matlab bootstrapping method to find the 95% confidence intervals for the estimate of the median.

Images were analyzed in MATLAB 2012 (Mathworks). Analysis pipeline is outlined in Figure 2.9, B-F. First, cells were segmented by their labeling with the HCS Cell Mask Blue cytoplasmic stain using a routine based on the watershed algorithm (`SegContour3.m`, Figure 2.9B). Next, total fluorescence in each fluorescence channel for each cell was calculated as follows. First, the value of the background fluorescence was computed in the neighborhood of the cell by taking the median of the unsegmented pixels in the neighborhood of the cell. Next, this background value was subtracted from each pixel's fluorescence value in the cell. Finally, all of the background-subtracted pixels were averaged to give the mean fluorescence for that cell.

After this automatic processing, manual correction of the data was performed. This included imposing a gate on the segmented cell area to filter out multiple cells and segmentation errors (Figure 2.9C). Next, cells were screened by eye such that cells in physical contact with another cell were rejected, and only single, isolated cells were included in the analysis (Figure 2.9D).

We found that for the same measured ligand-CFP level, we obtained different levels of surface availability, suggesting the ligands may reach the cell surface with different efficiencies. To account for this difference, we normalized total ligand-CFP fluorescence in the Notch1+Dll1 and Notch1+Jag1 cell lines. Total ligand was plotted as "Effective total ligand" (Figure 2.9E).

We then plotted each cells effective total ligand and availability fluorescence, and grouped cells

into bins logarithmically spaced along the effective total ligand axis. We plotted the median of these bins, and used a bootstrapped estimate of the median (MATLAB function `bootci.m`) to find the 95% confidence intervals of the bin median (Figure 2.9F).

For analysis with flow cytometry, cells were dissociated with .25% trypsin (Life Technologies), diluted in FACS buffer (1X Hanks Balanced Salt Solution (Gibco) with 2.5 mg/mL BSA), and filtered through 40μm strainers (BD Falcon). The cell suspension was screened for single-cell forward and side scatter and fluorescence intensity on a MacsQuant VYB instrument (Miltenyi Biotech). Data was imported into MATLAB 2012 for analysis. Analysis included imposing a gate on the forward and side-scatter area to omit dead cells and doublets and then analyzing the single-cell fluorescence intensity for each channel.

2.5 Movie-based dilution assay to measure and compare ligand-receptor *cis*-interaction strengths

A complementary method to evaluate *cis*-interactions is a movie-based method first introduced in Section 1.5 [51] (Figure 2.10 and Appendix). The advantage of this method is that is allows us to directly assess the effect of *cis*-ligand on the receiving ability of our cells. This method complements the availability assay, allowing us to see how both receptor availability and receiving ability change with increasing *cis*-ligand expression.

We began with cells expressing Notch, a fluorescent reporter for Notch activity, and an inducible ligand. The cells also contained a fluorescent nuclear CFP construct, to allow identification and segmentation of cell nuclei. Before the movie, we induced the cells to express high levels of *cis*-ligand. Then, we seeded the induced cells on plates coated with Dll1$^{\text{ext}}$-Fc and the Notch signaling inhibitor, DAPT. Right before the movie, we washed out the DAPT and the inducer. When the movie started, the cells gradually dilute out their *cis*-ligand levels with each round of cell division. When *cis*-ligand levels became low enough, *cis*-inhibition was relieved, and the Notch was free to respond to the Dll1$^{\text{ext}}$-Fc adsorbed to the plate.

2.5.1 Detailed methods for dilution assay

Cells were seeded onto glass-bottom plates (MatTek) coated with 5μg/mL fibronectin (Innovative Research) and 1μg/mL Dll1$^{\text{ext}}$-Fc in low-fluorescence imaging media, Alpha-MEM, that includes 5% FBS and omits phenol red, riboflavin, folic acid, and vitamin B12 (Life Technologies, custom made). Cells were maintained at 37C and 5% CO2 in a chamber enclosing the microscope, an inverted Olympus IX81 equipped with Zero Drift Control (ZDC), a 20x NA 0.7 objective, and an iKon-M CCD camera (Andor). All devices were controlled by Metamorph software.

Movies were analyzed in MATLAB. Cell nuclei in each frame were identified automatically based on the CFP nuclear fluorescence, and the total fluorescence from each channel in each cell nucleus was recorded. Background subtraction was applied to each fluorescence value. We then plotted the median ligand fluorescence and reporter fluorescence. The time when more than 50% of the cells activated, t_{on}, was found by recording the frame where the median YFP reached 10% of its final slope. We chose this metric instead of a hard threshold as it allows for a more careful comparison between cell lines that achieve different final slopes in their response curves. For example, receiver cells expressing Lfng respond strongly to Dll1, and achieve a higher final slope than their counterparts without Lfng.

2.6 The bottom up approach provides a way to form and test hypotheses about complex Notch signaling schemes

The methods described here can be used to investigate the interactions for any Notch ligand-receptor pair. With the measurements of how individual ligand-receptor pairs interact, we can return to the model in Section 2.1 and add additional terms to study and make predictions about the behavior of cells with multiple components. The experimental methods can then allow us to test these predictions by adding components from our parts list to our cell lines. Are the pairwise interactions sufficient to specify Notch signaling behaviors, or do higher-level interactions occur among multiple components? This bottom up approach allows us to address this key question, and in doing so to build up a more predictive understanding of Notch signaling.

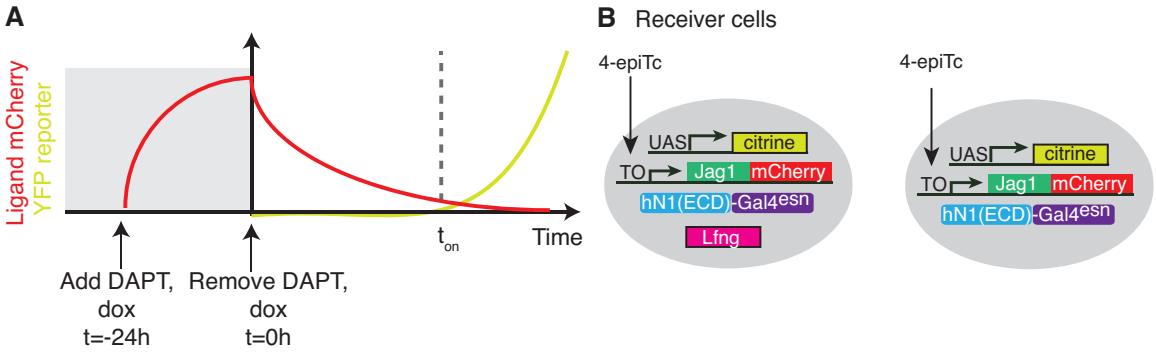

Figure 2.10: Movie protocol for evaluating *cis* interactions. (A) Schematic of the movie protocol. Before the movie, ligand expression is induced with doxycycline/4-epiTc and cells are seeded on plates coated with $Dll1^{ext}$-Fc in the presence of DAPT. At the start of the movie, DAPT and doxycycline are washed out. Ligand levels gradually dilute away with cell division. When *cis*-ligand levels are low enough, the cells can respond to the ligand on the plate, and the reporter activates, at time noted t_{on}. (B) Cell lines used in the dilution movies. Cells contain a diverted Notch1 receptor, a fluorescent reporter for Notch signaling, and an inducible *cis*-ligand construct. Constitutive Fringe was added to these parental cell lines to observe the effects of Fringe in the movie assay. Corresponding cell lines were made with Dll1 as the *cis*-ligand.

Construct name	Promoter	Gene	Mammalian selection	Role
pcDNA3-hN1(ΔICD)-$Gal4^{esn}$	pEF	hN(ΔICD)-$Gal4^{esn}$	Neomycin	Diverted Notch1 receptor in test cell lines
pcDNA3-hN1(ΔICD)-$Gal4^{esn}$	CMV	hN(ΔICD)-$Gal4^{esn}$	Neomycin	Diverted Notch1 receptor in movie cell lines
pcDNA-TO-Dll1-cerulean	CMV-TO	Dll1-cerulean	Hygromycin	Inducible Dll1 in test cell lines
pcDNA-TO-Jag1-cerulean	CMV-TO	Jag1-cerulean	Hygromycin	Inducible Jag1 in test cell lines
piggyBAC-CMV-Lfng	CMV	Lfng	Puromycin	Constitutive Lfng in test cell lines
piggyBAC-CMV-Mfng	CMV	Mfng	Puromycin	Constitutive Mfng in test cell lines
piggyBAC-CMV-Rfng	CMV	Rfng	Puromycin	Constitutive Rfng in test cell lines
pExchange-CMV-Lfng	CMV	Lfng	Puromycin	Constitutive Lfng in movie cell lines
pcDNA6-UAS-H2B03x-citrine	UAS	H2B-3x-citrine	Zeomycin	Fluorescent reporter for signaling from hN1(ΔICD)-$Gal4^{esn}$

Table 2.1: Table of plasmids used in this work.

Cell line name	Selection	Notes
CHO-K1 + TetR	Blasticidin 10μg/mL	Background staining control
CHO-K1 + TetR + pEF-hN(ΔICD)-Gal4^{esn}	Blasticidin 10μg/mL, Geneticin 600μg/mL	Background staining control, Notch expression $\Delta\Delta$CT $\approx$2.7 (to β-actin)
CHO-K1 + TetR + pEF-hN(ΔICD)-Gal4^{esn} + TO-Dll1-cerulean	Blasticidin 10μg/mL, Geneticin 600μg/mL, Hygromycin 500μg/mL	Notch + Dll1
CHO-K1 + TetR + pEF-hN(ΔICD)-Gal4^{esn} + TO-Jag1-cerulean	Blasticidin 10μg/mL, Geneticin 600μg/mL, Hygromycin 500μg/mL	Notch + Jag1
CHO-K1 + TetR + pEF-hN(ΔICD)-Gal4^{esn} + TO-Dll1-cerulean + piggyBac CMV-Lfng	Blasticidin 10μg/mL, Geneticin 600μg/mL, Hygromycin 500μg/mL, Puromycin 3μg/mL	Notch + Dll1 + Lfng, Lfng expression $\Delta\Delta$CT = 1.89 (to β-actin)
CHO-K1 + TetR + pEF-hN(ΔICD)-Gal4^{esn} + TO-Dll1-cerulean + piggyBac CMV-Mfng	Blasticidin 10μg/mL, Geneticin 600μg/mL, Hygromycin 500μg/mL, Puromycin 3μg/mL	Notch + Dll1 + Mfng, Mfng expression $\Delta\Delta$CT = 1.96 (to β-actin)
CHO-K1 + TetR + pEF-hN(ΔICD)-Gal4^{esn} + TO-Dll1-cerulean + piggyBac CMV-Rfng	Blasticidin 10μg/mL, Geneticin 600μg/mL, Hygromycin 500μg/mL, Puromycin 3μg/mL	Notch + Dll1 + Rfng, Rfng expression $\Delta\Delta$CT = 3.865 (to β-actin)
CHO-K1 + TetR + pEF-hN(ΔICD)-Gal4^{esn} + TO-Jag1-cerulean + piggyBac CMV-Lfng	Blasticidin 10μg/mL, Geneticin 600μg/mL, Hygromycin 500μg/mL, Puromycin 3μg/mL	Notch + Jag1 + Lfng, Lfng expression $\Delta\Delta$CT = 2.13 (to β-actin)
CHO-K1 + TetR + pEF-hN(ΔICD)-Gal4^{esn} + TO-Jag1-cerulean + piggyBac CMV-Mfng	Blasticidin 10μg/mL, Geneticin 600μg/mL, Hygromycin 500μg/mL, Puromycin 3μg/mL	Notch + Jag1 + Mfng, Mfng expression $\Delta\Delta$CT = 1.72 (to β-actin)
CHO-K1 + TetR + pEF-hN(ΔICD)-Gal4^{esn} + TO-Jag1-cerulean + piggyBac CMV-Rfng	Blasticidin 10μg/mL, Geneticin 600μg/mL, Hygromycin 500μg/mL, Puromycin 3μg/mL	Notch + Jag1 + Rfng, Rfng expression $\Delta\Delta$CT = .525 (to β-actin)
CHO-K1 + TetR + pEF-hN(ΔICD)-Gal4^{esn} + TO-Jag1-mCherry + UAS-H2B-citrine	Blasticidin 10μg/mL, Geneticin 600μg/mL, Hygromycin 500μg/mL, Zeocin 400μg/mL,	Notch1 + Jag1 reporter cell line, Lfng expression $\Delta\Delta$CT $\approx$ 2 (to β-actin)
CHO-K1 + TetR + pEF-hN(ΔICD)-Gal4^{esn} + TO-Jag1-mCherry + UAS-H2B-citrine + pExchange-Lfng	Blasticidin 10μg/mL, Geneticin 600μg/mL, Hygromycin 500μg/mL, Zeocin 400μg/mL ,Puromycin 3μg/mL	Notch1 + Jag1 + Lfng reporter cell line, Lfng expression $\Delta\Delta$CT $\approx$ 2 (to β-actin)
CHO-K1 + TetR + pEF-hN(ΔICD)-Gal4^{esn} + TO-Dll1-mCherry + UAS-H2B-citrine	Blasticidin 10μg/mL, Geneticin 600μg/mL, Hygromycin 500μg/mL, Zeocin 400μg/mL,	Notch1 + Dll1 reporter cell line, Lfng expression $\Delta\Delta$CT $\approx$ 2 (to β-actin)
CHO-K1 + TetR + pEF-hN(ΔICD)-Gal4^{esn} + TO-Dll1-mCherry + UAS-H2B-citrine + pExchange-Lfng	Blasticidin 10μg/mL, Geneticin 600μg/mL, Hygromycin 500μg/mL, Zeocin 400μg/mL ,Puromycin 3μg/mL	Notch1 + Dll1 + Lfng reporter cell line, Lfng expression $\Delta\Delta$CT $\approx$ 2 (to β-actin)

Table 2.2: Table of cell lines constructed for this work.

Chapter 3

Quantitative measurements of Notch-ligand *trans* and *cis* interactions

In this chapter, we use the methods from Chapter 2 to study and compare the interactions between different Notch ligand-receptor pairs. With four Notch receptors and five DSL ligands, there are 20 possible ligand-receptor pairs (Figure 1.4). We initially focused on Notch1-Dll1 and Notch1-Jag1. These pairs have been relatively well-characterized *in vitro*, and previous studies have show qualitatively different effects of Lfng and Mfng on the *trans*-activation for these pairs, allowing us to explore a range of possible signaling states [26, 57].

First, we compared the *trans*-activation capabilities of Dll1 and Jag1 and found that Dll1 is a stronger activator. Second, we examined the *cis* interactions for both pairs. We show that Dll1 is a also a stronger *cis*-inhibitor of Notch1 than Jag1, suggesting that *cis* and *trans* interaction strengths may be correlated. We offer direct evidence of mutual *cis*-inhibition by showing that Notch1 expression reduces both Dll1 and Jag1 ligand availability.

Finally, we examined if Fringe proteins affected *cis* interactions. We found that in addition to modulating the *trans*interactions between each ligand-receptor pair, expression of Fringe proteins also modulates their *cis*interactions. Interestingly, Fringe affects *cis* and *trans* interactions in the same direction: Lfng and Mfng strengthen Notch1-Dll1 interactions, in *trans* and in *cis*, and weaken Notch1-Jag1 interactions, in *trans* and in *cis*, while Rfng strengthens the interactions between both pairs. We will discuss the implications of these results in Chapter 4.

3.1 Dll1 *trans*-activates Notch1 more strongly than Jag1

We compared the abilities of Dll1 and Jag1 to *trans*-activate Notch1 using the two methods from Chapter 2. First, we plated receiver cells on plates coated with increasing concentrations of $Dll1^{ext}$-Fc or $Jag1^{ext}$-Fc (0-20μg/mL, serial dilutions). For both ligands, we observed the characteristic

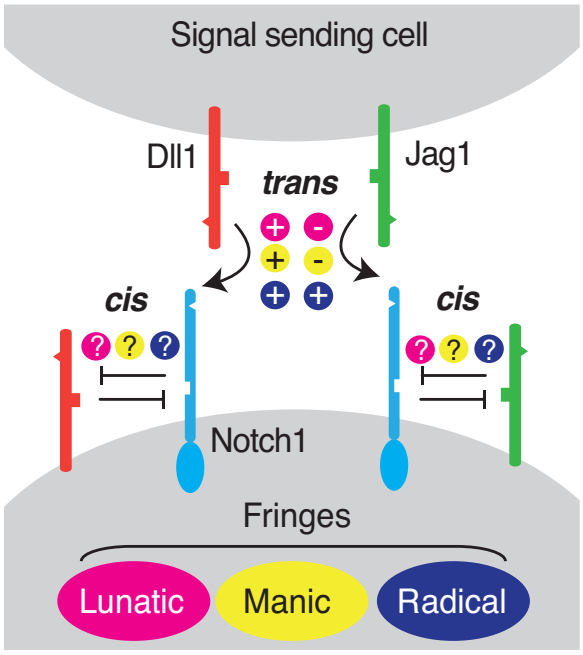

Figure 3.1: Known and unknown interactions between Notch1, Dll1, and Jag1. There are multiple potential ways in which Notch1 could interact in *cis* and *trans* with Jag1 and Dll1 ligands, and in which Fringe proteins could modulate these interactions. Known interactions are indicated by + and − for positive and negative regulation, respectively. Unknown ways in which Fringe proteins could modulate these interactions are indicated by question marks.

graded activation profile in response to increasing ligand levels [51]. We found that while both Dll1 and Jag1 ligands could activate our receiver cells, Dll1 activated much more strongly, with approximately four times more Jag1^{ext}-Fc than Dll1^{ext}-Fc needed to reach the same level of Notch activity (Figure 3.2A).

Next, we used the cell-based ligand presentation method from Section 2.3 to see if we obtained similar results. We co-cultured Dll1 and Jag1 sender cells with Notch1 receiver cells and measured the reporter fluorescence in the receivers. From this experiment, we observed that Dll1 and Jag1 sender cells also could activate our receiver cells in a graded fashion, and we confirmed our finding that Dll1 elicits more Notch activity than Jag1 (Figure 3.2B). Further, we found that when we compared the ligand availability at each 4-epiTc level for the two sender cell lines, four times more cell-based Jag1 compared to cell-based Dll1 was needed to elicit the same level of Notch activity, consistent with the results of the plate-bound ligand assay.

Together, these data suggest that Dll1 is a stronger *trans*-activator of Notch1 than Jag1. Approximately four times more Jag1 than Dll1 is needed to achieve the same level of Notch activity.

3.2 Dll1 *cis*-inhibits Notch1 more strongly than Jag1

Using the receptor and ligand availability assays, we compared the abilities of Dll1 and Jag1 to *cis*-inhibit the Notch1 receptor. We measured the levels of available receptors and ligands on the cell lines expressing Notch1 and Dll1 (denoted Notch1+Dll1) and Notch1 and Jag1 (denoted Notch1+Jag1). We induced ligand expression in the Notch1+Dll1 and Notch1+Jag1 cell lines with varying concentrations of 4-epiTc. After 48 hours of induction, we measured the available Notch1 receptor and available ligand on the cell surface as a function of ligand-Cerulean expression.

We observed that both Dll1 and Jag1 can fully *cis*-inhibit Notch1 receptors when the ligands are expressed at high levels (Figure 3.3A,B). Available Notch1 levels decreased in a dose-dependent fashion with increasing expression of either Dll1 or Jag1. At maximal induction levels, both cell lines showed no available Notch1, with the levels of Notch1 availability fluorescence overlapping with the distribution of background fluorescence from the CHO-K1 cell line (Figure 3.3A,B). To confirm that this reduction in Notch availability was not an artifact of ligand overexpression, we transiently transfected a mutated version of Dll1 into a cell line expressing Notch1. This mutated Dll1 contains a point mutation converting a phenylalanine residue in the DSL domain to alanine (F199A), and has been shown to be have a reduced capability to both i*trans*-activated and *cis*-inhibit Notch receptors [7]. The Dll1-F199A ligand could not reduce Notch availability to background levels (Figure 3.3C). Together, these results suggest that both Dll1 and Jag1 ligands can reduce Notch availability.

We also observed that Dll1 appeared to be somewhat more potent than Jag1 as a *cis*-inhibitor of Notch1. Approximately twice as much available Jag1 on the cell surface was needed to reduce Notch availability by 50% compared to Dll1 (Figure 3.3D). Dll1 appears to also be more potent than Jag1 as an activator of Notch1 in *trans* (Figure 2.8), raising the possibility that *cis* and *trans* interaction strengths between a receptor and ligand could be related. Structural evidence suggests that *cis* and *trans* interaction do involve common surfaces on the receptor and ligand [7] and this work suggests that this could translate into correlated affinities for both types of interaction.

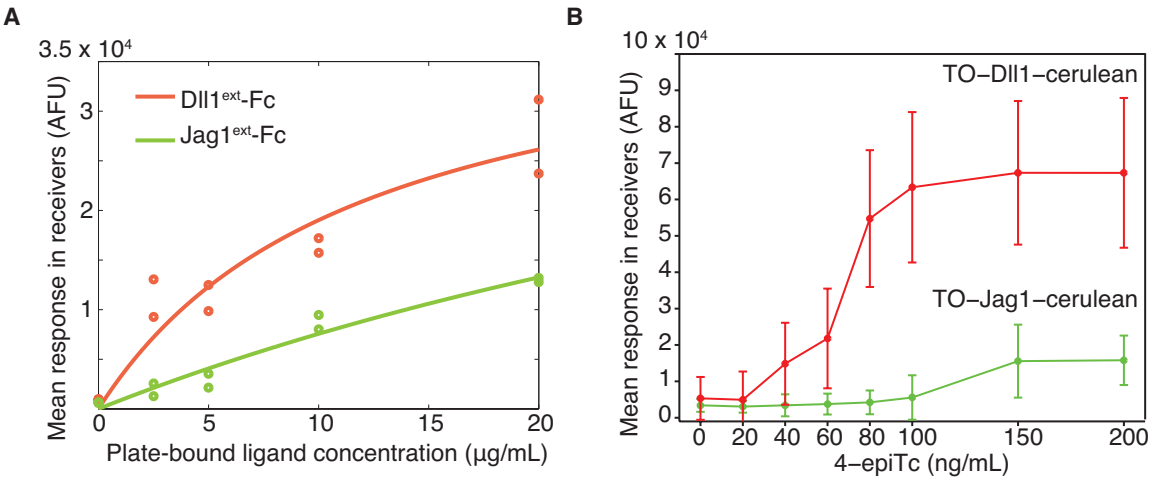

Figure 3.2: Dll1 is a stronger *trans*-activator of Notch1 than Jag1. (A) Receiver cells were plated on increasing concentrations of Dll1^{ext}-Fc (red points) or Jag1^{ext}-Fc (green points) and the fluorescence from the Notch activity reporter was measured on the flow cytometer. Points show the mean fluorescence of two replicates. Lines are a fit of the model from 2.1. Four times more Jag1 is needed to reach the same Notch activity as Dll1 (compare Jag1 at 20 μg/mL and Dll1 at 5μg/mL. (B) Results of a co-culture of receiver cells with either TO-Dll1-cerulean (red points) or TO-Jag1-cerulean (green points) senders. Points are the mean fluorescence from the Notch activity reporter in the the top ten percent responders of the receiver cells. Error bars are the standard deviation. Cells were analyzed on the flow cytometer. When ligand availability was measured at each 4-epiTc level, again the results of the co-culture suggest that four times more Jag1 ligand is needed to achieve the same level of Notch activity as Dll1.

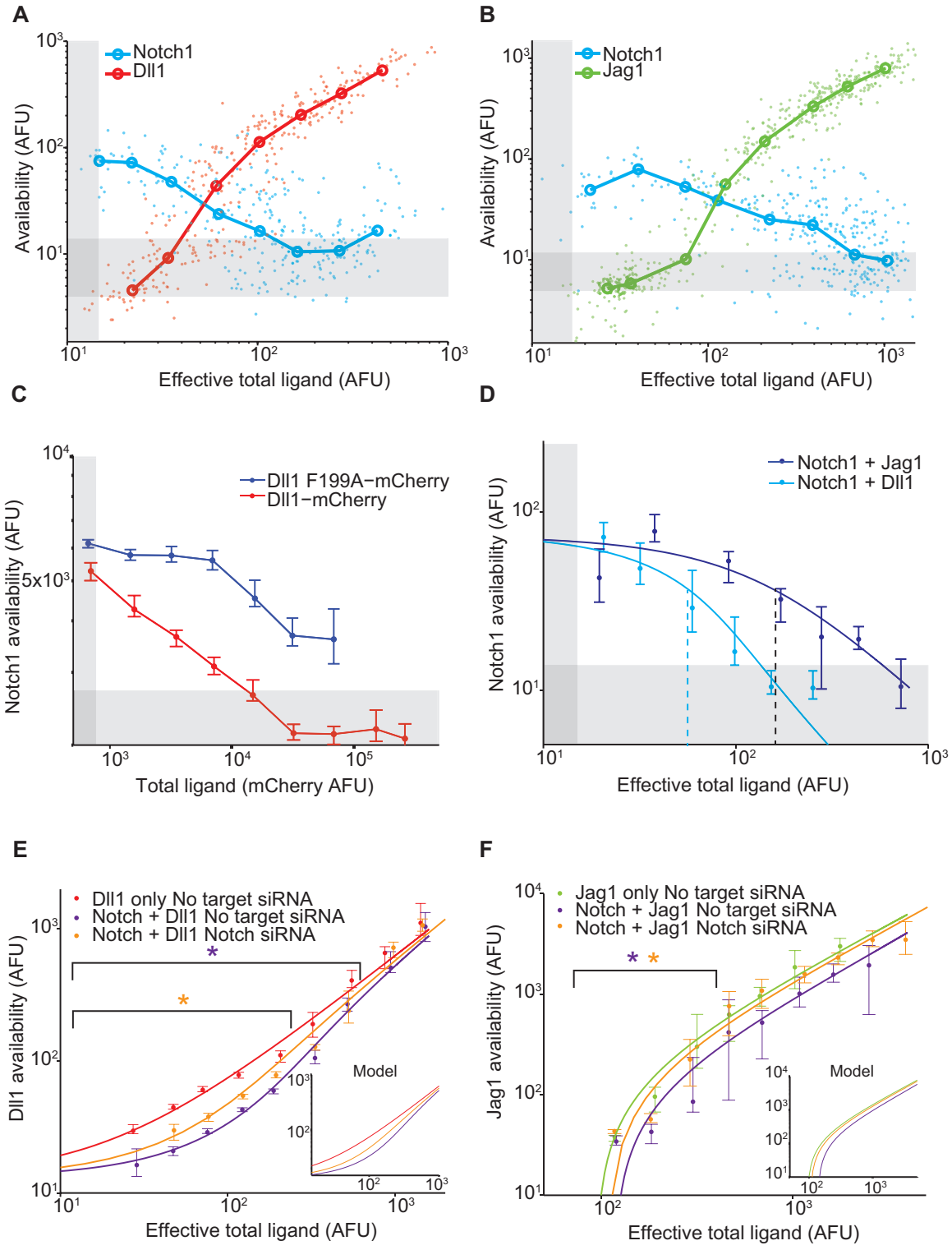
A
Notch1
Dll1
Availability (AFU)
Effective total ligand (AFU)
B
Notch1
Jag1
Availability (AFU)
Effective total ligand (AFU)
C
Dll1 F199A−mCherry
Dll1−mCherry
Notch1 availability (AFU)
5x10³
Total ligand (mCherry AFU)
D
Notch1 + Jag1
Notch1 + Dll1
Notch1 availability (AFU)
Effective total ligand (AFU)
E
Dll1 only No target siRNA
Notch + Dll1 No target siRNA
Notch + Dll1 Notch siRNA
Dll1 availability (AFU)
Model
Effective total ligand (AFU)
F
Jag1 only No target siRNA
Notch + Jag1 No target siRNA
Notch + Jag1 Notch siRNA
Jag1 availability (AFU)
Model
Effective total ligand (AFU)

Figure 3.3

Figure 3.3 *(previous page)*: Dll1 is a stronger *cis*-inhibitor of Notch1 than Jag1. (A-B) Single cell data show decreasing receptor availability and increasing ligand availability as total ligand expression increases. Circles denote the medians of data points in logarithmically spaced bins along the x-axis. Effective total ligand refers to the ligand availability observed at a given ligand-CFP fluorescence value in a cell line expressing only ligand. For receptor availability data in A, n = 299 and in B, n = 352. For the ligand availability data in A, n = 323 and in B, n = 530. Gray bars in all panels represent background levels, defined as the 25-75 percentile range of fluorescence from parental CHO-K1 cells that do not express Notch1 or ligand-Cerulean constructs. (C) Transient expression of wild-type Dll1-mCherry (n = 8817), but not the Dll1-mCherry F199A mutant (n = 14292), reduced Notch availability to background levels in a Notch1 cell line. Cells were analyzed by flow cytometry. Error bars in all panels denote 95% confidence interval for the bootstrapped estimate of the median. (D) Comparison of Notch availability in the Notch1+Dll1 and Notch1+Jag1 cell lines. Lines are fits to a model of receptor-ligand cis-interactions (Supplementary). (E) Comparison of ligand availability in cell lines expressing Dll1. Ligand availability a cell line expressing Dll1 only (n = 1146). Notch1 reduces ligand availability (purple, n = 1131), and this effect is rescued by siRNA against Notch1 (orange, n = 972). In the purple starred region, cells differ significantly in ligand availability between Notch1 or no target siRNA samples, while the orange star denotes regions where Dll1 and Notch1+Dll1 cells transfected with no target siRNA differ significantly. Significance was determined by applying the Wilcoxon rank sum test. Inset shows the model behavior for parameters derived from the fit in D. Knockdown of Notch was measured to be 50%. (F) Comparisons of ligand availability in a cell line expressing Jag1 only (green, n = 733), Notch1+Jag1 (orange, n = 532), and Notch1+Jag1 with siRNA against Notch (purple, n = 1163). Starred regions indicate significance as in E. Inset shows model behavior using parameters measured in D. Knockdown of Notch was measured to be 70%.

3.3 Ligand availability assay reveals mutual *cis*-inhibition between ligands and receptors

Next, we observed that the Notch1 receptor reduces both Dll1 and Jag1 availability, supporting the mutual inhibition model of *cis* interactions [51]. We compared the ligand availability in cell lines expressing only inducible ligand constructs to that of cell lines that also expressed Notch1. As expected, increasing ligand expression led to a corresponding increase in ligand availability. However, in the Notch+Jag1 and Notch+Dll1 cell lines, we observed significantly reduced ligand availability compared to their ligand-only counterparts at the same levels of total ligand expression. In these cell lines, we could restore ligand availability by knocking down expression of Notch1 with siRNA (Figure 3.3D,E). Because ligand availability correlates with sending ability (Figure 2.8), these results support a role for Notch1 decreasing Dll1 and Jag1 sending ability in *cis*, consistent with the mutual inhibition model of *cis* interactions.

3.4 Mammalian Fringes modulate Notch1+Dll1 and Notch+Jag1 *cis* interactions differently

To determine whether and how Fringe enzymes modulate *cis* interactions, we introduced each of the three Fringe genes into the Notch+ligand-Cerulean cell lines. We transfected plasmids encoding Lfng, Mfng, or Rfng under control of a constitutive promoter and selected stable populations, confirming Fringe expression with qPCR. As expected, these constructs increased the *trans* response to plate-bound Dll1 and decreased the response to Jag1, consistent with previous results [57].

To analyze the effect of Fringe enzymes on *cis* interactions, we repeated the availability assay in these cell lines and the corresponding parental cell lines that lacked ectopic Fringe expression.

For the Notch1+Dll1 cell lines expressing Lfng, Mfng, or Rfng, Notch1 availability decreased to background levels in response to Dll1 expression. Moreover, Fringe expression significantly reduced Dll1 availability compared to the parental cell lines without Fringe (Figure 3.4B). Together, these results suggest that all Fringe enzymes preserve, and may even strengthen, the Notch1-Dll1 *cis* interactions (Figure 3.4B). Note that absolute levels of availability fluorescence increased with Fringe expression, as can be observed at low total ligand levels in Figure 3.4A inset, because Fringes enhance binding of the $Dll1^{ext}$-Fc detection reagent to available Notch1. To account for this change in binding, we normalized the curves to the level of Notch availability measured when ligand levels were uninduced. After normalizing for this change, cell lines with Fringe expression appear to have stronger *cis* interactions (Figure 3.4A). Consistent with this, available Dll1 ligand assays revealed reduced available Dll1 when any of the Fringes was expressed (Figure 3.4B). Together, these results suggest that all three Fringe enzymes preserve, or strengthen, Notch1-Dll1 *cis* interactions.

The effects of Fringe enzymes on Notch1-Jag1 *cis* interactions were markedly different. In cell lines expressing Lfng or Mfng, Jag1 was not sufficient to reduce Notch availability to background levels even at very high expression levels (Figure 3.4C). In contrast, when Rfng was expressed, reduction of Notch availability was depleted to background levels with increasing *cis*-Jag1 expression. Thus, Lfng and Mfng, but not Rfng, appear to reduce *cis* interactions between Notch1 and Jag1. In the ligand availability assay, we did not detect a significant increase in Jag1 availability due to Lfng or Mfng expression (Figure 3.4D). Because the basal Jag1-Notch1 *cis*-inhibition strength is already weak compared to the Dll1-Notch1 *cis* interaction strength (Figure 3.3F), the Jag1 availability assay may not be sensitive enough to detect further reductions in *cis*-inhibition. Note that here, as in Figure 3.4A, we observed an increased binding of the $Dll1^{ext}$-Fc detection reagent in cell lines expressing Fringe proteins. However, when Lfng or Mfng is expressed, only Dll1, and not Jag1, is able to reduce Notch availability to background levels.

Together, these results suggest that Fringe expression modulates *cis*-inhibition between Notch1 receptor and ligands. Lfng and Mfng preserve and possibly strengthen interactions between Notch1

and Dll1, in *cis* and in *trans*, and weaken interactions between Notch1 and Jag1, in *cis* and in *trans*, while Rfng preserves or enhances the cis interactions with both ligands. Thus, the effects of Fringe proteins on *cis* interactions are in the same direction (strengthening or weakening) as their effects on *trans* interactions.

3.5 Lfng enables cells to receive from Dll1 ligands at high *cis*-Jag1 levels

Because Lfng or Mfng expression weakens Notch1-Jag1 *cis* interactions, a Lfng-expressing cell could maintain high expression levels of *cis*-Jag1 without compromising its ability to receive signals from *trans*-Dll1 ligands through Notch1. To test this prediction, we used the movie assay (2.5) to titrate ligand levels over time in individual cells.

We constructed cell lines constitutively expressing the diverted Notch1 receptor and activity reporter, along with the tetracycline-inducible Jag1-mCherry ligand (Components from Figure 1.4). Finally, to analyze the effect of Lfng on Notch1-Jag1 *cis*-inhibition, we added to this parental cell line a stably-integrated, constitutively-expressed Lfng gene. We also constructed similar cell lines with Dll1-mCherry in place of Jag1-mCherry.

In the parental cell lines without Lfng, Notch reporter activation was delayed until Jag1-mCherry levels diluted away, becoming active after 24h, indicative of *cis*-inhibition (Figure 3.5B). By contrast, the cell line with Lfng responded earlier to the plate-bound Dll1^{ext}-Fc despite high *cis*-Jag1 levels, and not significantly later than in cells lacking ligand expression altogether, indicating that Lfng reduces Notch1-Jag1 *cis* interactions. Thus, Lfng prevents high *cis*-Jag1 levels from blocking Notch activation (Figure 3.5B,C).

In contrast, when we performed the same experiment with cell lines expressing Dll1-mCherry, we observed no corresponding relief of *cis*-inhibition due to Lfng, suggesting that Lfng does not weaken Dll1-Notch1 *cis* interactions. These results, consistent with those from the availability assay, support the finding that Lfng inhibits Jag1-Notch1, but not Dll1-Notch1, *cis*-inhibition.

3.6 Summary of key findings

In summary, we compared the abilities of Dll1 and Jag1 to interact with Notch1 in *trans* and in *cis*. We found that the Notch1-Dll1 interaction was stronger than the Notch1-Jag1 in both cases. We also directly demonstrated that the *cis* interaction is mutually inhibitory by showing a decrease in ligand availability contingent on receptor expression. Finally, we showed that Fringe protein expression can modulate the *cis* interaction, and that they do so similarly to how they affect *trans* interactions. Lfng and Mfng strength the interactions between Notch1 and Dll1 while blocking the

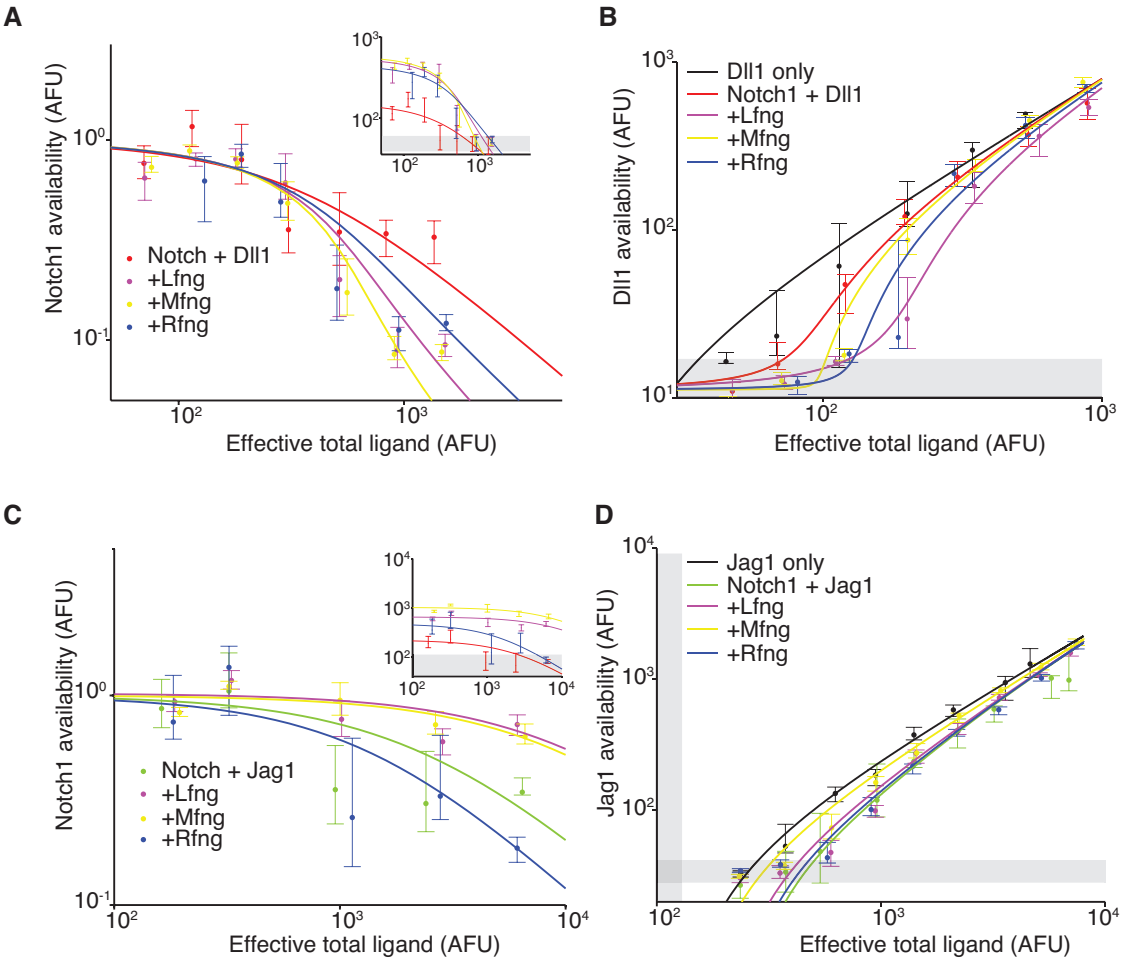

Figure 3.4: Mammalian Fringe proteins modulate *cis* interactions. (A) Available Notch1 levels for the Notch1+Dll1 cell line without Fringe (red) or with Lfng (magenta), Mfng (orange), or Rfng (blue). Lines are fits to model. Addition of any of the three Fringes accelerates the drop-off of Notch1 availability. In the inset, the same data, but unnormalized, shows that addition of any of the three Fringe proteins does not prevent available Notch1 from reaching background levels. (B) Dll1 availability for the cell lines from A. (C) Similar to A, but for the Notch1+Jag1 cell lines. Addition of Lfng and Mfng prevents the depletion of Notch1 availability, while addition of Rfng accelerates depletion of Notch1 availability. In the inset, the unnormalized data shows that Lfng or Mfng, but not Rfng, can block the ability of Jag1 to reduce Notch1 availability to background levels. (D) Jag1 availability for the cell lines in C. In all panels, points represent medians of data points in evenly spaced bins taken along the log of the x-axis. Error bars are the 95% confidence intervals of the bootstrapped estimated of the bin medians. Solid lines are model fits to the single-cell data. Gray bars denote the 25-75th percentile fluorescence range of stained parental CHO-K1 cells that do not express Notch1 or ligands.

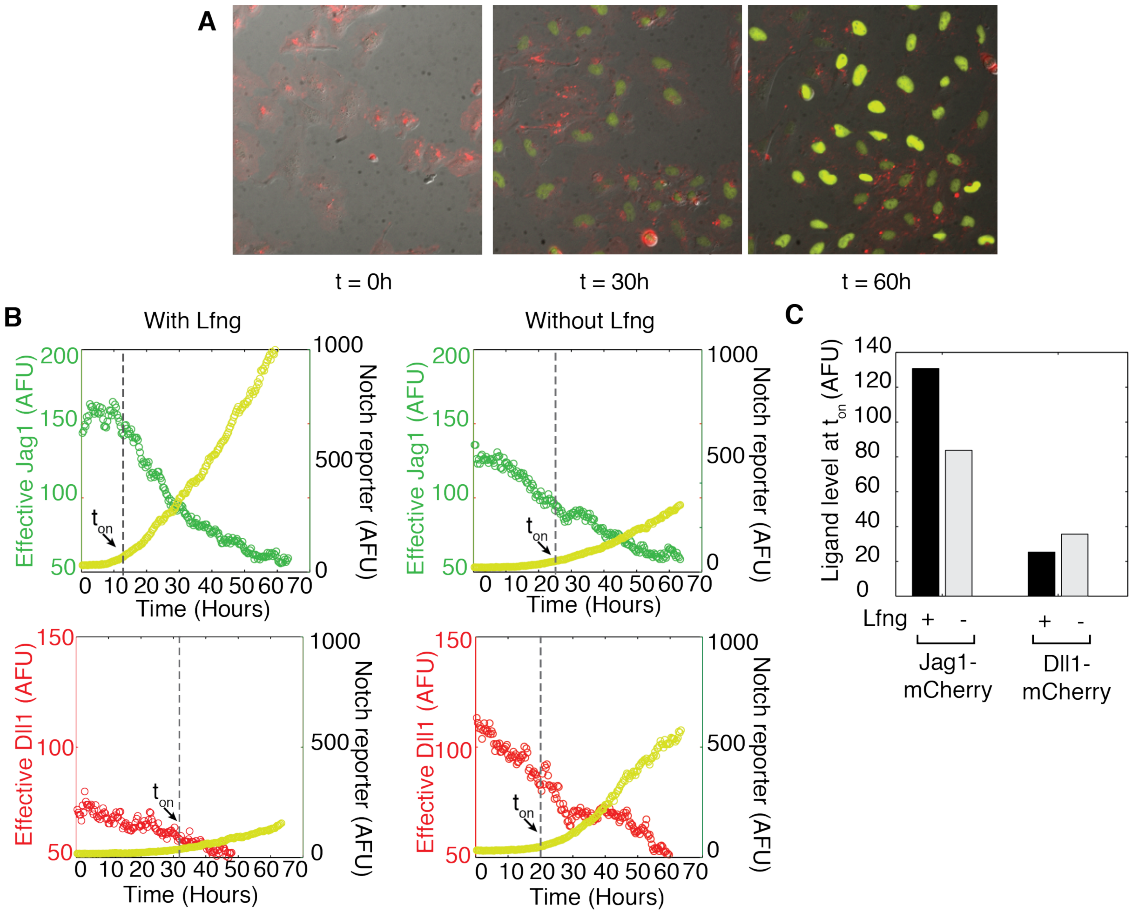

Figure 3.5: Lfng allows *trans*-signaling from Dll1 despite high *cis*-Jag1 levels. (A) Typical movie filmstrip. (B) Quantification of movies of the Notch1+Jag1 and Notch1+Dll1 cell lines, with and without Lfng. Points show the mean fluorescence of all cells in a single frame. The cell line with Lfng responds earlier than the cell line without Lfng, reflecting a weaker cis interaction between Jag1 and Notch1. The time when the YFP slope exceeds a threshold, defined as 10% of the final YFP slope, is marked as t_{on}. (C) Quantification of the ligand levels at ton for each cell line. Values are the average of two movies. Notch activity occurs even at high *cis*-Jag1 levels in the +Lfng, but not the Lfng, cell line. Notch responses occurred only at low ligand levels for the Dll1-mCherry cell lines, with and without Lfng.

interactions between Notch1 and Jag1. Rfng strengthens the ligand-receptor interactions for both pairs. Together, these data suggest that *cis* and *trans* interaction strengths are related and are modulated by Fringe modification similarly. In the next chapter, we explore what signaling states are enabled by our findings.

Chapter 4

Implications for developmental processes

In the previous chapter, we measured the interactions between different Notch receptor-ligand pairs and found distinct effects of Fringe expression on these interactions. In this chapter, we discuss the consequences of these findings for Notch-dependent developmental processes.

First, we show that the ability of Fringe proteins to modulate *cis* interactions can also be observed in the *in vivo* context of fly wing development. Next, we return to the concept of signaling states from Chapter 1 and show how our results constrain the set of possible signaling states. We show that a new signaling state enables a cell to send and receive signal simultaneously, and that this state may be used during a highly conserved Notch patterning circuit, Fringe-dependent boundary formation, first introduced in Chapter 1. Finally, we explore future directions for this work. We speculate on the landscape of signaling states that are as of yet unexplored, and what behaviors could be possible. Finally, we consider how this data and this approach could resolve outstanding puzzles related to Notch signaling.

4.1 Fringe differentially affects Delta-Notch and Delta-Serrate *cis*-inhibition phenotypes in *Drosophila* wing development

Our collaborators in the lab of Dr. Hamed Jafar-Nejad at Baylor are experts on the effects of glycosylation on Notch signaling and *Drosophila* genetics, and worked with us to develop experiments to test our cell-culture findings in fruit flies. To determine whether Fringe modulation of *cis* interactions occurs in a developmental context, we turned to the *Drosophila* wing imaginal disc as a model system. The Notch pathway in *Drosophila* has fewer components than in vertebrates, with just a single Notch receptor, two ligands, Delta and Serrate (related to vertebrate Jagged), and a

single Fringe (related to Lfng, Mfng, and Rfng). However, previous work has established both an effect of Fringe on *trans* interactions that is qualitatively similar to the mammalian Lfng and Mfng. *Drosophila* Fringe enhances Delta-Notch *trans*-activation and blocks Serrate (related to vertebrate Jagged ligands) *trans*-activation. Moreover, flies show a clear role for *cis*-inhibition of Notch by its ligands Delta and Serrate (related to mammalian Jag1) in wing disc development [10].

The adult *Drosophila* wing is patterned with five wing veins (Figure 4.1A). Along the edge of the wing is a smooth margin lined with bristles. Removing one copy of Notch results in thickening of the wing veins and the classic "notching" of the wing margin (Figure 1.1 and 4.1B and E). If Notch and its ligands were solely involved in *trans*-activation, one would expect these Notch haploinsufficient phenotypes would be enhanced by a simultaneous decrease in ligand expression. However, loss of one copy of Delta was reported to suppress the $Notch^{+/-}$ wing vein phenotype, indicating that the haploinsufficient phenotypes observed in $Notch^{+/-}$ animals are caused by *cis*-inhibition of Notch due to an increase in the relative levels of ligands to Notch [11].

Our results from Chapter 3 indicated that Lfng and Mfng preserve the *cis*-inhibition of Notch by Dll1 but weaken the *cis*-inhibition of Notch by Jag1. To examine whether *Drosophila* Fringe affects the ability of Delta and Serrate to *cis*-inhibit Notch in a manner similar to Lfng and Mfng, we performed genetic interaction studies in a $Notch^{+/-}$ background, which seems to be more sensitive to *cis*-inhibition by ligands.

First, we established that Delta and Serrate have distinct *cis*-inhibition phenotypes. To this end, we first generated transgenic flies harboring the Delta locus ($Dl^{gt\text{-}wt}$) or the Serrate locus ($Ser^{gt\text{-}wt}$), in which the expression of Delta or Serrate is driven by endogenous promoter/enhancers, and showed that these transgenes behave similarly to their endogenous counterparts in flies. Animals with one or two copies of the $Dl^{gt\text{-}wt}$ transgene in a wild-type background did not exhibit any wing defects. However, in $Notch^{+/-}$ animals, one additional copy of the $Dl^{gt\text{-}wt}$transgene (3x Delta dosage) resulted in a slight increase in the penetrance of mild wing margin defects adjacent to the L3 vein and a moderate enhancement of the wing vein thickening (Figure 4.1C). Two copies of $Dl^{gt\text{-}wt}$ (4x Delta dosage) strongly enhanced the wing vein thickening phenotype in $Notch^{+/-}$ animals (Figure 4.1D). These flies also showed a moderate enhancement of the wing margin loss phenotype (Figure 4.1D). These observations indicate that although Delta-Notch *cis*-inhibition affects both wing vein and wing margin formation, Notch is more sensitive to Delta *cis*-inhibition during wing vein formation.

The effects of increasing the gene dosage of Serrate on the Notch haploinsufficient phenotypes were quite different from those of increasing Delta dosage. Two copies of the $Ser^{gt\text{-}wt}$ transgene did not cause any wing abnormalities in a wild-type background. However, one copy of $Ser^{gt\text{-}wt}$ (3x Serrate dosage) significantly enhanced the wing margin loss phenotype of $Notch^{+/-}$ animals without affecting their wing vein phenotype (Figure 4.1F). A second copy of $Ser^{gt\text{-}wt}$ (4x Serrate dosage) further enhanced the wing margin loss (Figure 6F). Indeed, 43% of the $Notch^{+/-}$ $Ser^{gt\text{-}wt}$/ $Ser^{gt\text{-}wt}$

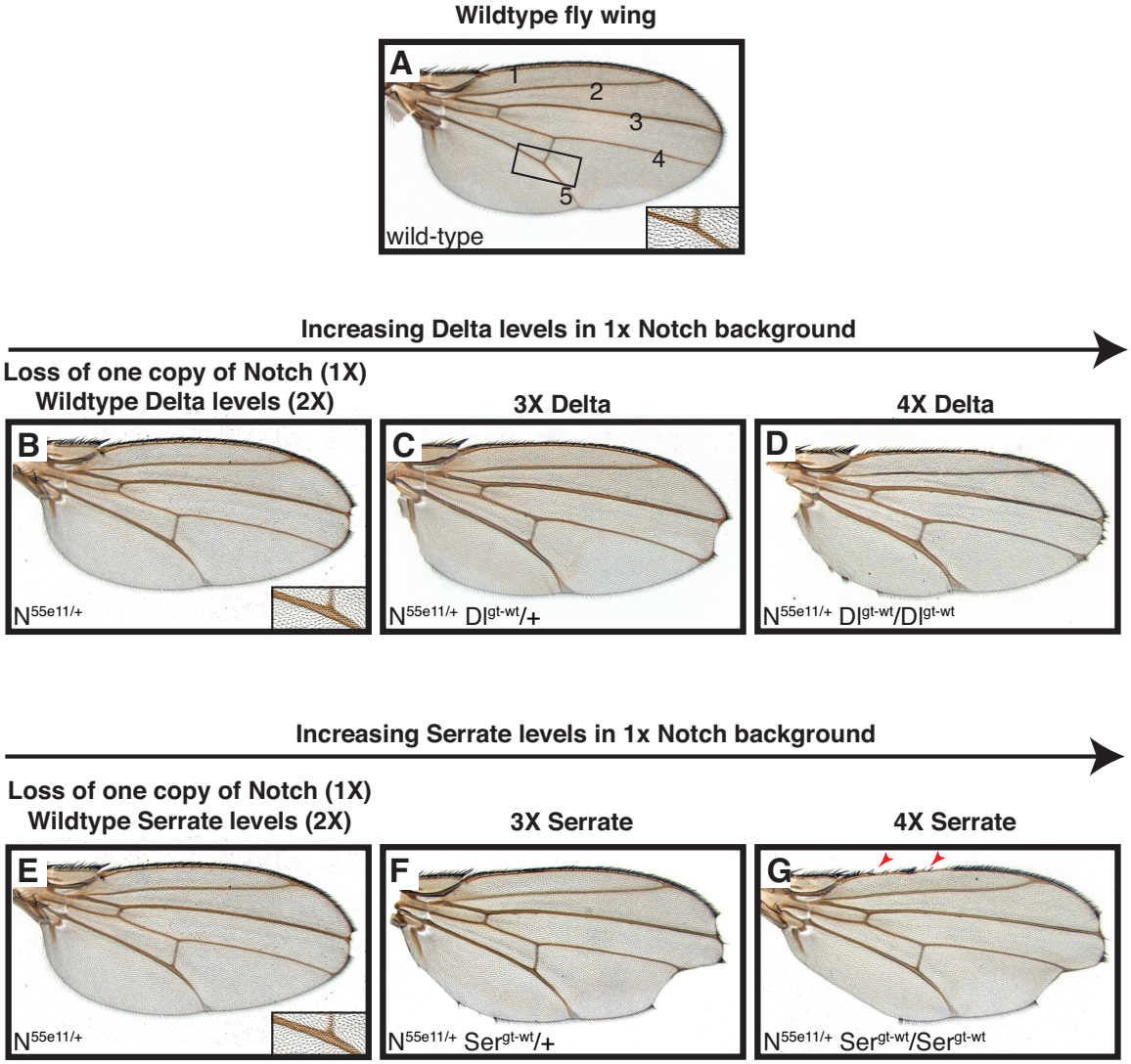

Figure 4.1: Delta and Serrate have distinct *cis*-inhibition phenotypes in the fly wing. (A) A wildtype fly wing, with each of the five wing veins numbered. (B) and (E) Fly wing with one copy of Notch removed (1X Notch). There is a slight wing margin loss in the L3 vein region. (B-D) The effects of increasing Delta dosage in a 1X Notch background. As the ratio of Delta to Notch expression increases, the vein thickening phenotype worsens, while the wing margin in the L3 vein region increases only slightly. (E-G) The effects of increasing Serrate dosage in a 1X Notch background are markedly different. As the ratio of Serrate to Notch expression increases, the wing margin defects grow more severe, extending to the L4 vein and to anterior regions of the wing (red arrows), while the vein width remains relatively normal.

wings showed severe wing margin loss extending to the L3 and L4 wing veins and also in anterior regions of the wing, which was not observed in any of the other genotypes analyzed (Figure 4.1F). Of note, despite their severe wing margin loss, Notch+/; $Ser^{gt\text{-}wt}/Ser^{gt\text{-}wt}$ animals only showed a mild enhancement of the wing vein thickening compared to $Notch^{+/-}$ flies (Figure 4.1G, compare to 4.1E). These observations indicate that although both Delta and Serrate can *cis*-inhibit Notch during wing development, Notch is more sensitive to *cis*-Delta during wing vein formation and more sensitive to *cis*-Serrate during wing margin formation.

Next, we tested whether and how altering Fringe activity changed these distinct Delta and Serrate *cis*-inhibition phenotypes. We used $fringe^{13}$ and $fringe^{L73}$ strains that harbor severe loss-of-function alleles with nonsense mutations in Fringe. Animals heterozygous for fringe have normal wings (ref). However, loss of one copy of Fringe alters the Notch haploinsufficient wing margin and wing vein phenotypes in opposite directions: it enhances the Serrate-dependent wing margin loss but suppresses the Delta-dependent wing vein thickening (Figure 4.2). Addition of one copy of Serrate, but not one copy of Dl, enhances the wing margin loss in $Notch^{+/-}$; $fng^{+/-}$ animals (Figure 4.2D, F). Indeed, even in $fng^{+/-}$ animals with wild-type Notch gene dosage, addition of a copy of Serrate results in a low penetrance mild wing margin loss (Figure 4.2F). Altogether, our observations strongly support the conclusion that during *Drosophila* wing development, Fringe increases the sensitivity of Notch to *cis*-Delta but decreases its sensitivity to *cis*-Serrate, similar to the effect of Lfng and Mfng in the mammalian context.

4.2 The repertoire of Notch signaling states with Notch and Dll1 or Jag1 ligands

Interactions between Notch ligands and receptors, both in *cis* and in *trans*, control the quantitative ability of cells to send or receive signals. Recent work with cells expressing one ligand and one receptor, Dll1 and Notch1, showed that strong and mutually inactivating *cis* interactions between Dll1 and Notch1 can force cells into mutually exclusive signaling states [51]. But does the exclusivity of sending and receiving states in this simple setting persist in more complex contexts that involve multiple ligands and modulation by Fringe proteins?

To answer this question, we must consider how *cis* and *trans* interactions, together with Fringe proteins, specify a particular set of signaling states, and how those states determine the directionality and specificity of signaling. With the data from Chapter 3, we can extrapolate to map the possible signaling states for cells expressing Notch1, Dll1 or Jag1 ligands, and one of the three mammalian Fringes. We consider signaling states for cells with extreme ratios of receptor to ligand and ligand to receptor, at either very low or very high Fringe levels. Signaling behaviors at intermediate receptor-to-ligand ratios and at lower Fringe levels may show different quantitative capacities to send or

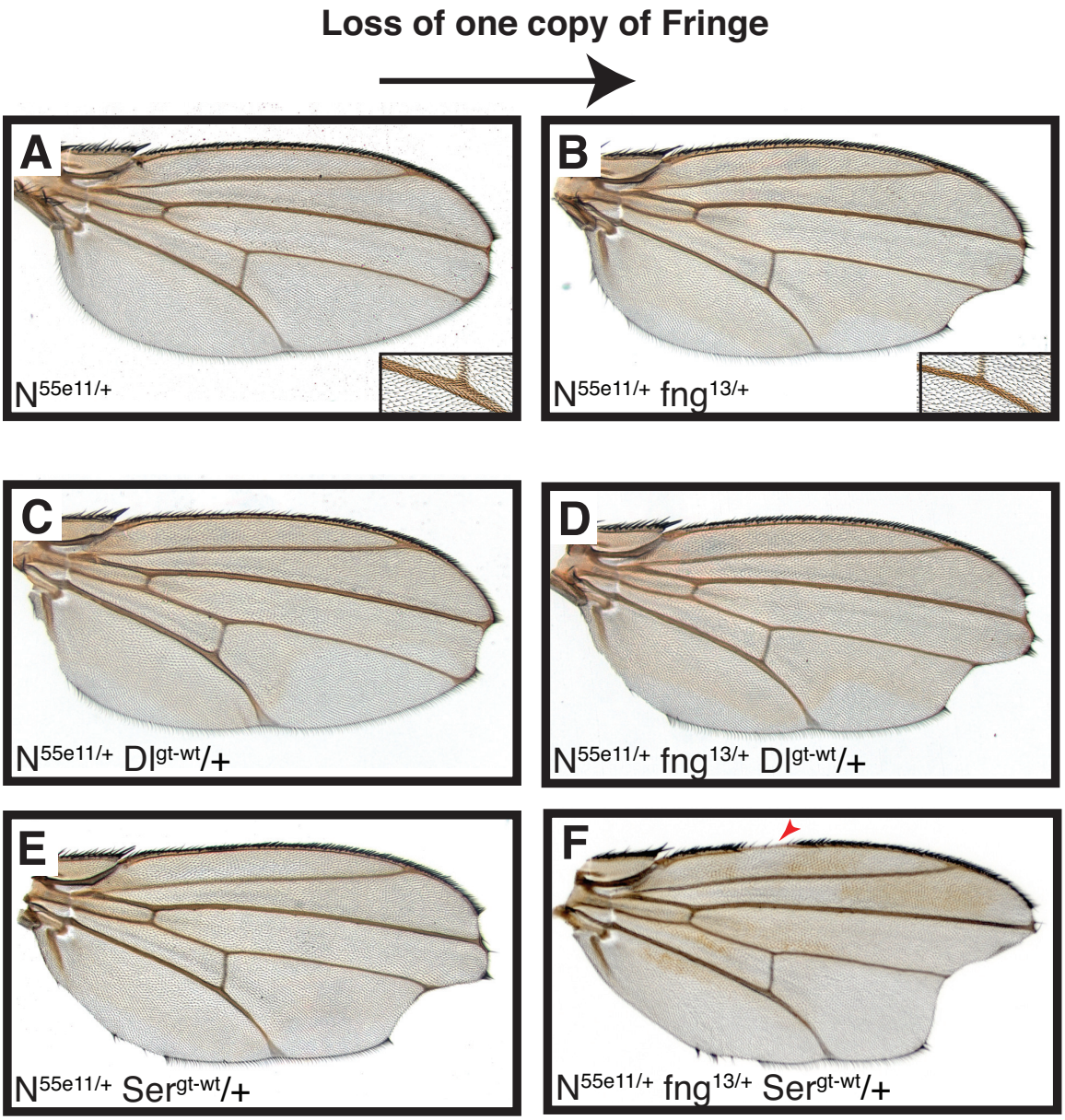

Figure 4.2: Decreasing Fringe activity improves Delta *cis*-inhibition phenotypes and worsens Serrate *cis*-inhibition phenotypes. (A) A wing of a fly missing one copy of Notch. (B) Removing a copy of Fringe from the fly in A results in more wing margin loss. (C) Fly from Figure 4.1C with one copy of Fringe removed and one copy of Delta added (1x Notch, 3x Delta). We see strong vein thickening while the margin loss from A is slightly increased. (D) Removing a copy of Fringe from the background in C results in an improvement of the wing vein phenotype. The wing margin loss is not significantly worse than that observed in the fly in B. (E) The fly from Figure 4.1F with one copy of Notch removed and one copy of Serrate added (1x Notch, 3x Serrate). (F) Removing a copy of Fringe from the background in E results in severe wing margin loss, much more than seen in B, with defects extending into anterior regions of the wing (red arrow). This phenotype resembles the 1x Notch 4x Serrate fly from Figure 4.1G.

receive signal, but should show qualitatively similar signaling states.

For the Notch1+Dll1 cells, all three Fringe proteins maintained or strengthened mutually inhibitory *cis* interactions between Dll1 and Notch1. Thus, with or without Fringe expression, the ability of cells to send or recieve depends on the relative levels of Notch1 and Dll1 (Figure 4.3A,B). Rfng preserves or strengthens Notch1 interactions with both Dll1 and Jag1, in *cis* and *trans*. As a result, Rfng expression maintains the same qualitative send or receive signaling states as observed without Rfng (Figure 4.3CA and 4.3CB, second and third panels). On the other hand, Lfng and Mfng preserve or strengthen Notch1-Dll1 *cis* interactions. Consequently, their expression leads a receiving state (only from Dll1, not Jag1) (Figure 4.3A, first panel), without affecting the sending state (Figure 4.3B, first and third panels). Thus, for a cell expressing Notch1 and Dll1, none of the Fringe proteins appear to disrupt the exclusivity of sending and receiving capabilities.

The picture is different, however, for Notch1+Jag1 cells (Figure 4.3C,D). Without Fringe, these cells exhibit exclusive send and receive states (Figure 4.3C). Rfng enhances *cis* and *trans* Notch1-Jag1 interactions (Figure 4.3D, first and second panels), maintaining exclusive sending and receiving signaling states. However, expression of Lfng or Mfng leads to a qualitatively different behavior: By weakening Jag1-Notch1 *cis* interactions, Lfng/Mfng expression enables cells to have Notch1 and Jag1 simultaneously available on the cell surface. A cell in this signaling state could use Notch1 to receive from *trans*-Dll1 ligands (but not from Jag1, as Lfng/Mfng block Jag1-Notch1 *trans* signaling), while also activating other cells with the Jag1 ligand (Figure 4.3CD, fourth panel). Thus, a cell expressing Lfng/Mfng, Jag1, and Notch1 can send and receive simultaneously, *but only using different ligands*.

A cell in this signaling state would not respond efficiently to Jag1 expressed by other cells in the same state because Lfng/Mfng reduces its response to *trans* Jag1. Evidently, the Notch pathway does allow for simultaneous sending and receiving, but the logic of the receptor and ligand interactions prevents this from occurring among cells in the same signaling state.

For the ligands we studied, Lfng and Mfng have identical effects on *cis* and *trans* interactions provoking the question of whether Lfng and Mfng have distinct roles. One possibility is suggested by recent experimental work on the subsequent sugar modifications to the Fringe-catalyzed GlcNAc residues on Notch [27]. Mutant CHO cells deficient in the addition of galactose to GlcNAc on Notch [27] were shown to be unable to support the Lfng or Mfng-dependent inhibition of Jag1-Notch1 *trans* signaling, further suggesting that Lfng and Mfng function redundantly in this aspect of Notch regulation. However, in mutant CHO cells, Lfng could not enhance *trans* signaling by Dll1, suggesting that galactose addition is required for this effect of Lfng. In sharp contrast, the ability of Mfng to promote Dll1-Notch1 *trans* signaling did not depend on galactose, and was indeed enhanced in galactosylation-deficient cells. The differential effects of each Fringe depending on the activity of downstream enzymes suggest that the Fringes are not functionally identical.

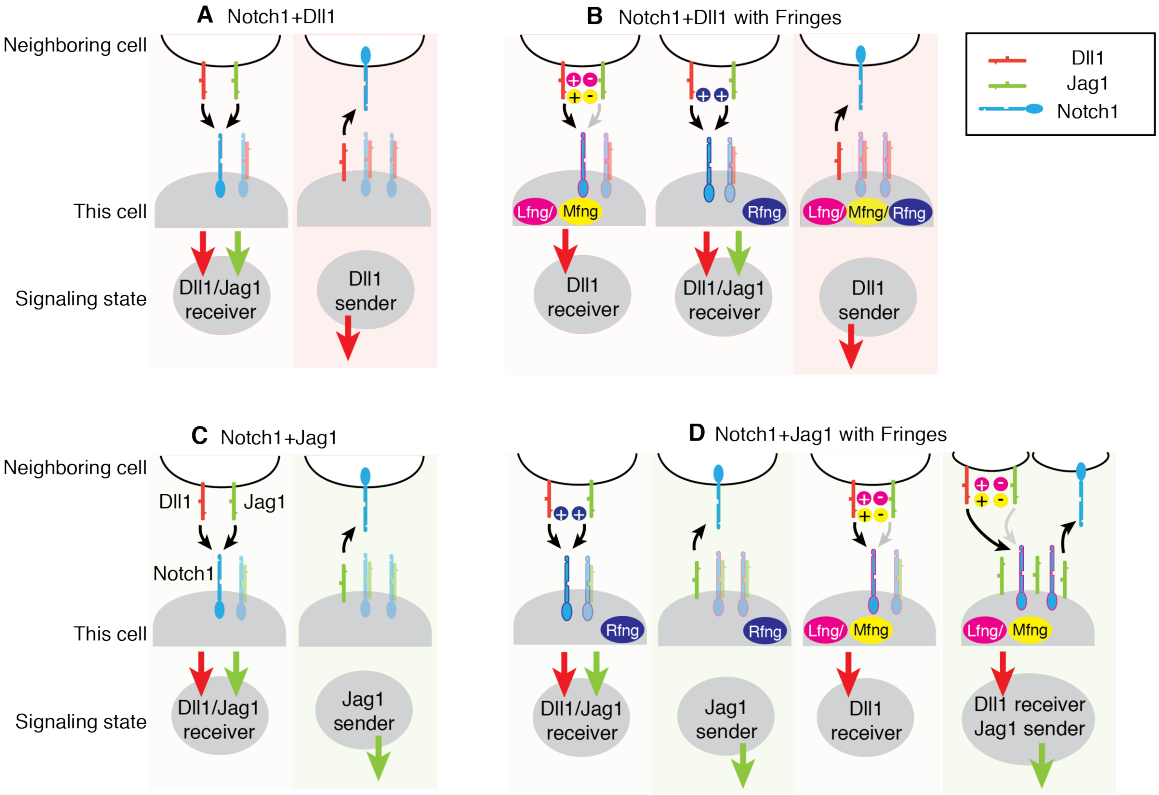

Figure 4.3: Signaling states of the Notch pathway. Each cartoon denotes a distinct configuration of Notch pathway components, with the resulting signaling state indicated schematically below. We consider extreme endpoints, where Notch1 expression is much higher than ligand expression (Notch1 > ligand, light shaded panels), and where ligand expression is much higher than Notch1 expression (Ligand > Notch1, dark shaded panels). We also consider either low (A and C) or very high levels of Fringe expression (B and D). (A) A cell expressing Notch1 and Dll1 can be in a receiving state, where it can be activated by *trans* Dll1 or Jag1, when Notch1 levels surpass Dll1 levels, left. A Dll1-sending state occurs when Dll1 exceeds Notch1, right. (B) With the addition of Lfng or Mfng, the receiving state in A becomes sensitive to *trans*-Dll1 but not *trans*-Jag1 (left). Rfng enhances receiving from both ligands (middle). Any of the three Fringe proteins support the Dll1 sending state when Dll1 exceeds Notch1 (right). (C) Co-expression of Notch1 and Jag1 permits exclusive sending (right) or receiving (left) signaling states, similar to those in A. (D) Cells expressing Notch1, Jag1, and Rfng show exclusive send or receive signaling states as in A and C (first two panels). However, addition of Lfng or Mfng inhibits Notch1-Jag1 *cis* interactions. As a result, these cells can receive signals from Dll1 but not Jag1 when Notch1 expression exceeds Jag1 expression (third panel). Finally, when Jag1 exceeds Notch1, the cell can send with Jag1 and receive from Dll1 simultaneously (right panel).

4.3 A proposed model for dorsoventral boundary formation in the wing disc

With our new knowledge of signaling states summarized in Figure 4.3, we return to the boundary formation process at the dorsoventral interface of the developing fly wing, first introduced in Section 1.9. We recall that cells within the dorsal and ventral compartments of the wing disc signal to one another, forming a sharp stripe of Notch activation at the interface between the two cell populations (Figure 1.8). This picture of boundary formation appeared to challenge our model of exclusive send and receive signaling states (Figure 1.6), because cells on either side of the boundary are all capable of receiving a signal [10]. But if all cells are in a receiving state, and signaling is occurring, then some cells must also possess the capacity to send signal. We propose a model that incorporates the ability of Fringe to modulate *cis* interactions, and show that we can resolve this apparent discrepancy.

In this patterning process, multiple ligands and Fringe are required for signaling. Cells in the dorsal compartment express Notch, Delta, Serrate, and Fringe, while cells in the ventral express Notch and Delta only (Figure 4.4). Because ventral cells only express Notch and Delta, they thus resemble our original one-ligand one-receptor model from Figure 1.6. Because ventral cells are initially capable of receiving, they should have an excess of Notch over Delta, as shown in Figure 4.4A (ventral).

Next, we turn to dorsal cells, which express multiple ligands—Delta and Serrate—and Fringe. Because dorsal cells are initially in a receiving state [10], their Delta must be eliminated in *cis* interactions with Notch. *cis*-inhibition of Delta could thus explain why dorsal cells do not signal to one another, even though they express and are responsive to Delta. At the same time, Fringe could allow Serrate and Notch to both remain available simultaneously (Figure 4.4 , dorsal), a state resembling that in Figure 4.3D (far right panel). Because Fringe blocks Serrate-Notch signaling, dorsal cells cannot signal to one another, but can signal to dorsal cells at the boundary. In this configuration, signaling can occur only from dorsal to ventral cells.

Notch activation in ventral cells causes them to up-regulate Delta expression, switching them to a Delta-sending state [10] [16] . Now, ventral cells are able to *trans*-activate dorsal cells, which remain responsive to Delta (Figure 4.4B).

Recent experimental results in the fly wing are consistent with this model of a two-step, sequential signaling process. Troost and Klein recently examined signaling at the boundary with higher time resolution than in previous work. They found that signaling occurred in two sequential phases [54]: first, dorsal cells signal via Serrate to ventral cells. Subsequently, ventral cells up-regulate Delta and signal back to dorsal cells. A similar model was proposed based on early studies of Delta-expressing clones at the boundary [16].

This model can also explain experimental results related to misexpression of ligands. Serrate

overexpression perpendicular to the DV boundary was found to block Notch signaling on both sides of this boundary. This result was taken as evidence that Fringe does not prevent *cis*-interactions [21]. However, in light of our model, we propose an alternative potential explanation: Serrate overexpression *cis*-inhibits ventral cells, interrupting the first step of signaling in the sequential signaling process. Our model predicts that dorsal cells would still be capable of receiving a signal even at high Serrate levels, as Fringe prevents Serrate-Notch *cis*-inhibition. A possible way to test this idea would be to misexpress Delta ligands in the region of Serrate overexpression to test if dorsal cells retain the ability to receive signals.

Evidence for *cis*-inhibition of a ligand by the Notch receptor has been observed in the late stages of dorsoventral boundary formation in the Drosophila wing [3]. Specifically, the Notch receptor was shown to *cis*-inhibit the Serrate ligand by promoting Serrate endocytosis in dorsal and ventral cells [3]. The observation that at this stage both dorsal and ventral cells express fringe [39] might seem not to be in agreement with our proposed model. We do not feel this observation conflicts with out hypothesis, as we propose that Notch-Serrate *cis*interactions are weakened, but not completely eliminated, by Fringe. Further, we make no claims as to the localization of the *cis*inhibition complexes; it is possible that receptor-ligand *cis*-inhibition between Notch and Delta does occur, but does not result in clearance of Delta from the surface. These ligand-specific differences in the ultimate location and fate of the receptor-ligand *cis*-inhibition complexes remain to be explored.

4.4 Exploration of signaling states with multiple pathway components

With even a few components and simple interactions, a cell's signaling behavior can be sufficiently complex to require mathematical modeling to predict outcomes. Using our model from Chapter 2 and incorporating our findings from Chapter 3, as well as data from other recent studies, we can begin to hypothesize the signaling behaviors of cells expressing complex configurations of components. We explore a few examples to illustrate the approach.

In the boundary formation model from Section 4.3, we predicted that a cell expressing Notch, Delta/Dll1, Serrate/Jagged and Fringe/Lfng or Mfng should be able to send with Serrate/Jag1 and receive from Delta/Dll1. We can investigate this behavior *in silico* by incorporating additional terms describing the *cis* interactions of a second ligand into Equations 2.4. We show that if the ratio of the *cis* interaction strengths is sufficiently large, we can see that the ligand with the stronger interaction in *cis* will be preferentially inactivated by Notch (Delta/Dll1), leaving the ligand with the weaker interaction (Serrate/Jag1) available on the surface; in fact, its availability is higher than would be observed if it were expressed alone (Figure 4.5).

We can go further to speculate on what could happen with additional ligands and receptors.

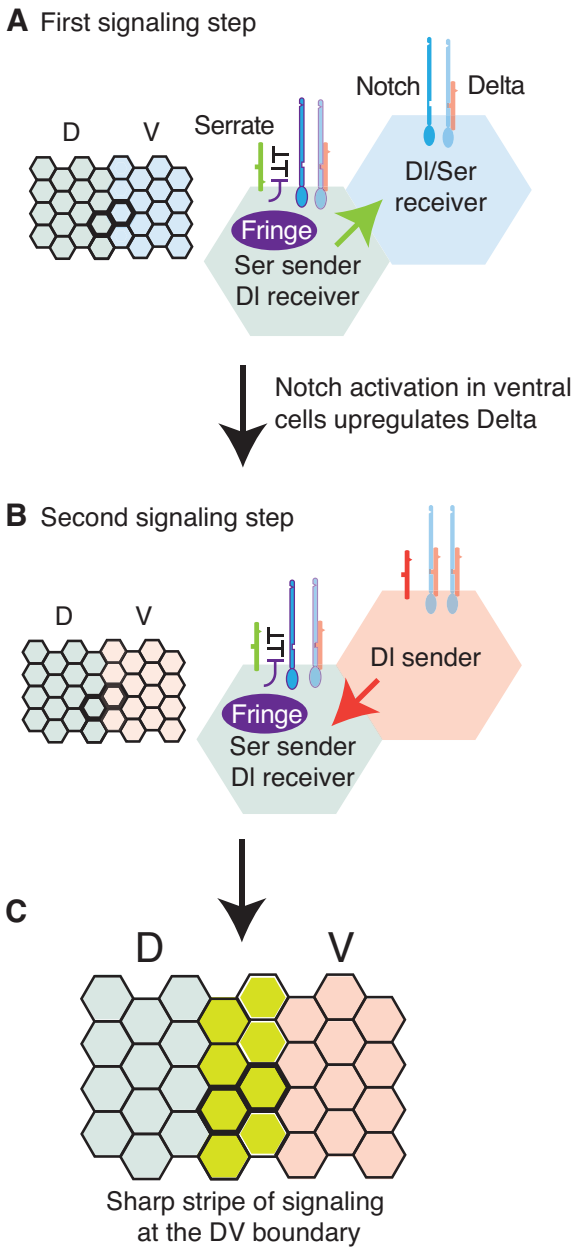

Figure 4.4: A model for Notch signaling states during dorsal-ventral boundary formation in the *Drosophila* wing disc. (A) Initially, ventral cells (light blue) express more Notch than Delta, and are able to receive signals. Dorsal cells (light green) express Serrate, Notch, Delta and Fringe. Fringe promotes Delta-Notch *cis* interactions but weakens Serrate-Notch cis interactions, enabling dorsal cells to simultaneously receive signals from Delta while sending signals with Serrate. Because Fringe reduces the response of Notch to trans-Serrate, dorsal cells cannot receive signals from other dorsal cells. Thus, the first signaling step occurs from dorsal to ventral cells (green arrow). (B) In response to Notch activation, ventral cells up-regulate Delta expression, switching to a sending state, and trans-activating dorsal cells. (C) The result is the observed pattern of Notch activation at the boundary of the dorsal and ventral compartments.

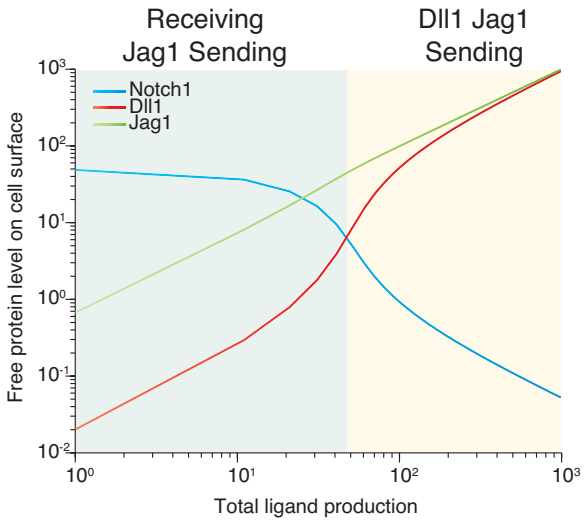

Figure 4.5: Model of a cell with Dll1, Jag1, and Notch1

There are to date few studies quantitatively comparing the interaction strengths in *cis* or in *trans* for different ligand-receptor pairs. However, one recent study showed that Dll4 is a stronger *trans*-activator of Notch1 than Dll1 [1]. Our findings so far suggest that the *cis*-interaction and *trans*-interaction are correlated; under the hypothesis that this relationship holds for every ligand-receptor pair, Dll4 should interact more strongly in *cis* with Notch1. This would lead to exclusive sending and receiving states for a cell expressing Notch1 and Dll4. The susceptibility of the Notch1-Dll4 interactions to Fringe modification will determine whether or not it is possible to send and receive simultaneously with this ligand.

It is not known what signaling states could be possible with the other Notch receptors. Preliminary work in immunology suggests that Notch3 shows an opposite preference for ligands compared to Notch1 [55]. That is, where Notch1 shows the strongest *trans*-signaling when Dll4 is the stimulating ligand, followed by Dll1/Jag2, with Jag1 as the weakest activating ligand, for Notch3 this hierarchy is inverted. If we hypothesize that *cis* and *trans* interaction strengths are correlated for all ligand-receptor pairs, and that Notch3 interactions are similarly susceptible to Fringe modification, it could be possible that a simultaneous send/receive signaling state could occur with Notch3 and Dll4. This hypothesis can be explored using our methods.

4.5 Our results could resolve contradictory findings

These results could help explain other puzzling observations. For example, one of the most striking vertebrate Notch phenotypes is disorganized somitogenesis in Notch pathway mutants [29]. In mice and chicks, Lfng is required for this process [34]. However, Lfng inhibits Notch1-Dll1 signaling [8], rather than promoting signaling as expected from previous analysis of its effect on *trans* interactions

[26]. The ability of Lfng to strengthen Dll1-Notch1 *cis* interactions could explain this phenomenon, since Lfng would tend to reduce the abundance of Dll1 and Notch1 available for *trans* signaling interactions.

Indeed, the phenotype of Lfng mutant mice bears a striking resemblance to mice mutant for Dll3, with mice showing skeletal malformations arising from disrupted somitogenesis [32, 58]. Dll3 is not able to *trans*-activate Notch, but can *cis*-inhibit Notch receptors [33]. Thus, the loss of Dll3 phenotype should reflect a loss of *cis*-inhibition and a gain of Notch signaling. Indeed, the Dll3 and Lfng knockout phenotypes also bear a resemblance to mice where Notch activity is constitutively driven with an NICD-GFP fusion [18]. Both the Dll3 and Lfng knockouts show distinctly different effects on somitogenesis compared to a Dll1 knockout [28]. Dll1 knockout mice show a loss of Notch signaling [18], as evidenced by a complete loss of Notch target gene expression. These animals are unable to form somites of any kind. Because loss of Lfng results in defects that resemble loss of Dll3, this implies that Lfng mutants reflect a loss of Notch activity due to *cis*-inhibition, and that the normal role of Lfng could be to promote *cis*-inhibition in this process. This hypothesis remains to be tested *in vivo*.

4.6 Future directions

Based on these results and others, different configurations of receptors and ligands, through *cis* interactions, could work to specify distinct signaling states in cells (Figure 4.3). These states are more complex than just 'send' and 'receive', but are still constrained by the logic of receptor-ligand interactions. Understanding what signaling states are possible, and how cells in different signaling states interact with one another, could provide a useful way to think about the Notch signaling system.

However, many questions remain. We still lack systematic measurements of the interaction strengths, in *cis* and in *trans* for the full repertoire of ligand-receptor pairs, and their quantitative dependence on Fringe expression levels. Given that multiple Fringe proteins are co-expressed in many systems, we will need to examine how Fringe proteins combine to influence Notch signaling. Are their effects additive or could one Fringe dominate the effects of another? The approach described here can distinguish between these hypotheses.

Another important avenue for research is the dynamics of Fringe modification. How quickly does it take to detect the effects of Fringe on Notch activity? This question is especially important given that Fringe expression is dynamically regulated in some contexts [8]. We can use the cell lines and movie-based assays described in this thesis to explore this aspect of Notch regulation.

Finally, additional components beyond ligands, receptors, and Fringes may need to be incorporated into our model in order to develop a predictive view of Notch signaling. Nevertheless, we

anticipate that the experimental approaches developed here can be generalized to address these questions and provide a deeper understanding of the basic design principles of the Notch signaling pathway.

Bibliography

[1] M. B. Andrawes, X. Xu, H. Liu, S. B. Ficarro, J. A. Marto, J. C. Aster, and S. C. Blacklow. Intrinsic selectivity of Notch 1 for Delta-like 4 over Delta-like 1. *J Biol Chem*, 288(35):25477–89, 2013.

[2] S. Artavanis-Tsakonas, M. D. Rand, and R. J. Lake. Notch signaling: Cell fate control and signal integration in development. *Science*, 284(5415):770–6, 1999.

[3] I. Becam, U. M. Fiuza, A. M. Arias, and M. Milan. A role of receptor Notch in ligand *cis*-inhibition in *Drosophila*. *Curr Biol*, 20(6):554–60, 2010.

[4] R. Benedito, C. Roca, I. Sorensen, S. Adams, A. Gossler, M. Fruttiger, and R. H. Adams. The notch ligands Dll4 and Jagged1 have opposing effects on angiogenesis. *Cell*, 137(6):1124–35, 2009.

[5] S. J. Bray. Notch signalling: A simple pathway becomes complex. *Nat Rev Mol Cell Biol*, 7(9):678–89, 2006.

[6] K. Bruckner, L. Perez, H. Clausen, and S. Cohen. Glycosyltransferase activity of Fringe modulates Notch-Delta interactions. *Nature*, 406(6794):411–5, 2000.

[7] J. Cordle, S. Johnson, J. Z. Tay, P. Roversi, M. B. Wilkin, B. H. de Madrid, H. Shimizu, S. Jensen, P. Whiteman, B. Jin, C. Redfield, M. Baron, S. M. Lea, and P. A. Handford. A conserved face of the Jagged/Serrate DSL domain is involved in Notch *trans*-activation and textitcis-inhibition. *Nat Struct Mol Biol*, 15(8):849–57, 2008.

[8] J. K. Dale, M. Maroto, M. L. Dequeant, P. Malapert, M. McGrew, and O. Pourquie. Periodic Notch inhibition by Lunatic Fringe underlies the chick segmentation clock. *Nature*, 421(6920):275–8, 2003.

[9] M. H. Dallas, B. Varnum-Finney, C. Delaney, K. Kato, and I. D. Bernstein. Density of the Notch ligand Delta1 determines generation of B and T cell precursors from hematopoietic stem cells. *J Exp Med*, 201(9):1361–6, 2005.

[10] J. F. de Celis and S. Bray. Feed-back mechanisms affecting Notch activation at the dorsoventral boundary in the Drosophila wing. *Development*, 124(17):3241–51, 1997.

[11] J. F. de Celis and S. J. Bray. The Abruptex domain of Notch regulates negative interactions between Notch, its ligands and Fringe. *Development*, 127(6):1291–302, 2000.

[12] J. F. de Celis, A. Garcia-Bellido, and S. J. Bray. Activation and function of Notch at the dorsal-ventral boundary of the wing imaginal disc. *Development*, 122(1):359–69, 1996.

[13] A. de-la Concha, U. Dietrich, D. Weigel, and J. A. Campos-Ortega. Functional interactions of neurogenic genes of *Drosophila melanogaster*. *Genetics*, 118(3):499–508, 1988.

[14] M. De Smedt, I. Hoebeke, K. Reynvoet, G. Leclercq, and J. Plum. Different thresholds of Notch signaling bias human precursor cells toward b-, nk-, monocytic/dendritic-, or t-cell lineage in thymus microenvironment. *Blood*, 106(10):3498–506, 2005.

[15] D. del Alamo, H. Rouault, and F. Schweisguth. Mechanism and significance of *cis*-inhibition in Notch signalling. *Curr Biol*, 21(1):R40–7, 2011.

[16] D. Doherty, G. Feger, S. Younger-Shepherd, L. Y. Jan, and Y. N. Jan. Delta is a ventral to dorsal signal complementary to serrate, another notch ligand, in drosophila wing formation. *Genes Dev*, 10(4):421–34, 1996.

[17] B. D'Souza, L. Meloty-Kapella, and G. Weinmaster. Canonical and non-canonical notch ligands. *Curr Top Dev Biol*, 92:73–129, 2010.

[18] J. Feller, A. Schneider, K. Schuster-Gossler, and A. Gossler. Noncyclic Notch activity in the presomitic mesoderm demonstrates uncoupling of somite compartmentalization and boundary formation. *Genes Dev*, 22(16):2166–71, 2008.

[19] U. M. Fiuza, T. Klein, A. Martinez Arias, and P. Hayward. Mechanisms of ligand-mediated inhibition in Notch signaling activity in Drosophila. *Dev Dyn*, 239(3):798–805, 2010.

[20] R. J. Fleming, K. Hori, A. Sen, G. V. Filloramo, J. M. Langer, R. A. Obar, S. Artavanis-Tsakonas, and A. C. Maharaj-Best. An extracellular region of Serrate is essential for ligand-induced *cis*-inhibition of Notch signaling. *Development*, 140(9):2039–49, 2013.

[21] M. Glittenberg, C. Pitsouli, C. Garvey, C. Delidakis, and S. Bray. Role of conserved intracellular motifs in Serrate signalling, cis-inhibition and endocytosis. *Embo j*, 25(20):4697–706, 2006.

[22] M. Gossen and H. Bujard. Tight control of gene expression in mammalian cells by tetracycline-responsive promoters. *Proc Natl Acad Sci U S A*, 89(12):5547–51, 1992.

[23] I. Greenwald. Notch and the awesome power of genetics. *Genetics*, 191(3):655–69, 2012.

[24] K. G. Guruharsha, M. W. Kankel, and S. Artavanis-Tsakonas. The Notch signalling system: recent insights into the complexity of a conserved pathway. *Nat Rev Genet*, 13(9):654–66, 2012.

[25] S. Hammond, M. Kaplarevic, N. Borth, M. J. Betenbaugh, and K. H. Lee. Chinese hamster genome database: An online resource for the CHO community at www.CHOgenome.org. *Biotechnol Bioeng*, 109(6):1353–6, 2012.

[26] C. Hicks, S. H. Johnston, G. diSibio, A. Collazo, T. F. Vogt, and G. Weinmaster. Fringe differentially modulates Jagged1 and Delta1 signalling through Notch1 and Notch2. *Nat Cell Biol*, 2(8):515–20, 2000.

[27] X. Hou, Y. Tashima, and P. Stanley. Galactose differentially modulates lunatic and manic Fringe effects on Delta1-induced Notch signaling. *J Biol Chem*, 287(1):474–83, 2012.

[28] M. Hrabe de Angelis, n. McIntyre, J., and A. Gossler. Maintenance of somite borders in mice requires the Delta homologue Dll1. *Nature*, 386(6626):717–21, 1997.

[29] K. D. Irvine. Fringe, Notch, and making developmental boundaries. *Curr Opin Genet Dev*, 9(4):434–41, 1999.

[30] A. C. Jaleco, H. Neves, E. Hooijberg, P. Gameiro, N. Clode, M. Haury, D. Henrique, and L. Parreira. Differential effects of Notch ligands Delta-1 and Jagged-1 in human lymphoid differentiation. *J Exp Med*, 194(7):991–1002, 2001.

[31] R. Kopan and M. X. Ilagan. The canonical Notch signaling pathway: Unfolding the activation mechanism. *Cell*, 137(2):216–33, 2009.

[32] K. Kusumi, E. S. Sun, A. W. Kerrebrock, R. T. Bronson, D. C. Chi, M. S. Bulotsky, J. B. Spencer, B. W. Birren, W. N. Frankel, and E. S. Lander. The mouse pudgy mutation disrupts Delta homologue Dll3 and initiation of early somite boundaries. *Nat Genet*, 19(3):274–8, 1998.

[33] E. Ladi, J. T. Nichols, W. Ge, A. Miyamoto, C. Yao, L. T. Yang, J. Boulter, Y. E. Sun, C. Kintner, and G. Weinmaster. The divergent DSL ligand Dll3 does not activate Notch signaling but cell autonomously attenuates signaling induced by other DSL ligands. *J Cell Biol*, 170(6):983–92, 2005.

[34] J. Lewis. Notch signalling and the control of cell fate choices in vertebrates. *Semin Cell Dev Biol*, 9(6):583–9, 1998.

[35] C. Y. Logan and R. Nusse. The Wnt signaling pathway in development and disease. *Annu Rev Cell Dev Biol*, 20:781–810, 2004.

[36] U. Marklund, E. M. Hansson, E. Sundstrom, M. H. de Angelis, G. K. Przemeck, U. Lendahl, J. Muhr, and J. Ericson. Domain-specific control of neurogenesis achieved through patterned regulation of Notch ligand expression. *Development*, 137(3):437–45, 2010.

[37] L. Meloty-Kapella, B. Shergill, J. Kuon, E. Botvinick, and G. Weinmaster. Notch ligand endocytosis generates mechanical pulling force dependent on dynamin, epsins, and actin. *Dev Cell*, 22(6):1299–312, 2012.

[38] C. A. Micchelli, E. J. Rulifson, and S. S. Blair. The function and regulation of cut expression on the wing margin of Drosophila: Notch, Wingless and a dominant negative role for Delta and Serrate. *Development*, 124(8):1485–95, 1997.

[39] M. Milan and S. M. Cohen. Temporal regulation of apterous activity during development of the Drosophila wing. *Development*, 127(14):3069–78, 2000.

[40] A. C. Miller, E. L. Lyons, and T. G. Herman. cis-inhibition of Notch by endogenous Delta biases the outcome of lateral inhibition. *Curr Biol*, 19(16):1378–83, 2009.

[41] O. L. Mohr. Character Changes Caused by Mutation of an Entire Region of a Chromosome in Drosophila. *Genetics*, 4(3):275–82, 1919.

[42] D. J. Moloney, V. M. Panin, S. H. Johnston, J. Chen, L. Shao, R. Wilson, Y. Wang, P. Stanley, K. D. Irvine, R. S. Haltiwanger, and T. F. Vogt. Fringe is a glycosyltransferase that modifies Notch. *Nature*, 406(6794):369–75, 2000.

[43] T. H. Morgan. *The Theory of the Gene*. New Haven,Yale University Press;, 1928. http://www.biodiversitylibrary.org/bibliography/5978.

[44] T. H. Morgan and C. B. Bridges. *Sex-Linked Inheritance in Drosophila*. Washington, Carnegie Institution of Washington. http://www.biodiversitylibrary.org/bibliography/22854.

[45] T. K. Noah and N. F. Shroyer. Notch in the intestine: Regulation of homeostasis and pathogenesis. *Annu Rev Physiol*, 75:263–88, 2013.

[46] N. Perrimon, C. Pitsouli, and B. Z. Shilo. Signaling mechanisms controlling cell fate and embryonic patterning. *Cold Spring Harb Perspect Biol*, 4(8):a005975, 2012.

[47] L. K. Phng and H. Gerhardt. Angiogenesis: A team effort coordinated by Notch. *Dev Cell*, 16(2):196–208, 2009.

[48] R. G. Ramos, B. G. Grimwade, K. A. Wharton, T. N. Scottgale, and S. Artavanis-Tsakonas. Physical and functional definition of the Drosophila Notch locus by p element transformation. *Genetics*, 123(2):337–48, 1989.

[49] K. Shimizu, S. Chiba, K. Kumano, N. Hosoya, T. Takahashi, Y. Kanda, Y. Hamada, Y. Yazaki, and H. Hirai. Mouse Jagged1 physically interacts with Notch2 and other Notch receptors. Assessment by quantitative methods. *J Biol Chem*, 274(46):32961–9, 1999.

[50] D. Sprinzak, A. Lakhanpal, L. LeBon, J. Garcia-Ojalvo, and M. B. Elowitz. Mutual inactivation of Notch receptors and ligands facilitates developmental patterning. *PLoS Comput Biol*, 7(6):e1002069, 2011.

[51] D. Sprinzak, A. Lakhanpal, L. Lebon, L. A. Santat, M. E. Fontes, G. A. Anderson, J. Garcia-Ojalvo, and M. B. Elowitz. Cis-interactions between Notch and Delta generate mutually exclusive signalling states. *Nature*, 465(7294):86–90, 2010.

[52] P. Stanley and T. Okajima. Roles of glycosylation in Notch signaling. *Curr Top Dev Biol*, 92:131–64, 2010.

[53] G. Struhl and A. Adachi. Nuclear access and action of Notch in vivo. *Cell*, 93(4):649–60, 1998.

[54] T. Troost and T. Klein. Sequential Notch signalling at the boundary of Fringe expressing and non-expressing cells. *PLoS One*, 7(11):e49007, 2012.

[55] I. Van de Walle, E. Waegemans, J. De Medts, G. De Smet, M. De Smedt, S. Snauwaert, B. Vandekerckhove, T. Kerre, G. Leclercq, J. Plum, T. Gridley, T. Wang, U. Koch, F. Radtke, and T. Taghon. Specific Notch receptor-ligand interactions control human TCR-$\alpha\beta/\gamma\delta$ development by inducing differential Notch signal strength. *J Exp Med*, 210(4):683–97, 2013.

[56] A. Xu, N. Haines, M. Dlugosz, N. A. Rana, H. Takeuchi, R. S. Haltiwanger, and K. D. Irvine. *In vitro* reconstitution of the modulation of *Drosophila* Notch-ligand binding by Fringe. *J Biol Chem*, 282(48):35153–62, 2007.

[57] L. T. Yang, J. T. Nichols, C. Yao, J. O. Manilay, E. A. Robey, and G. Weinmaster. Fringe glycosyltransferases differentially modulate Notch1 proteolysis induced by Delta1 and Jagged1. *Mol Biol Cell*, 16(2):927–42, 2005.

[58] N. Zhang, G. V. Martin, M. W. Kelley, and T. Gridley. A mutation in the Lunatic fringe gene suppresses the effects of a Jagged2 mutation on inner hair cell development in the cochlea. *Curr Biol*, 10(11):659–62, 2000.

Appendix: Cis interactions between Notch and Delta generate mutually exclusive signaling states

This paper appeared in the May 6, 2010 edition of *Nature*. I contributed to the experimentation and data analysis for the main figures, and also to the Discussion section.

Abstract

The Notch-Delta signalling pathway allows communication between neighbouring cells during development [1]. It has a critical role in the formation of 'fine-grained' patterns, generating distinct cell fates among groups of initially equivalent neighbouring cells and sharply delineating neighbouring regions in developing tissues [2-5]. The Delta ligand has been shown to have two activities: it transactivates Notch in neighbouring cells and *cis*-inhibits Notch in its own cell. However, it remains unclear how Notch integrates these two activities and how the resulting system facilitates pattern formation. Here we report the development of a quantitative time-lapse microscopy platform for analysing Notch-Delta signalling dynamics in individual mammalian cells, with the aim of addressing these issues. By controlling both *cis*- and *trans*-Delta concentrations, and monitoring the dynamics of a Notch reporter, we measured the combined *cis*-*trans* input-output relationship in the Notch-Delta system. The data revealed a striking difference between the responses of Notch to *trans*- and *cis*- Delta: whereas the response to *trans*-Delta is graded, the response to *cis*-Delta is sharp and occurs at a fixed threshold, independent of *trans*-Delta. We developed a simple mathematical model that shows how these behaviours emerge from the mutual inactivation of Notch and Delta proteins in the same cell. This interaction generates an ultrasensitive switch between mutually exclusive sending (high Delta/low Notch) and receiving (high Notch/low Delta) signalling states. At the multicellular level, this switch can amplify small differences between neighbouring cells even without transcription-mediated feedback. This Notch-Delta signalling switch facilitates the formation of sharp boundaries and lateral-inhibition patterns in models of development, and provides insight into previously unexplained mutant behaviours.

Letter

Notch and Delta are single-pass transmembrane protein families found in metazoan species. Delta in one cell can bind to, and transactivate, Notch in a neighbouring cell. This interaction results in proteolytic release of the Notch intracellular domain, which translocates to the nucleus and activates target genes6 (Fig. 1a). Delta also has a second role, inhibiting Notch activity in its own cell (*cis*-inhibition) [7-10]. *Cis*-inhibition has been shown to involve direct interaction of the two proteins [11], but current understanding is incomplete [12].

To understand how concentrations of *cis*- and *trans*-Delta are integrated by the Notch pathway (Fig. 1b), we constructed cell lines that allowed us to modulate the concentrations of *cis*- and *trans*-Delta independently, and to monitor quantitatively the transcriptional response of a Notch reporter (Fig. 1c and Supplementary Fig. 1). These cell lines stably expressed Notch receptors and corresponding yellow fluorescent protein (YFP) reporters of Notch activity (Supplementary Figs 1 and 2). They also contained a doxycycline-inducible chimaeric rat Dll1-mCherry fusion gene (Delta-mCherry; Supplementary Fig. 3). In our main cell line, hN1G4$^{\mathrm{esn}}$, the intracellular domain of human NOTCH1 was replaced with a minimal variant of the transcriptional activator Gal4, denoted Gal4$^{\mathrm{esn}}$ [13], to avoid activation of endogenous Notch targets [14-16]. A second cell line, hN1, containing the full-length human NOTCH1 was analysed as a control (Supplementary Fig. 1). Notch messenger RNA expression levels in these cells were comparable to those observed in early T-cell progenitors where Notch is active [17] (Supplementary Information).

We first asked how Notch activity depends on the concentration of *trans*-Delta. We adsorbed fusion proteins, consisting of immunoglobin-G (IgG) fused to the extracellular domain of human DLL1 (Delta$^{\mathrm{ext}}$), to the surface of plates at different concentrations, denoted $\mathrm{D}_{\mathrm{plate}}$ (Fig. 2a and Supplementary Fig. 4) [18,19], and recorded time-lapse movies of Notch activation. Before the start of each movie ($t < 0$), we inhibited Notch activation using the γ-secretase inhibitor *N*-[*N*-(3,5-difluorophenacetyl)-L-alanyl]- *S*-phenylglycine t-butyl ester (DAPT). At $t = 0$, DAPT was washed out, allowing the fluorescent reporter to accumulate at a rate determined by Notch activity (Fig. 2b, c and Supplementary Movie 1). The YFP production rate showed a graded response to $\mathrm{D}_{\mathrm{plate}}$, well-fitted by a Hill function with a modest Hill coefficient (Fig. 2d).A similar response was observed in the hN1 cell line (Supplementary Figure 1). This graded response was not due to the use of plate-bound ligands: when cells expressing only Delta were co-cultured with cells expressing only Notch, we observed a similarly graded dependence of Notch activity on the level of Delta expression, but with greater variability (Supplementary Fig. 5).

We next set out to quantify the response of Notch to varying concentrations of *cis*-Delta in the hN1G4$^{\mathrm{esn}}$ cell line. We used a scheme in which Delta-mCherry was expressed in a pulse before the start of the movie and subsequently allowed to dilute, effectively titrating its concentration

[20] (Fig. 3a). These experiments were performed at low cell density, where relatively weak intercellular activation of Notch is observed (Supplementary Fig. 6), and transactivation was induced predominantly by D_{plate}. At the beginning of the movie, Notch reporter expression was fully inhibited by high Delta- mCherry concentrations (Fig. 3b and Supplementary Movie 2). Subsequently, Delta-mCherry concentrations gradually declined on a timescale of $\tau_D = 32 \pm 2.5$ h, consistent with dilution by cell growth and division (Fig. 3c). At $t_{on} \approx 40$ h, we observed a sharp onset of reporter expression in the median response of the population (Fig. 3c). Even sharper responses were evident in individual cell lineages (Fig. 3d-f and Supplementary Fig. 13). Similar behaviour was observed in the hN1 cell line (Supplementary Fig. 7)

To quantify the sharpness of *cis*-inhibition, we computed the rise time, denoted τ_{rise}, required for Notch activity to increase by a factor of e in individual cells (Fig. 3e and Fig. 3a, inset). The distribution of τ_{rise} showed a median of 2.6 h, which is considerably less than τ_D (Fig. 3f). For comparison, an equivalently sharp Hill function of *cis*-Delta would require a Hill coefficient of $\tau_D/\tau_{rise} < 12$.

We repeated the experiment for a variety of D_{plate} values, allowing us to directly measure the integrated response of Notch across the two-dimensional input space of *cis*- and *trans*-Delta concentrations (Fig. 3g and Supplementary Fig. 14). Activation occurred at a similar value of t_{on} and, therefore, a similar *cis*-Delta concentration, regardless of D_{plate}, as indicated by the fixed position of the transition from black to green points in Fig. 3g. In addition, the activation remained sharp at all D_{plate} values for which it could be clearly measured.

Thus, an explanation for the observed *cis*- and *trans*-signal integration must simultaneously account for the three key features of the experimental data: a graded response to *trans*-Delta (Fig. 2d), a sharp response to *cis*-Delta (Fig. 3c-f) and a fixed threshold for *cis*-inhibition across varying concentrations of *trans*-Delta (Fig. 3g). We show here that a simple model can explain these observations in a unified way (Box 1 and Fig. 3h). The model's key assumption is that Notch and Delta in the same cell mutually inactivate each other. As shown in Box 1, strong enough mutual inactivation can produce an ultrasensitive switch between two mutually exclusive signalling states: cells can be in a predominantly 'sending' state, with high Delta concentration and low Notch concentration, or a 'receiving' state, with high Notch concentration and low Delta concentration, but cannot be in both states at the same time. Alternative models that do not include mutual inactivation fail to account for the observed data (Supplementary Fig. 8).

The three features described above emerge naturally in this model. First, in the absence of *cis*-Delta, the rate of Notch activation is proportional to the *trans*-Delta concentration, generating a graded response. Second, a sharp response to *cis*-Delta results from mutual inactivation, which causes an excess of either protein to strongly diminish the activity of the other. Finally, the switching point occurs when Notch and *cis*-Delta concentrations are comparable, and is therefore only weakly

dependent on *trans*-Delta.

The mutual-inactivation model predicts cis-inhibition, not just of Notch by Delta but also of Delta by Notch. This interaction is supported by results in other systems [12,21,22]. We tested this prediction in our system using a transactivation assay based on co-culture of Delta-expressing sending cells with Notch reporter cells. Expression of Notch in the Delta-expressing cells reduced their ability to transactivate, as predicted (Supplementary Fig. 9). The exact biochemical mechanism of mutual inactivation remains unclear, but we observed no sharp drop in the total cellular Delta-mCherry fluorescence during switching, suggesting that the inactive complex may be stable in these conditions (Fig. 3c, d).

This signalling switch has important implications for multicellular patterning. To understand these implications, consider two neighbouring cells that produce Notch and Delta at constant rates (Fig. 4a). A slight excess of Notch production in one cell and a slight excess of Delta production in its neighbour can generate a strong signalling bias in one direction: the first cell becomes a receiver and the second becomes a sender. In this way, a small difference in production rates between cells is amplified into a much larger difference in Notch activity (Fig. 4b). This amplification does not require transcriptional regulation or feedback.

The send-receive signalling switch can facilitate formation of sharp boundaries. For example, in Drosophila Notch and Delta sharply delineate wing vein boundaries [4,5]. In this system, Delta production is initially expressed in a graded profile transverse to the vein. Eventually, Notch signalling is restricted to two sharp side bands on either side of the vein axis.

As a simplified model, we simulated the development of a field of cells with a graded rate of Delta production and a uniform rate of Notch production (Fig. 4c). The mutual-inactivation model generated sharply defined side bands of Notch signalling at positions where the two production rates intersect, that is, where sender and receiver cells are next to each other (Fig. 4c). Moreover, this model explains a striking mutant behaviour that occurs in the *Drosophila* wing vein system. Although Notch and Delta are individually haploinsufficient (causing thicker veins), the $\text{Notch}^{+/-}$ $\text{Delta}^{+/-}$ double mutant restores the wild-type phenotype [23]. This suppression of the single-mutant phenotypes in the double mutant emerges automatically in the model because proportional rescaling of the Notch and Delta production rates does not move their intersection points (Fig. 4d). This suppression is maintained across a broad range of parameter values and persists even with additional feedbacks (Supplementary Fig. 10c), but is difficult to explain in other models (Supplementary Fig. 10a and Supplementary Information).

The send-receive signalling switch can also facilitate lateral-inhibition patterning. When Notch transcriptionally downregulates Delta expression, the resulting intercellular positive-feedback loop can generate 'checkerboard' patterns of Notch activity [24,25] (Fig. 4e). Without mutual inactivation, pattern formation requires a minimum Hill coefficient of $n = 2$, or higher, in the regulatory

feedback loop (Fig. 4f, left, and Supplementary Information). Although we cannot rule out such cooperativity, or additional feedback loops, no evidence for strongly cooperative transactivation was observed here or previously (Fig. 2d and Supplementary Fig. 1). In contrast, mutual inactivation allows patterning even without cooperativity, by introducing a sharp response to changes in Delta expression (Fig. 4f, right). In addition, for strong enough *cis*-inhibition, mutual inactivation allows cells with high Delta concentrations to coexist next to one another in the steady state, leading to a broader range of possible patterns (Supplementary Fig. 17). Finally, we note that low concentrations of free Notch and Delta exist in sender and, respectively, receiver cells for finite mutual-inactivation strengths (Supplementary Fig. 11). The resulting signalling between like cells (senders or receivers) can have a role in lateral-inhibition patterning dynamics.

Modeling box

Here we describe a simple model of Notch-Delta interactions that explains the experimental data and provides insight into developmental patterning processes. The model involves several reactions. First, during intercellular signalling, Notch in one cell binds to extracellular Delta, of concentration D_{trans}, leading to release of the Notch intracellular domain and degradation of its extracellular domain [6]. Similarly, Notch in a neighbouring cell, N_{trans}, can bind to Delta. Second, Notch binds irreversibly to Delta in the same cell to form a stable, inactive, complex, which is effectively removed from the system [12]. Finally, Notch and Delta are produced at constant rates, and degraded and/or diluted at a constant rate, in addition to being removed through the interactions described above.

These reactions can be expressed as a set of ordinary differential equations for the concentrations of free Notch, N, and free Delta, D, in an individual cell. An additional equation represents the intracellular domain of Notch, S, which activates expression of the fluorescent reporter gene:

$$\begin{aligned}
\frac{dN}{dt} &= \beta_N - \gamma N - \frac{DN}{k_c} - \frac{D_{trans}N}{k_t}, \\
\frac{dD}{dt} &= \beta_D - \gamma D - \frac{DN}{k_c} - \frac{DN_{trans}}{k_t}, \\
\frac{dS}{dt} &= \frac{D_{trans}N}{k_t} - \gamma_S S.
\end{aligned}$$

Here D_{trans} represents $\mathrm{D_{plate}}$ in Figs 2 and 3, but could also represent Delta concentration in one or more neighbouring cells (Supplementary Information). Similarly, D in these equations corresponds to *cis*-Delta in the experiments, and β_N and β_D denote the production rates of Notch and Delta, respectively. The combined degradation and dilution rate, γ, is assumed for simplicity to be the same for Notch and Delta, and γ_S is the rate of decay of S. We write k_c and k_t to denote the strengths of *cis*-inhibition and transactivation, respectively. See Supplementary Information for a

more detailed description.

In the steady state, mutual inactivation leads to a switch between two qualitatively distinct behaviours, depending on the relative production rates of Delta and Notch. When $\beta_D > \beta_N$, excess Delta effectively inactivates almost all Notch, allowing cells to send, but not efficiently receive, signals. Conversely, when $\beta_D < \beta_N$, excess Notch effectively inactivates Delta, allowing cells to receive, but not efficiently send, signals. Thus, the system approaches two mutually exclusive signalling states: high Delta/low Notch ('sending'; pink shading in Figure), and high Notch/low Delta ('receiving'; blue shading in Figure). We note that this switch is not bistable.

In the steady state, the transition between the two regimes is ultrasensitive: near the threshold, a relatively small change in β_D or β_N can lead to a much larger change in signalling (Supplementary Fig. 11). Related biochemical kinetics occur in bacterial small RNA and protein sequestration [27-29]. In Fig. 3, ultrasensitivity occurs dynamically in response to the decay of the total Delta concentration (Supplementary Information).

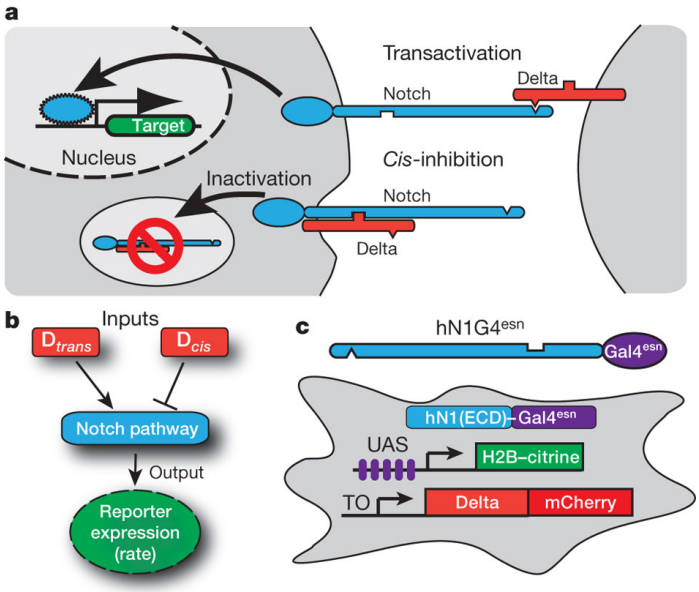

Figure 1: System for analyzing signal integration in the Notch-Delta pathway. a, Notch (blue) and Delta (red) interactions are indicated schematically. b, Notch activity integrates *cis*-and *trans*-Delta. c, T-REx-CHO-K1 cell line for analysing Notch activity. The hN1G4^{esn} cell line stably incorporates a variant of human NOTCH1 in which the activator Gal4^{esn} replaces the Notch intracellular domain (here hN1(ECD) is the extracellular domain of hN1). This cell line also contains genes for histone 2B (H2B)citrine (YFP) reporter controlled by an upstream activating sequence (UAS) promoter, a tetracycline-inducible (TO) DeltamCherry fusion protein and a constitutively expressed H2Bcerulean (cyan fluorescent protein, or CFP) for image segmentation (not shown). A similar cell line expressing full-length human NOTCH1 (the hN1 cell line) was also analysed (Supplementary Figs 1 and 2). These cells exhibit no detectable endogenous Notch or Delta activities. NotchDelta interactions are indicated schematically and do not represent molecular interaction mechanisms [11].

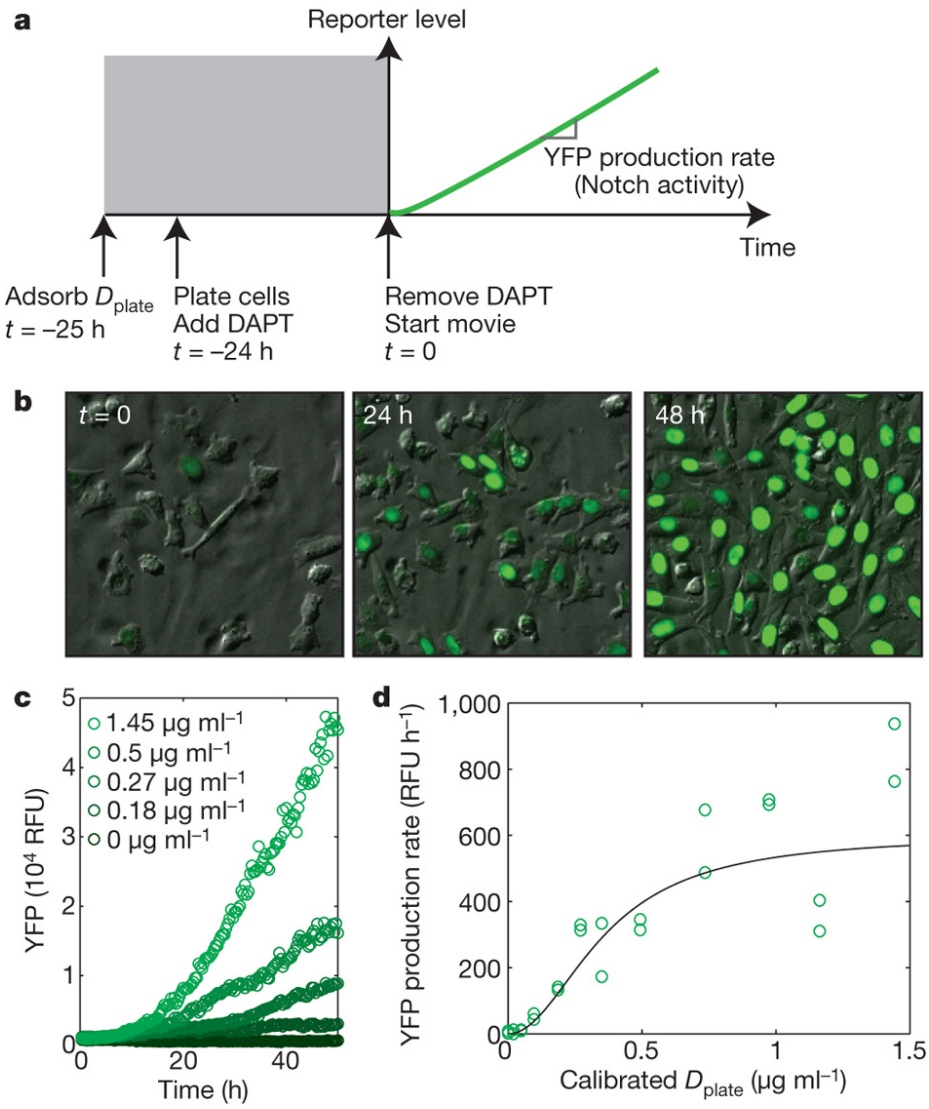

Figure 2: Transactivation of Notch occurs in a graded fashion. a, Experimental design. The rate of increase of fluorescence (slope of green line) is a measure of Notch activity. b, Typical hN1G4^{esn} filmstrip showing activation of Notch reporter (green), with $D_{plate} = 1.16$ μg ml^{-1} and frame times as indicated (Supplementary Movie 1; compare with Supplementary Fig. 6). c, hN1G4^{esn} cells respond in a graded manner to variations in D_{plate}. The data show the median fluorescence of individual cells within a single field of view for the indicated values of D_{plate} (see Supplementary Fig. 15 for distributions). RFU, relative fluorescence unit. d, The relationship between D_{plate} and Notch activity (in RFU per hour, from the linear regime in c). The Hill-function fit is indicated by the black line, which has Hill coefficient $n = 1.7$ (95% confidence interval, $n = 0.8 - -2.7$). Similar results were obtained using the hN1 cell line (Supplementary Fig. 1). We note that doxycycline does not directly affect Notch activation or cell growth, nor does D_{plate} affect cell growth (Supplementary Fig. 12).

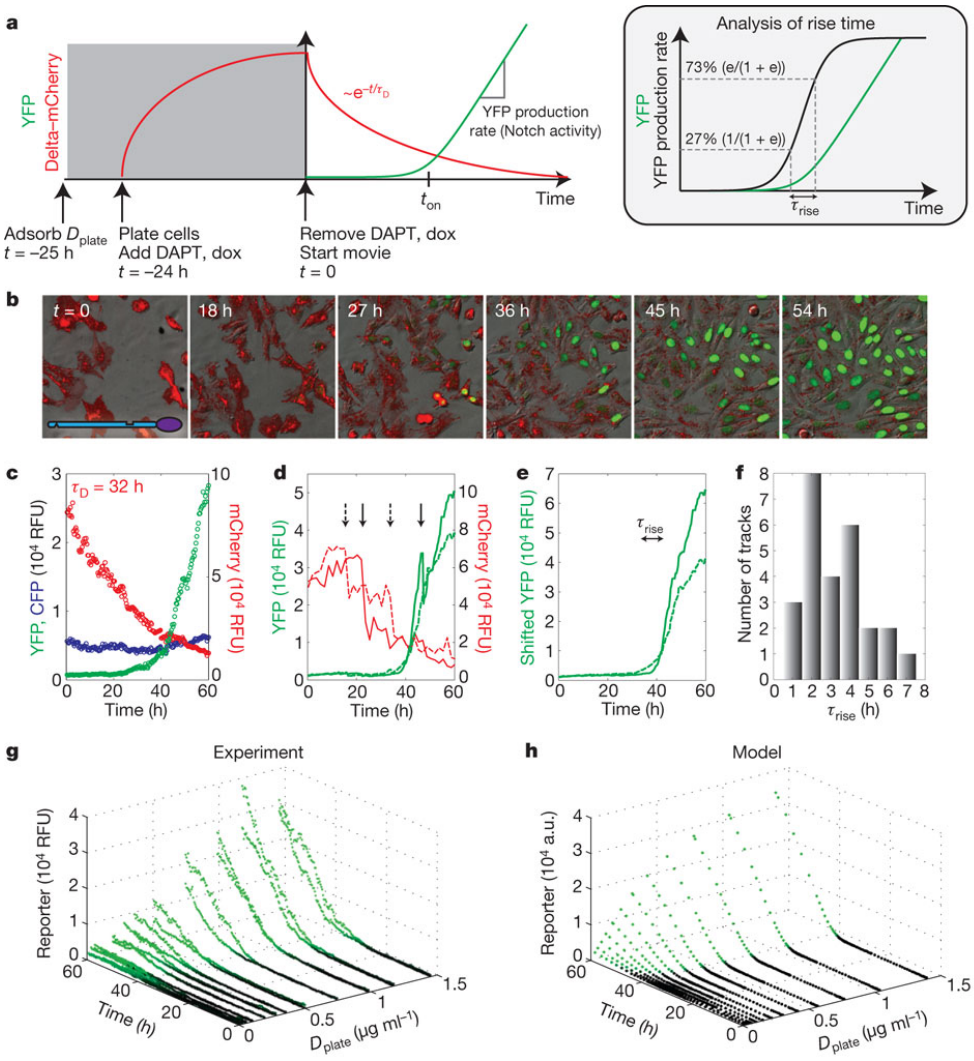

Figure 3: *Cis-trans* signal integration by Notch. a, Experimental protocol. Inset, the rise time, τ_{rise}, is the time required for Notch activity (black line or slope of green line) to change by a factor of e. dox, doxycycline. b, Filmstrip of hN1G4$^{\mathrm{esn}}$ cells, with $D_{plate} = 1.45$ μg ml^{-1} (Supplementary Movie 2), showing Delta-mCherry fluorescence (red) and concomitant activation of Notch reporter (green) at the indicated times (compare with Supplementary Fig. 6). c, Population average (median) response for the same movie shows a slow decay of Delta-mCherry fluorescence (red data), but a sharp response of reporter expression (green data). Constitutively expressed pCMV-H2B-cerulean (blue data) remains constant (control). Compare with the single-cell tracks in Supplementary Fig. 13 and the response to modulation of doxycycline in Supplementary Fig. 14. d, Single-cell response for two individual cells (solid and dashed lines, colours as in c). Black arrows mark cell divisions. e, Single-cell traces in d replotted, but shifted up after each cell division event to 'add back' sister-cell fluorescence, to show the continuity of Notch activity (see also Supplementary Fig. 13). f, Histogram of τ_{rise} from 26 non-overlapping cell lineages (Supplementary Fig. 13). g, Notch response to both *cis*- and *trans*-Delta. Data shown are from two duplicate movies acquired at each of 12 D_{plate} values for hN1G4$^{\mathrm{esn}}$ cells. Green colouring indicates data that exceed a detection threshold. Note that onset (the black-to-green transition) occurs at approximately the same time for all D_{plate} values. h, Simulations based on the model in Box 1 are qualitatively similar to data in g (see Supplementary Information and Supplementary Fig. 16 for model details). a.u., arbitrary units.

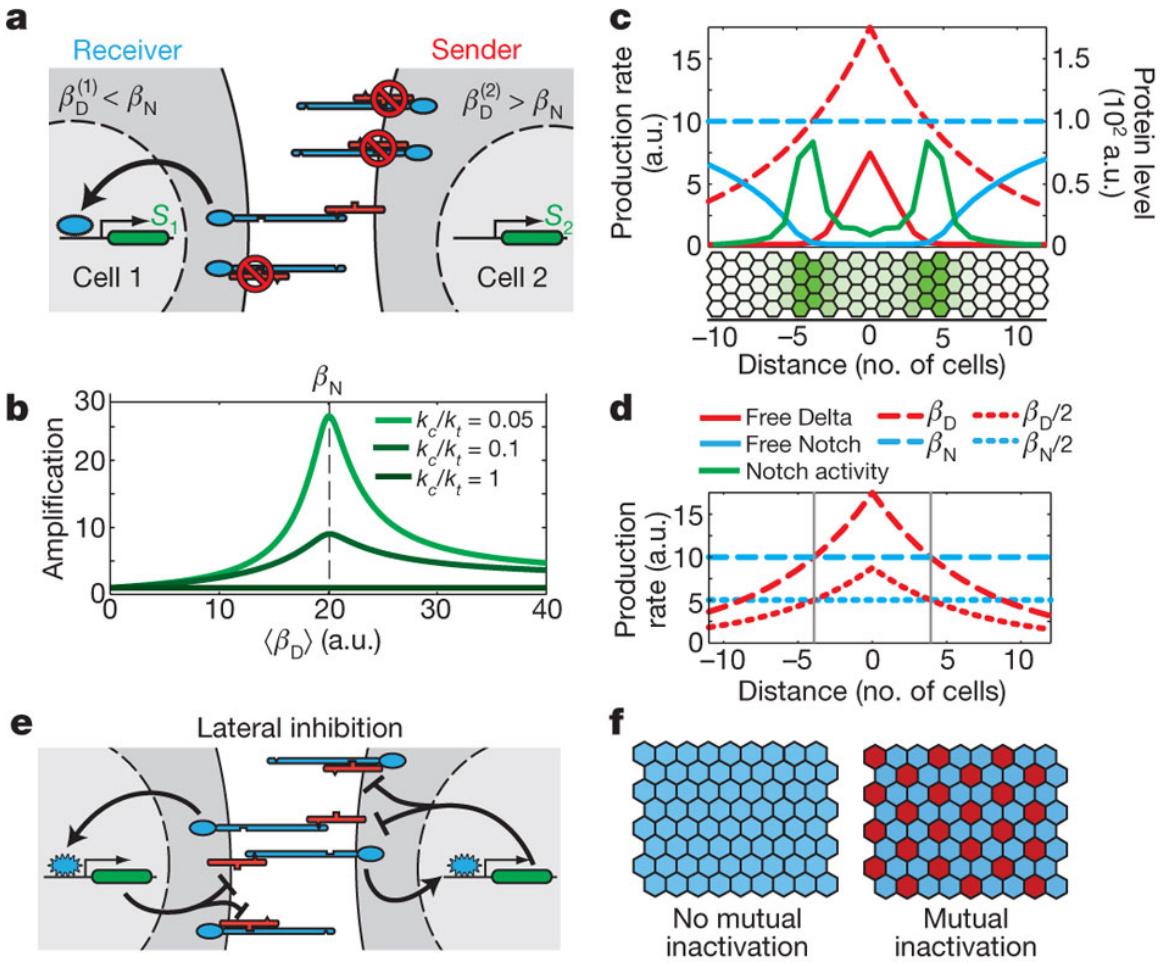

Figure 4: The mutual-inactivation model in multicellular patterning. a, Signal amplification. The two interacting cells have the same amount of Notch (here, two molecules) but different amounts of Delta (one or three molecules). Owing to the *cis*-interaction between Notch and Delta, signalling is strongly biased to cell 1. b, Notch amplifies differences between cells. Signal amplification, $(S_1/S_2 - 1)/(\beta_D^{(2)}/\beta_D^{(1)} - 1)$, for two interacting cells, with different Delta production rates, $\beta_D^{(2)} = 1.35\beta_D^{(1)}$ (see model in Supplementary Information). The x axis shows the average Delta production rate, $\langle\beta_D\rangle = (\beta_D^{(2)} + \beta_D^{(1)})/2$. Maximum amplification occurs when Delta production rates flank β_N (vertical dashed line). Stronger mutual inactivation (smaller k_c/k_t) increases signal amplification. c, d, Sharp boundary formation in response to a gradient of Delta production. c, Simulation of a field of interacting cells in which Delta production rates decay exponentially from the centre, according to $\beta_D(x) = \beta_D^0 \exp(-x/x_0)$ with $x_0 = 7$ cells (dashed red line). The Notch production rate, β_N, is constant (dashed blue line). The resulting free Notch and Delta protein levels are indicated (solid lines). Notch activation occurs in two sharply defined columns of cells (green line in plot and green cells in cellular diagram). d, Suppression of mutant phenotypes is explained by the mutual-inactivation model. Grey lines indicate positions where $\beta_N = \beta_D(x)$, leading to Notch activity peaks. Simultaneous reduction of both Notch and Delta production rates by half maintains boundary positions (dotted lines) (Supplementary Fig. 10). e, f, Mutual inactivation facilitates lateral inhibition patterning (e). In the absence of cooperativity in regulatory feedback, a standard lateral-inhibition model [24] cannot pattern (f, left) but a model of lateral inhibition with mutual inactivation can (f, right).

Methods summary

We assembled genetic constructs and cell lines by standard methods (Supplementary Table 1). All cell lines used in the main text (Supplementary Table 2) were derived from T-REx-CHO-K1(Invitrogen). Cell lines were constructed by sequential rounds of Lipofectamine 2000 (Invitrogen) transfection and selection. We isolated stably transfected clones by limiting dilution or FACS.

Time-lapse microscopy was performed with cells plated on 24-well glass-bottom plates (MatTek). For plate-bound Delta experiments, IgG-Delta^{ext} was adsorbed to the plate together with 5 μg ml^{-1} hamster fibronectin (Innovative Research) before cell plating. Before imaging, cells were switched to a low-fluorescence medium, consisting of 5% FBS in αMEM lacking riboflavin, folic acid, phenol red and vitamin B12. Movies were acquired using an Olympus IX81-ZDC microscope, equipped with an environmental chamber at 37°C supplying 5% CO_2, a $\times$20, numerical-aperture-0.7 objective, and automated acquisition software (METAMORPH (version 7.5.6.0), Molecular Devices).

We obtained Western blots for Gal4 using standard protocols. Blots were probed using rabbit anti-Gal4 DBD primary antibody (sc-577, Santa Cruz Biotechnology; 1:200) followed by incubation with horseradish peroxidaselabelled anti-rabbit IgG secondary antibody (Amersham; 1:2,000). Bands were quantified using a VersaDoc gel imaging system (Bio-Rad). Quantitative PCR with reverse transcription was performed using standard protocols based on the RNeasy kit (Qiagen) and the iScript cDNA synthesis kit (Bio-Rad).

We analysed co-culture experiments for YFP fluorescence using a FACScalibur flow cytometer (Becton Dickinson) and standard protocols. Movies were analysed in several stages. First, individual cell nuclei were identified in CFP images using a custom algorithm (MATLAB, MathWorks R2007a) based on edge detection and thresholding of constitutively expressed H2B-cerulean fluorescence. Then, for analysis of single-cell expression trajectories, individual nuclei were tracked across frames using custom software (MATLAB, C) based on the softassign algorithm (Supplementary Information). All single-cell trajectories were validated manually. For further details, see Supplementary Information.

References

1. Artavanis-Tsakonas, S., Rand, M. D. & Lake, R. J. Notch signaling: Cell fate control and signal integration in development. *Science* **284**, 770-776 (1999).

2. Goodyear, R. & Richardson, G. Pattern formation in the basilar papilla: Evidence for cell rearrangement. *J. Neurosci.* **17**, 6289-6301 (1997).

3. Heitzler, P. & Simpson, P. The choice of cell fate in the epidermis of Drosophila. *Cell* **64**, 1083-1092 (1991).

4. Huppert, S. S., Jacobsen, T. L. & Muskavitch, M. A. Feedback regulation is central to Delta-Notch signalling required for Drosophila wing vein morphogenesis. *Development* **124**, 3283-3291 (1997).

5. De Celis, J. F., Bray, S. & Garcia-Bellido, A. Notch signalling regulates veinlet expression and establishes boundaries between veins and interveins in the Drosophila wing. *Development* **124**, 1919-1928 (1997).

6. Bray, S. J. Notch signalling: A simple pathway becomes complex. *Nature Rev. Mol. Cell Biol.* **7**, 678-689 (2006).

7. de Celis, J. F. & Bray, S. Feed-back mechanisms affecting Notch activation at the dorsoventral boundary in the Drosophila wing. *Development* **124**, 3241-3251 (1997).

8. Micchelli, C. A., Rulifson, E. J. & Blair, S. S. The function and regulation of cut expression on the wing margin of Drosophila: Notch, Wingless and a dominant negative role for Delta and Serrate. *Development* **124**, 1485-1495 (1997).

9. Klein, T., Brennan, K. & Arias, A. M. An intrinsic dominant negative activity of Serrate that is modulated during wing development in Drosophila. *Dev. Biol.* **189**, 123-134 (1997).

10. Miller, A. C., Lyons, E. L. & Herman, T. G. cis-Inhibition of notch by endogenous delta biases the outcome of lateral inhibition. *Curr. Biol.* **19**, 1378-1383 (2009).

11. Cordle, J. *et al.* A conserved face of the Jagged/Serrate DSL domain is involved in Notch trans-activation and cis-inhibition. *Nature Struct. Mol. Biol.* **15**, 849-857 (2008).

12. Matsuda, M. & Chitnis, A. B. Interaction with Notch determines endocytosis of specific Delta ligands in zebrafish neural tissue. *Development* **136**, 197-206 (2009).

13. Kakidani, H. & Ptashne, M. GAL4 activates gene expression in mammalian cells. *Cell* **52**, 161-167 (1988).

14. Struhl, G. & Adachi, A. Nuclear access and action of notch in vivo. *Cell* **93**, 649-660 (1998).

15. Aster, J. C. *et al.* Essential roles for ankyrin repeat and transactivation domains in induction of T-cell leukemia by Notch1. *Mol. Cell. Biol.* **20**, 7505-7515 (2000).

16. Yang, L. T. *et al.* Fringe glycosyltransferases differentially modulate Notch1 proteolysis induced by Delta1 and Jagged1. *Mol. Biol. Cell* **16**, 927-942 (2005).

17. Rothenberg, E. V., Moore, J. E. & Yui, M. A. Launching the T-cell-lineage developmental programme. *Nature Rev. Immunol.* **8**, 9-21 (2008).

18. Varnum-Finney, B. *et al.* Immobilization of Notch ligand, Delta-1, is required for induction of notch signaling. *J. Cell Sci.* **113**, 4313-4318 (2000).

19. Wang, S. *et al.* Notch receptor activation inhibits oligodendrocyte differentiation. *Neuron* **21**, 63-75 (1998).

20. Rosenfeld, N., Young, J. W., Alon, U., Swain, P. S. & Elowitz, M. B. Gene regulation at the single-cell level. *Science* **307**, 1962-1965 (2005).

21. Jacobsen, T. L., Brennan, K., Arias, A. M. & Muskavitch, M. A. Cis-interactions between Delta and Notch modulate neurogenic signalling in Drosophila. *Development* **125**, 4531-4540 (1998).

22. Shaye, D. D. & Greenwald, I. LIN-12/Notch trafficking and regulation of DSL ligand activity during vulval induction in Caenorhabditis elegans. *Development* **132**, 5081-5092 (2005).

23. De Celis, J. F. & Bray, S. J. The Abruptex domain of Notch regulates negative interactions between Notch, its ligands and Fringe. *Development* **127**, 1291-1302 (2000).

24. Collier, J. R., Monk, N. A., Maini, P. K. & Lewis, J. H. Pattern formation by lateral inhibition with feedback: A mathematical model of Delta-Notch intercellular signalling. *J. Theor. Biol.* **183**, 429-446 (1996).

25. Plahte, E. Pattern formation in discrete cell lattices. *J. Math. Biol.* **43**, 411-445 (2001).

26. Melen, G. J., Levy, S., Barkai, N. & Shilo, B. Z. Threshold responses to morphogen gradients by zero-order ultrasensitivity. *Mol. Syst. Biol.* **1**, doi:10.1038/ msb4100036 (2005).

27. Levine, E., Zhang, Z., Kuhlman, T. & Hwa, T. Quantitative characteristics of gene regulation by small RNA. *PLoS Biol.* **5**, e229 (2007).

28. Buchler, N. E. & Louis, M. Molecular titration and ultrasensitivity in regulatory networks. *J. Mol. Biol.* **384**, 1106-1119 (2008).

29. Lenz, D. H. *et al.* The small RNA chaperone Hfq and multiple small RNAs control quorum sensing in Vibrio harveyi and Vibrio cholerae. *Cell* **118**, 69-82 (2004).

Supplementary Information

Construct Name	Promoter	Gene	Mammalian Selection	Role in this work
pEV-UAS-H2B-citrine	UAS	H2B-citrine	Zeocin	Reporter for hN1-Gal4^{esn}
pEV-12xCSL-H2B-citrine	12xCSL	H2B-citrine	Zeocin	Reporter for hN1
pcDNA3-hN1-mod1	CMV	hNotch1	Neomycin	hN1 construct
pcDNA3-hN1-mcherry	CMV	hN1-mcherry	Neomycin	hN1 construct (used)
pCDNA3-hNECD – Gal4^{esn}	CMV	hNECD – Gal4^{esn}	Neomycin	hN1-Gal4^{esn} construct
pcDNA5/TO-hNICD-Gal4^{esn}	CMV-TO	hNICD-Gal4^{esn}	Hygromycin	hNICD-Gal4^{esn}
pcDNA5/TO-Delta-mcherry	CMV-TO	Delta-mcherry	Hygromycin	Inducible Delta-mCherry
pcDNA5/TO-Gal4^{esn}	CMV-TO	Gal4^{esn}	Hygromycin	Inducible Gal4^{esn}
pCS-H2B-cerulean	CMV	H2B-cerulean	-	Segmentation color
pcDNA6-UAS-H2B-citrine	UAS	H2B-citrine	Blasticidin	Reporter in dual reporter line
pEV-12xCSL-H2B-mcherry	12xCSL	H2B-mcherry	Zeocin	Reporter in dual reporter line

Figure : Supplementary Table S1: Table of plasmids/constructs

Stable Cell Line	Parental Line	Transfected Construct	Antibiotic Selection
T-REx-CHO-K1 (Invitrogen)	-	-	Blasticidin (10 ug/ml)
12xCSL-H2B-Citrine	T-REx-CHO-K1	pEV-12xCSL-H2B-Citrine	Zeocin (400 ug/ml), Blasticidin (10 ug/ml)
UAS-H2B-Citrine + CMV-H2B-Cerulean	T-REx-CHO-K1	pEV-UAS-H2B-Citrine pCS-H2B-Cerulean	Zeocin (400 ug/ml), Blasticidin (10 ug/ml)
hN1-No-Delta	12xCSL-H2B-Citrine	pcDNA3-hN1-mCherry	Zeocin (400 ug/ml), Blasticidin (10 ug/ml), Geneticin (600 ug/ml)
hN1G4^{esn}-No-Delta	UAS-H2B-Citrine + CMV-Cerulean	pcDNA3-hNECD-Gal4^{esn}	Zeocin (400 ug/ml), Blasticidin (10 ug/ml), Geneticin (600 ug/ml)
hN1	hN1-No-Delta	pcDNA5-TO-Dl-mCherry pCS-H2B-Cerulean	Zeocin (400 ug/ml), Blasticidin (10 ug/ml), Geneticin (600 ug/ml), Hygromycin (500 ug/ml)
hN1G4^{esn}	hN1G4^{esn}-No-Delta	pcDNA5-TO-Dl-mCherry	Zeocin (400 ug/ml), Blasticidin (10 ug/ml), Geneticin (600 ug/ml), Hygromycin (500 ug/ml)
TO-DMC	T-REx-CHO-K1	pcDNA5-TO-Dl-mCherry	Hygromycin (500 ug/ml), Blasticidin (10 ug/ml)
TO-DMC+hN1G4^{esn} (for fig. S9)	TO-DMC	pcDNA3-hNECD-Gal4^{esn}	Hygromycin (500 ug/ml), Blasticidin (10 ug/ml), Geneticin (600 ug/ml)
TO-Gal4^{esn}	UAS-H2B-Citrine + CMV-H2B-Cerulean	pcDNA5/TO-Gal4^{esn}	Zeocin (400 ug/ml), Blasticidin (10 ug/ml), Hygromycin (500 ug/ml)
UAS-H2B-Citrine	CHO-K1 (CCL-61)	pcDNA-UAS-H2B-Citrine	Blasticidin (10 ug/ml)
UAS-H2B-Citrine + 12xCSL-H2B-mCherry (dual reporter)	UAS-H2B-Citrine	pEV-12xCSL-H2B-Citrine	Zeocin (400 ug/ml), Blasticidin (10ug/ml)

Figure : Supplementary Table S2: Table of cell lines

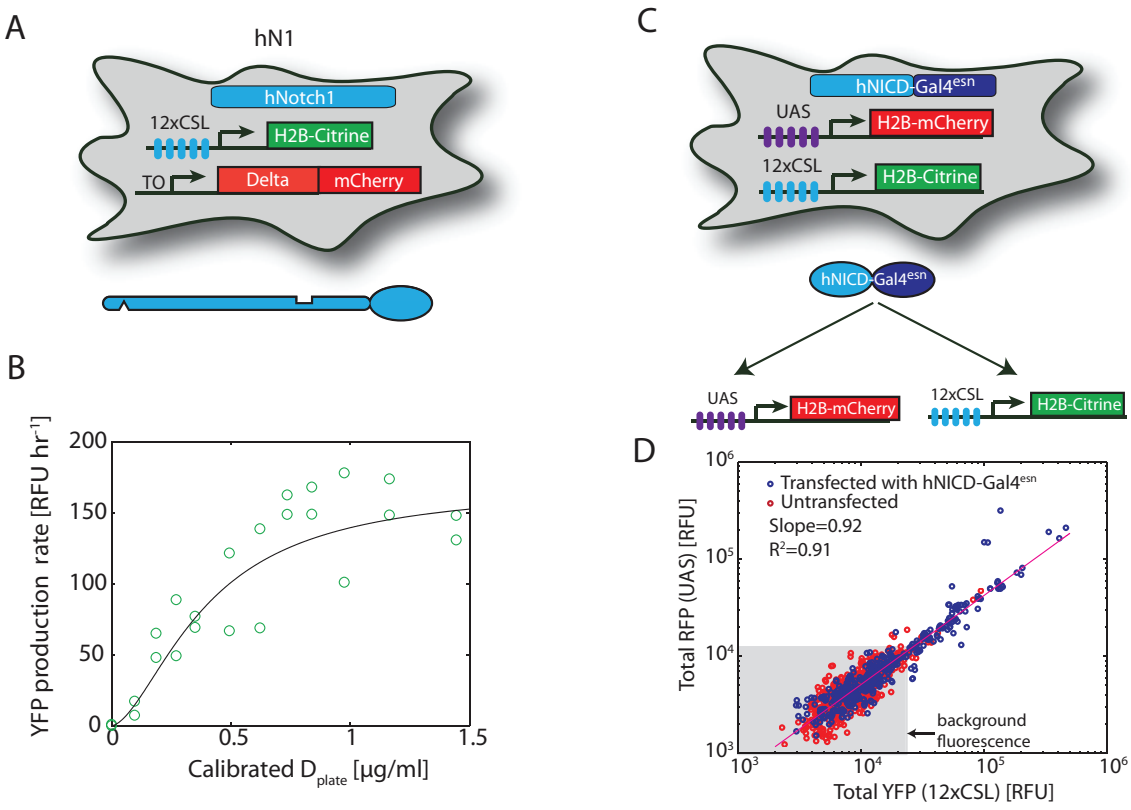

Figure : Figure S1: hN1G4^{esn} and hN1 cell lines exhibit similar response. (A) The hN1 cell line stably incorporates genes for full length hNotch1, Histone 2B (H2B)-Citrine (YFP) reporter controlled by a synthetic 12XCSL promoter[30], and a Tet-inducible Delta-mCherry fusion protein. It also constitutively expresses H2B-Cerulean (CFP) for image segmentation (not shown). Note that the hN1 cell line includes an mCherry domain fused to the C-terminus of hNotch1, which is not detectable experimentally and therefore omitted in the diagram. These cells exhibit no detectable endogenous Notch or Delta activities. (B) Notch response to trans-Delta in the hN1 cell line is similar to the one in hN1G4^{esn} (Fig. 2). Hill coefficient $n = 1.6$ (95% CI: 0.6-2.5). (C-D) Co-linear response of the 12xCSL and the UAS promoters. (C) A fusion protein consisting of Gal4^{esn} and the Notch Intracellular Domain (ICD) was transiently transfected into a CHO-K1 cell line containing two stably integrated reporters: 12xCSL-H2B-Citrine and UAS-H2B-mCherry. (C) Total RFP fluorescence versus total YFP fluorescence for transfected (blue circles) or untransfected (red circles) cells shows a co-linear response of the two reporters to the fusion activator (plotted on a log-log scale). A linear regression fit shows a slope of 0.92 ($R^2 = 0.91$), corresponding to a nearly linear relation between the two reporters (red line). Background fluorescence (gray area) is due to basal leakiness of reporters. Note that, due to the finite transfection efficiency of the transient transfection, only some of the cells contain the fusion activator. Data points are extracted from fluorescence images of cells, and analyzed using the techniques described in the text and methods. This result together with the non-cooperative behavior of the Gal^{esn}-UAS system shown in Fig. S2 is consistent with a non-cooperative activation of the 12xCSL promoter by Notch ICD.

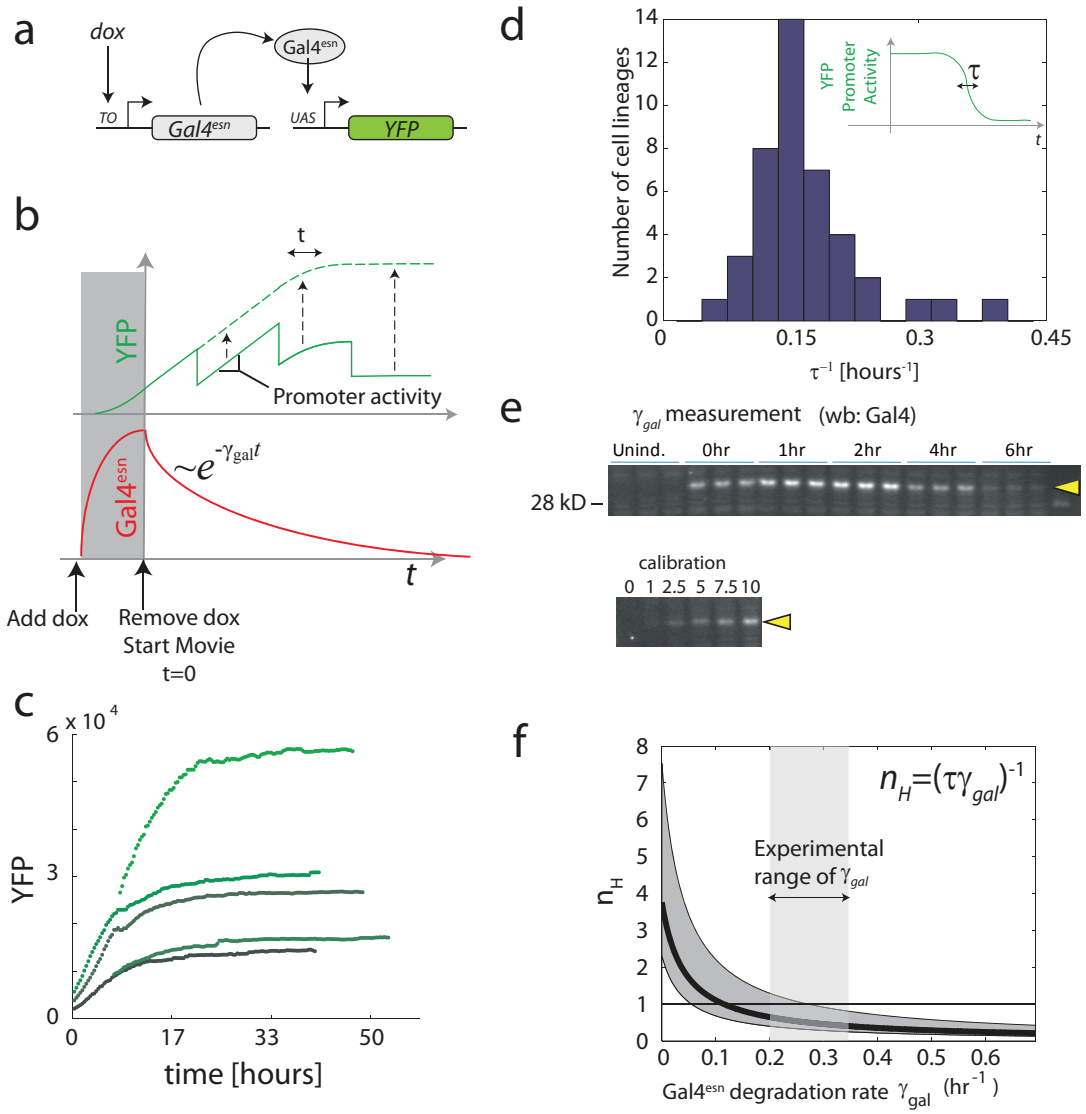

Figure S2 (caption on next page)

Figure *(previous page)*: Figure S2 (previous page): The Gal4^{esn}-UAS transcription factor-promoter interaction shows no cooperativity. This figure describes a measurement of the relationship between Gal4^{esn} concentration and the transcriptional activity of its target UAS promoter. As in Fig. 3A and ref. 2, the approach involves allowing the transcription factor to decay and/or dilute while following the activity of its target promoter. (a) Schematic of cell line design. In this cell line, Gal4^{esn} is expressed from a *tet*-dependent promoter under the control of the doxycyline inducer. Gal4^{esn} activates expression of an H2B-YFP (Citrine) reporter gene. (b) Schematic of experimental design. Prior to the start of the movie, cells were induced with a pulse of doxycycline, which was then washed out immediately before the beginning of time-lapse movie recording. Consequently, Gal4^{esn} was expressed, and then allowed to degrade and/or dilute over time (red curve, bottom panel), while H2B-YFP fluorescence was monitored in individual cell lineages (top panel). γ_{gal} denotes the effective decay rate of Gal4^{esn}. For large enough pulses of Gal4^{esn} expression, the resulting data (shown schematically) would be expected to show constant rates of production of YFP (slopes of green line), interrupted by a 2-fold decrease in YFP levels at cell division events, due to partitioning of the YFP to daughter cells. To avoid discontinuities inherent to cell division events, the "lost" fluorescence after division is replaced (computationally) after each cell division event (dashed line and arrows). The slope of the resulting (dashed) trace is directly related to the activity of the UAS promoter, shown in the inset of (d). Here we focus on τ, the relative timescale required for the slope to fall from 73% to 23% of its initial value as Gal4^{esn} decays (cf. Fig. 3A). (c) Observed YFP accumulation in individual cell lineages. These traces have been corrected for cell division events as shown in (b). (d) Histogram of measured τ values determined from traces like those in (c) shows that, despite variability in initial levels of expression, the timescales, τ, required for turn off were relatively constant. (e) Using a time-course Western blot against Gal4^{esn}, we observed the Gal4^{esn} half-life to be between 3-5 hours (i.e. $\gamma_{gal} \sim 0.2 - 0.33$). A calibration with varying levels of cell lysate was also run to test linearity of measurement (bottom). (f) Inferring the Hill coefficient of the Gal4^{esn}-UAS interaction based on the measured values of τ and γ_{gal}, using the relationship shown in equation, inset. The black line shows how measurements of γ_{gal} constrain the possible range of underlying Hill coefficients. The dark gray region indicates the range of n_H values consistent with variability in the measurement of τ in (f). The light gray region indicates the measured range of γ_{gal}. The intersection between the two gray regions provides the range of likely for n_H values. This result shows that the effective cooperativity of the Gal4^{esn}-UAS interaction does not significantly exceed 1.

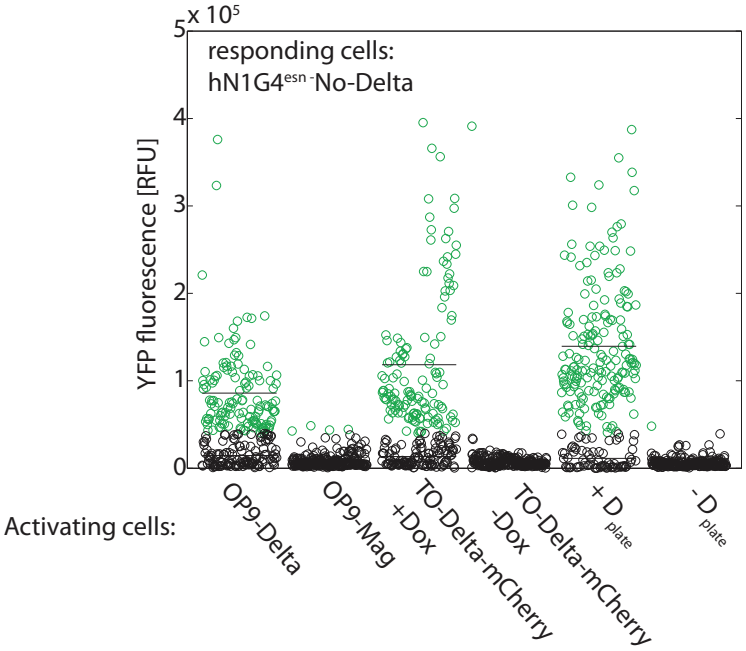

Figure : Figure S3: TO-Delta-mCherry cells trans-activate as efficiently as OP9-Delta cells. We compared the relative abilities of the TO-Delta-mCherry cell line, the OP9-Delta cell line, and D_{plate} to trans-activate Notch. Stromal OP9 cells stably expressing mDll1 (OP9-Delta) and control OP9 cells not expressing Delta[1] (both are a generous gift from Ellen Rothenberg) and inducible CHO TO-Delta-mCherry cells were co-cultured with hN1G4^{esn}-No-Delta cells (containing Notch and a reporter only–see Fig. S5). Cells were plated at a ratio of (70% Delta cells :30% Notch cells) at cell density of 1×10^5 cells/ml and incubated for 48 hours, and then imaged in an epifluorescence microscope. TO-Delta-mCherry cells were either induced with 100ng/ml Dox or not induced, as indicated. A set of controls with Notch reporter cells grown with or without plate-bound Delta (indicated by $+D_{plate}$ and $-D_{plate}$, respectively) were measured at the same time. Green and Black circles correspond to YFP fluorescence of activated and non-activated Notch cells, respectively (n=259 cells in each sample).

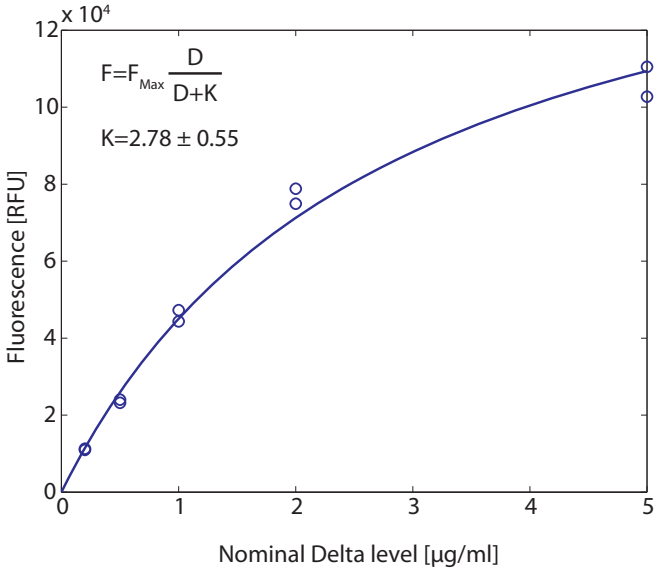

Figure : Figure S4: Calibration of plate bound Delta. Plates were incubated with different concentrations of IgG-Delta^{ext} (see methods for complete protocol). We determined the relationship between the concentration of IgG-Delta^{ext} used during incubation and the amount of IgG-Delta^{ext} actually adsorbed to the plate using a fluorescence binding assay. Right after incubation, plates were treated with anti-human-IgG conjugated to Alexa488 (Invitrogen). Fluorescence levels were measured using a plate reader (Wallac 1420, Perkin-Elmer). As seen in the figure, the binding of IgG-Delta^{ext} starts to saturate at concentrations bigger than 2ug/ml and is well-fit by the Michaelis-Menten curve $D_{plate} = \frac{D_{nominal}}{1+D_{nominal}/K}$, with $K = 2.78$ and where $D_{nominal}$ is the concentration of IgG-Delta^{ext} used in the incubation step. In addition, to assess the spatial uniformity of D_{plate}, we took snapshots of the bound antibody using a fluorescence microscope (not shown). We estimate the plate-plate variation in D_{plate} at 10-20%.

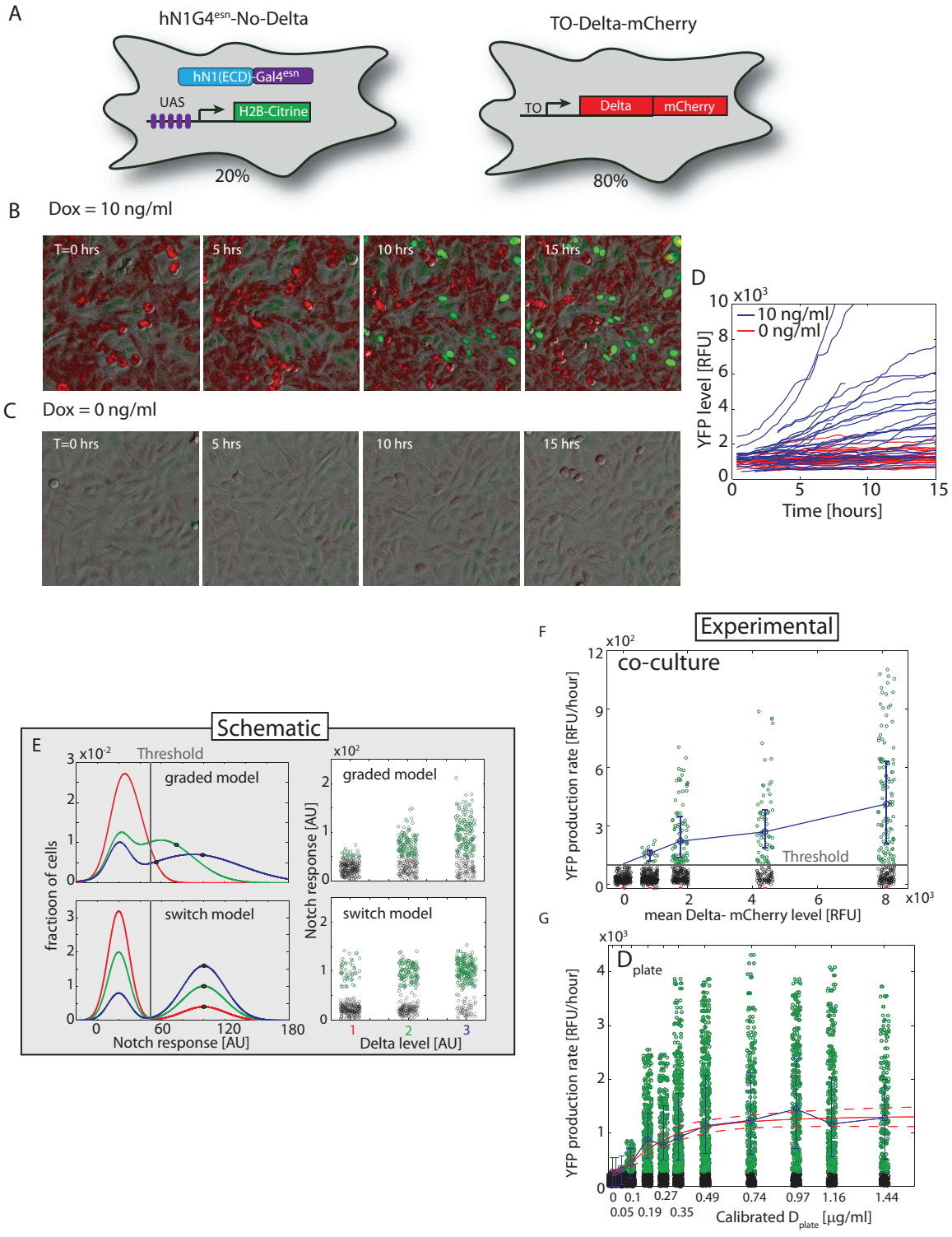

Figure S5 (caption on next page)

Figure : Figure S5 (previous page): Notch activity responds to *trans*-activation by cell-bound Delta in a graded fashion. (A) In order to analyze *trans*-activation between cells, we co-cultured two cell lines, one expressing hN1G4^{esn} and a reporter (hN1G4^{esn}-No-Delta cell line, left), and one containing only inducible Delta-mCherry (TO-DMC cell line, right). See Table S2 for strain descriptions. (B) Filmstrip of intercellular trans-activation taken from Movie S3. Here, the hN1G4^{esn}-No-Delta cell line (green nuclei) was co-cultured with the TO-DMC cell line induced with 10ng/ml doxycycline to express Delta-mCherry (red cytoplasmic staining). Cell lines were co-cultured at a density ratio of 80:20 (TO-DMC: hN1G4^{esn}-No-Delta). Note the increasing Notch reporter fluorescence over time. (C) In contrast, without induction (no doxycycline), we observed much lower activation of Delta-mCherry expression and Notch activity in the reporter cell lines. Note that color (intensity) scales in (B) and (C) are the same. (D) Single cell tracks from the two movies shown in B and C. (E) Distinguishing between two possible models of activation in this experiment: graded and switch-like (schematic). Both models assume that some fraction of the cells do not respond even at maximal activation (here, we assume 20% 'non responders'). In the graded model, the responding population shows an increase of its median (black circles) response above a threshold, with higher induction levels (coefficient of variation is kept fixed). In the switch-like model, cells are in either the 'on' or 'off' states; only the fraction of cells occupying the 'on' state increases with Delta. Note that the two models predict qualitatively different responses of the mean number of activated cells with increasing Delta. (F) Experimental analysis of Notch reporter activation in individual cells (YFP production rates) at different levels of mean Delta-mCherry induction. The green circles correspond to single cell YFP production rates in the hN1G4^{esn}-No-Delta cell line above the threshold, determined by the basal expression without any Delta-mCherry induction in the TO-DMC cell line (a). The black circles correspond to cells that do not respond or that respond at levels below the threshold. The blue circles correspond to the median of activated cells. Error bars denote the 25 and 75 percentiles of the activated cells' distributions. The response is consistent with a graded, rather than switch-like, model of trans-activation (e). (G) For comparison, a similar analysis was performed on the plate-bound Delta induction data shown in Fig. 2 c,d. Here, individual data points correspond to rates of YFP production. Note the graded, saturating response of the median response (blue data points and line) to D_{plate}. The red lines indicate a best fit of these median responses to a Hill function, with 95% confidence intervals bounded by the dashed red lines. The best fit Hill coefficient was 1.8 ± 0.9, in agreement with values obtained in Fig. 2D. Note that the relative fluorescence unit (RFU) scales in (F) and (G) are different due to the use of different imaging conditions. Together, these results show, first, that plate-bound and cell-expressed Delta trans-activate with similar cooperativity, and second, that the analysis based on population average response shown in Fig. 2D for plate-bound Delta produces equivalent results to the single-cell analysis of activation by cellular Delta.

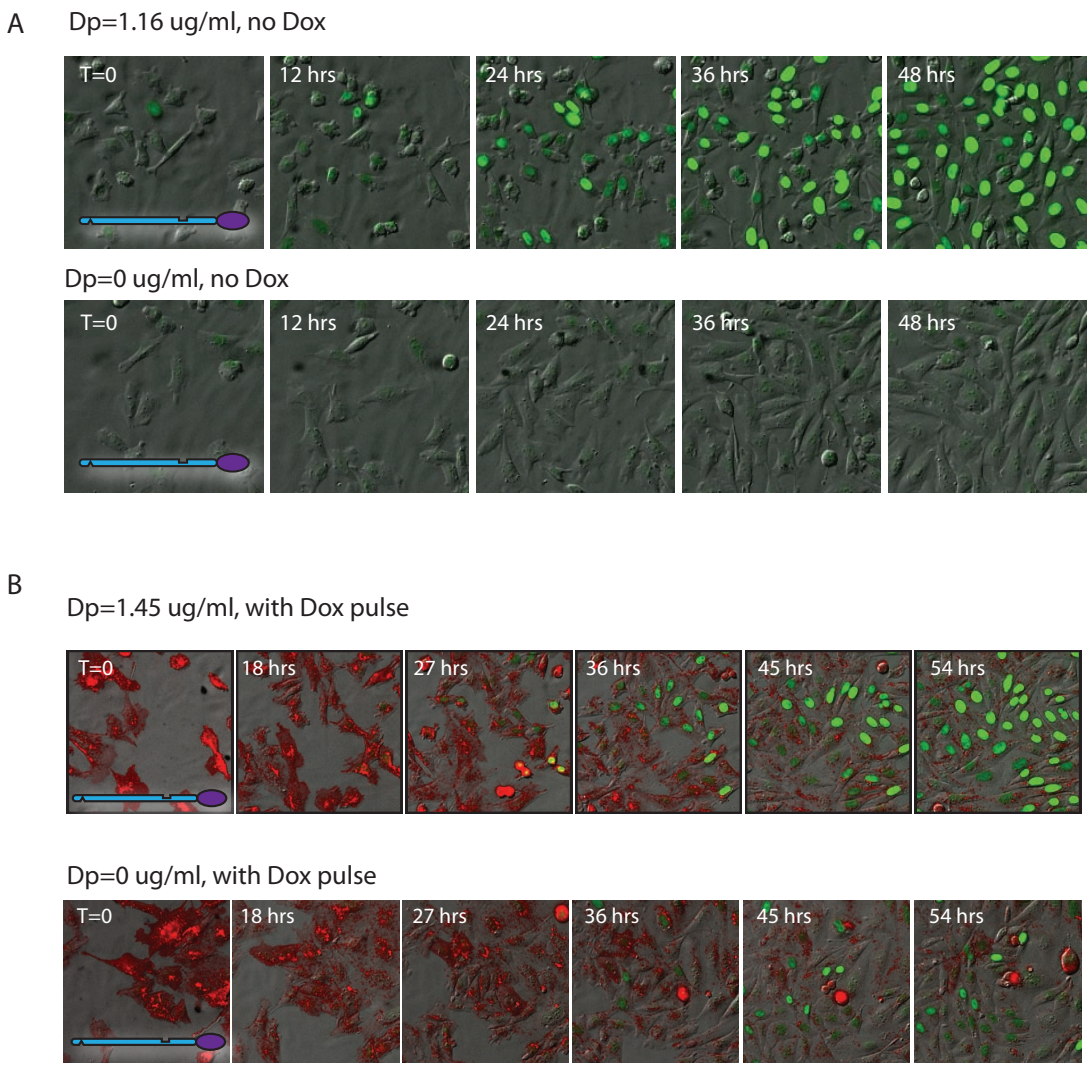

Figure : Figure S6: Induction at D_{plate}=0 is small compared to higher D_{plate} levels. (A) Filmstrips comparing activation of hN1G4^{esn} cells at D_{plate}=0 and D_{plate}=1.16 μg/ml (Fig. 2B). No induction is observed at D_{plate}=0. (B) Filmstrips comparing activation of hN1G4^{esn} cells induced with a doxycycline pulse at D_{plate}=0 and D_{plate}=1.16ug/ml (Fig. 2B). Only very few cells are induced in this case compared to higher D_{plate}. Thus, at this cell density transactivation between hN1G4^{esn} cells has only a small effect (this is also seen in the average data in Fig. 3G).

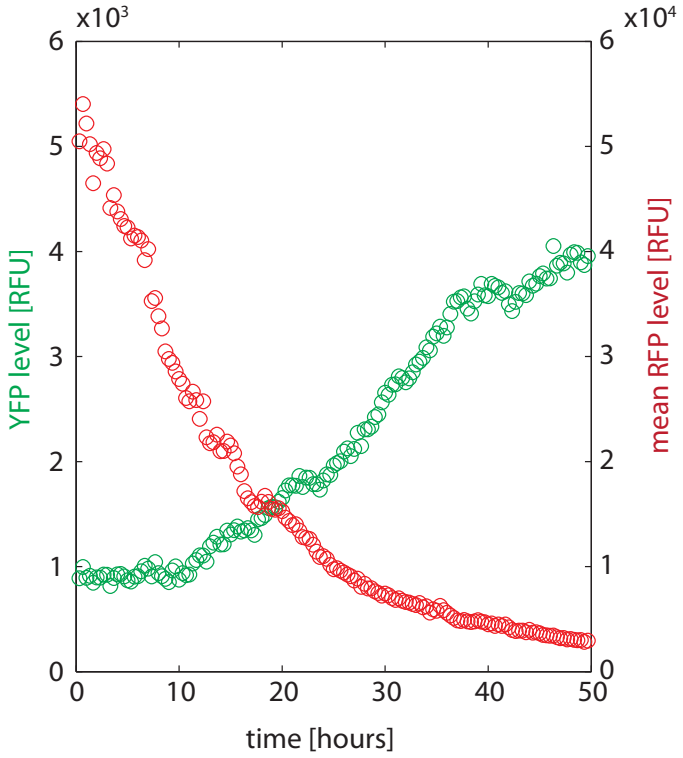

Figure : Figure S7: The hN1 cell line also shows an ultrasensitive response. hN1 cells show delayed turn-on in Notch signaling in response to slow decay of Delta-mCherry. Protocol is as described in Fig. 3A.

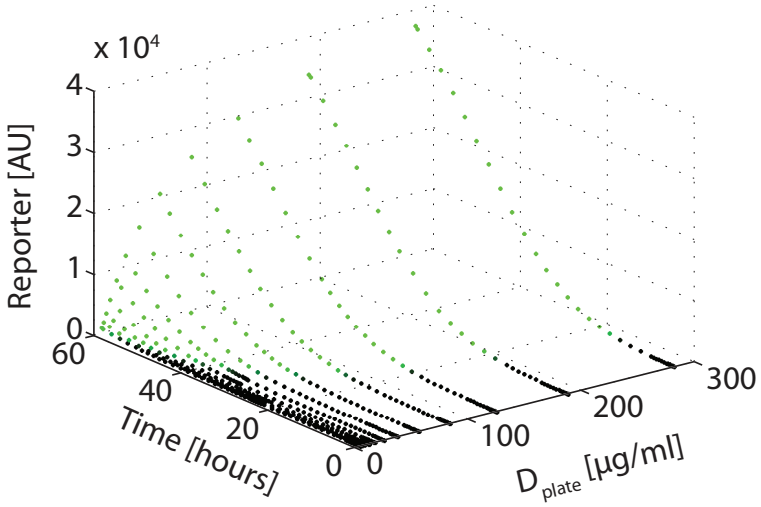

Figure : Figure S8: Delta inactivation by Notch is required for sharp responses to *cis*-Delta at fixed threshold. We simulated a model in which Delta inactivates Notch catalytically. In this model Delta is assumed to be recycled back after interaction with Notch (see theoretical supplementary for derivation and parameters). Note that, unlike the simulations based on the mutual inactivation model (Fig. 3H), here the turn-on curves do not exhibit sharp responses, and the threshold positions vary with D_{plate}. Note that the range of D_{plate} was scaled up to show the full response spectrum because a much higher D_{plate} is required to overcome the effect of D_{cis}.

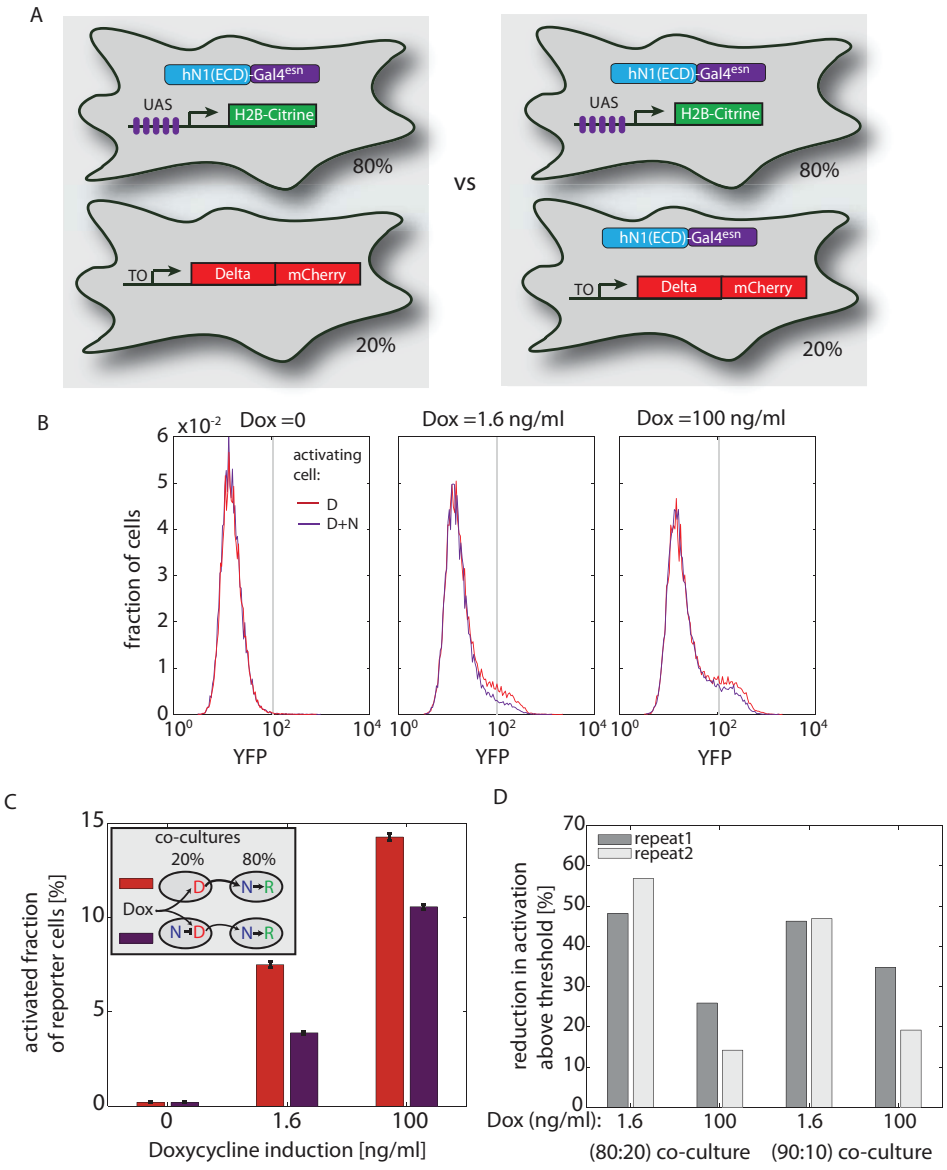

Figure S9 (caption on next page)

Figure : Figure S9 (previous page): Notch cis-inactivates Delta. (A) Cells expressing hN1G4^{esn} and a UAS-H2B-Citrine reporter (hN1G4^{esn}-No-Delta) were co-cultured with cells expressing Delta (TO-DMC) or cells expressing Notch and Delta (TO-Delta-mCherry+hN1G4^{esn}). Note that TO-Delta-mCherry+hN1G4^{esn} cell line does not contain a reporter. This enables measurement of the response only from the Notch reporter cells. The level of Delta-mCherry in both of the inducing cell lines is similar across a wide dox induction range (not shown) providing evidence that Notch does not induce Delta degradation. Experimental procedure: Cells were co-cultured at the indicated ratios and plated at 1×10^5 cells/ml. Cells were subjected to a 12 hour doxycycline pulse (weak induction) with different dox levels. FACS analysis was performed 24 hours after the dox pulse using a FACSCalibur. (B) Fluorescence distributions in co-culture experiments. A total of 50,000 cells were measured for each sample. Only cells containing the Notch reporter are shown. The activation threshold (gray vertical line) is defined as a fluorescence level greater than that of 99.5% of negative control (dox=0). (C) Fraction of cells above threshold for the co-culture experiments shown in (B). Standard errors were estimated using a bootstrapping method by calculating the standard error of 20 non-overlapping subsamples. Note that the difference in the fraction of activated cells between the two samples is largest at intermediate Delta induction. This is consistent with the mutual inactivation model since the titration level of Notch should have larger effect at lower Delta expressions. (D) Qualitatively similar results were obtained in a repeat performed on a different day (dark gray vs light gray). Furthermore the relative reduction in activation of cells between the two samples remains similar even when the relative fractions of the two cell lines are changed to 10% Delta (or Delta+ Notch) cells and 90% Notch reporter cells.

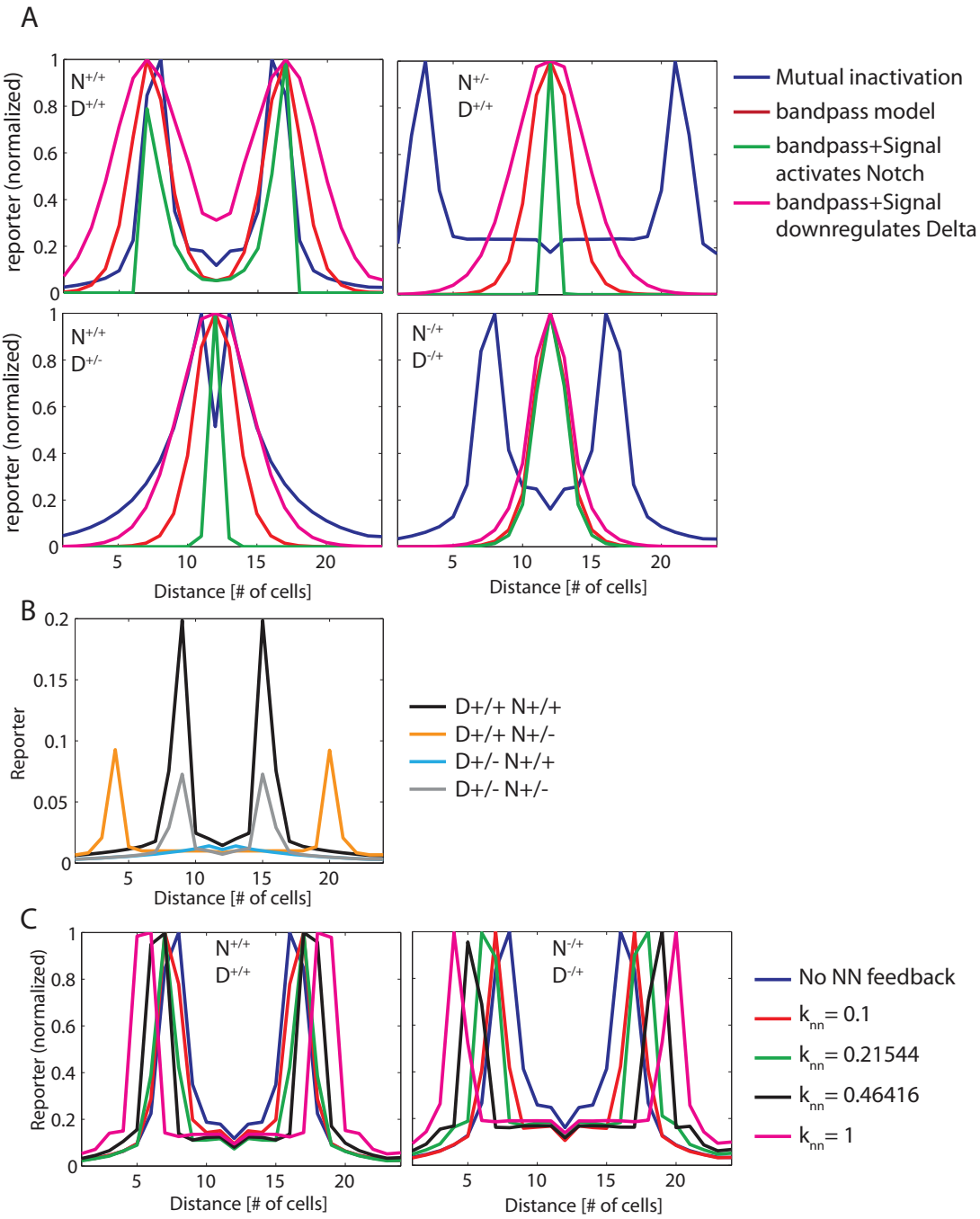

Figure S10 (caption on next page)

Figure : Figure S10 (previous page): Comparison of the mutual inactivation model to alternative models of boundary formation. (A) Three alternative models are compared to the mutual inactivation model discussed in the main text (blue). The 'band-pass' model (red) assumes that the Notch target promoter responds only to a narrow range ("band") of Notch signaling levels. This band-pass function was represented by a product of activating and repressing Hill functions, each with Hill coefficient, $n = 8$ (see Section III of the supplementary modeling text). The high Hill coefficient is required to match the sharpness of the pattern generated with that obtained in the mutual inactivation model. For simplicity, no *cis*-inhibition was considered in this case. The second alternative model ("bandpass + signal activates Notch", green) adds an additional transcriptional feedback of Notch signaling on the production rate of Notch, so that Notch signaling activates expression of Notch. Such feedback makes the outer edge of the pattern sharper. The third alternative model (magenta, "bandpass + signal downregulates Delta") adds feedback through Delta (Notch signaling downregulates production of Delta). This lateral inhibition type feedback tends to broaden the signal response. All models are defined in the supplementary theory section. See Table S3 for parameter values. Note that the two feedback models require fine tuning of the parameters to show a qualitative effect of the feedbacks (i.e. to differentiate the feedback models from the simple bandpass). The four different panels correspond to Notch signaling profiles of the different models for $N^{+/+}$, $D^{+/+}$, and $N^{+/-}$ $D^{+/-}$ heterozygous mutants. All profiles were normalized to their maximal level to allow comparison of the boundary positions in different heterozygous mutant combinations. Top left corresponds to the wild-type case. Top right: Only the mutual inactivation model (blue) is consistent with the observed broad but sharp wing vein phenotypes of the $N^{+/-}$ mutant[3]. Bottom left: The $D^{+/-}$ phenotype of the mutual inactivation model (blue), but not the other models, shows broadening of the signaling profile (note the extended tails at a distance of approximately five cell diameters on the x-axis) and eliminates sharp side-bands (note that the central "dip" is an effect of the sharp kink in the morphogen profile at 0, and would not occur with a more realistic morphogen profile). These effects occur when the $D^{+/-}$ mutation makes the Delta production rate smaller than the Notch production rate. See also discussion in (B). Bottom right: In the mutual inactivation model, but not the other models, the double mutant $N^{+/-}$ $D^{+/-}$ regains the wild-type phenotype due to the ratiometric property discussed in Fig. 4D, Box 1, and in the text. This suppression is independent of the exact shape and length scale of the gradient. (B) Strong *cis*-inhibition selectively reduces signaling in the $D^{+/-}$ mutant. Here we plot the four un-normalized mutant profiles for the mutual inactivation model with a different parameter set (Table S3), with stronger *cis*-inhibition. The reporter level for the $N^{+/+}$ $D^{+/-}$ mutant is substantially smaller than those of the wild type and all other mutants at all positions along the morphogen gradient. Such ubiquituous subthreshold activity of the reporter can be expected to resemble the null Delta phenotype of thicker and less sharply defined veins. Note that suppression in the double mutant persists for these new parameters, as shown by the invariance of the positions of the bands between wild-type and $N^{+/-}$ $D^{+/-}$. More generally, suppression in the double mutant is maintained across a wide range of parameter values. (C) Positive feedback through Notch has a modest effect on suppression in the double mutant. Here we considered a variant of the mutual inactivation model in which Notch activity leads to increased expression of Notch. The strength of this feedback is quantified by the parameter k_{nn}, which denotes the amount of Notch signaling necessary to half-maximally induce the additional Notch production (supplementary theory section). Only intermediate values of k_{nn} change the spatial pattern (i.e. broaden it) without destroying its qualitative shape. Within this range, suppression is generally maintained except for a modest expansion ($<\sim 1$ cell) in the double mutant compared to wild-type.

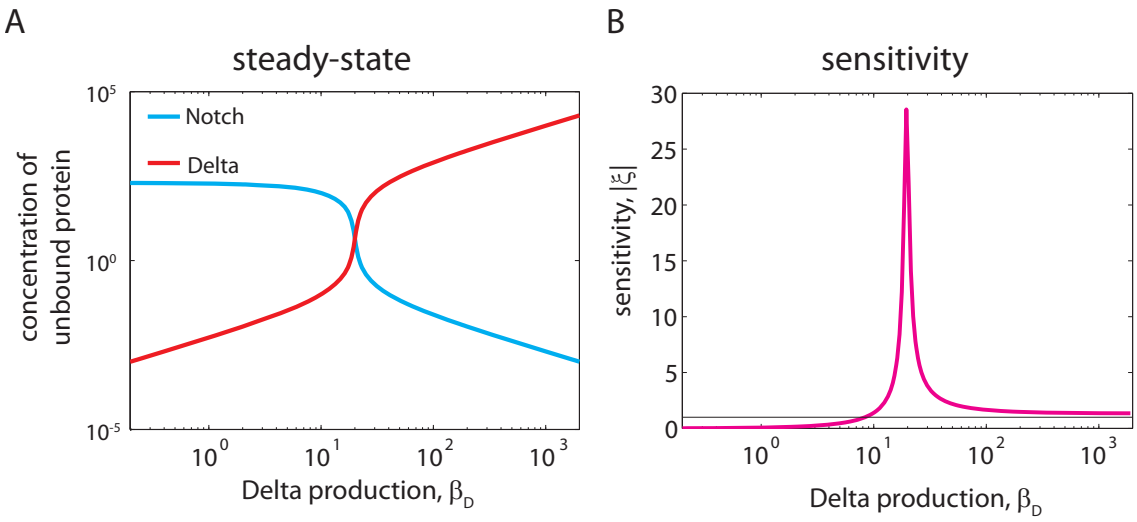

Figure : Figure S11: Steady-state sensitivity of the mutual inactivation switch. (A) The steady state levels of Notch (blue) and Delta (red) are shown with respect to the production rate of Delta, β_D, in a log-log plot, for the case presented in the Box Figure (values given in the Supplementary Table S3). This plot reveals a rapid change in Notch and Delta for a small change in the β_D near the switch location. (B) Steady-state sensitivity of the system, as defined in Box 1, for the conditions of plot A. Note that the sensitivity of the system remains larger than 1 for a very broad range of Delta production rates (to the right of the threshold).

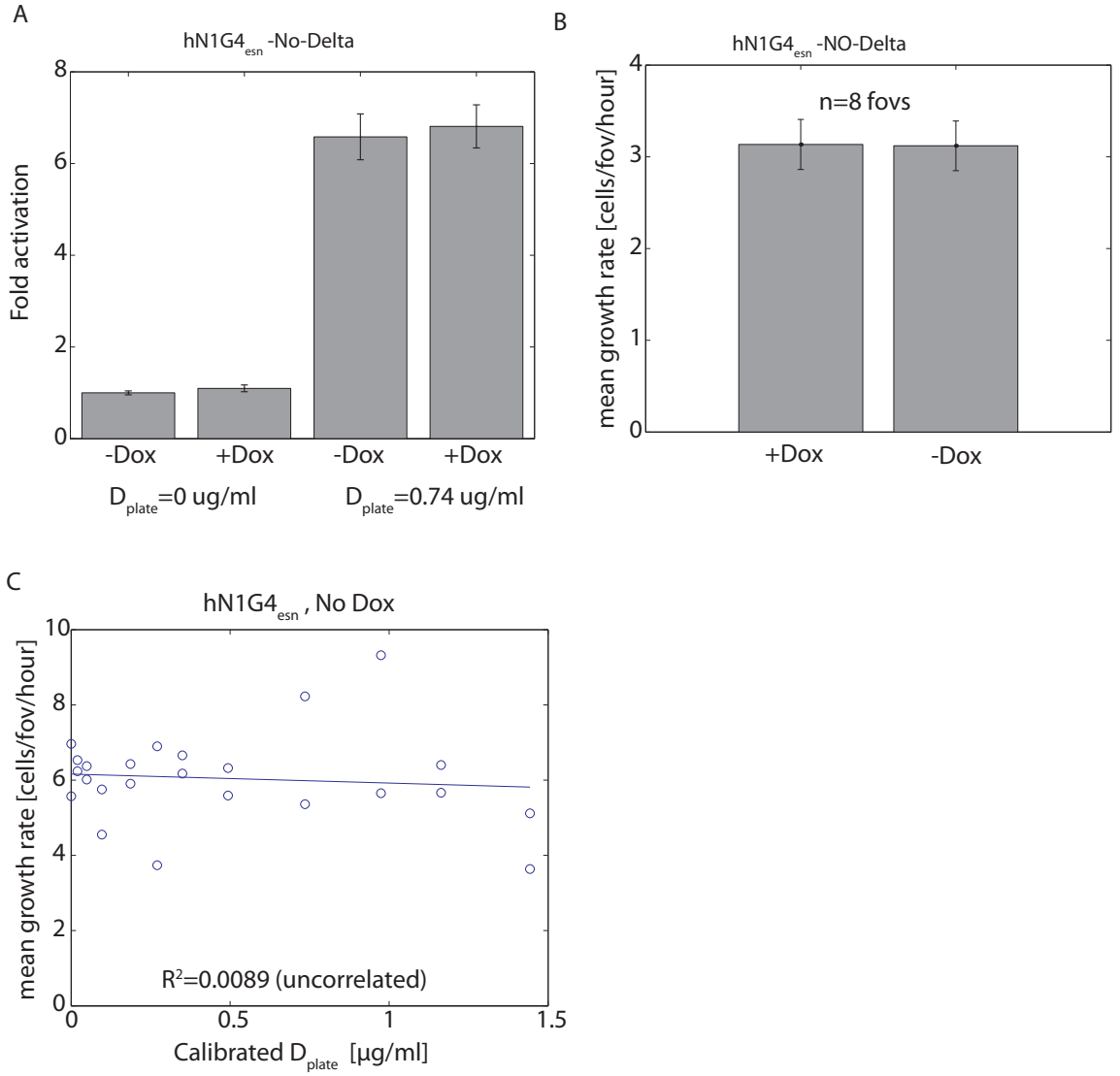

Figure : Figure S12: Negative controls show that Notch signaling is not affected by doxycycline, and growth rate is not affected by doxycycline and D_{plate}. (A) Cells expressing Notch ($hN1G4^{esn}$ -No-Delta) were induced by D_{plate} to similar levels of Notch activity in the presence or absence of 100ng/ml doxycycline (protocol was similar to the ones used in Fig.2), showing that Notch activity is not influenced directly by doxycycine. (B) The growth rate of the Notch reporter cells was not affected by presence of doxycycline. (C) Mean growth rate of the cells shown in Fig. 2C,D,E is not affected by D_{plate}. Growth rate was defined as the rate of increase in the number of cells per field of view (fov) over time.

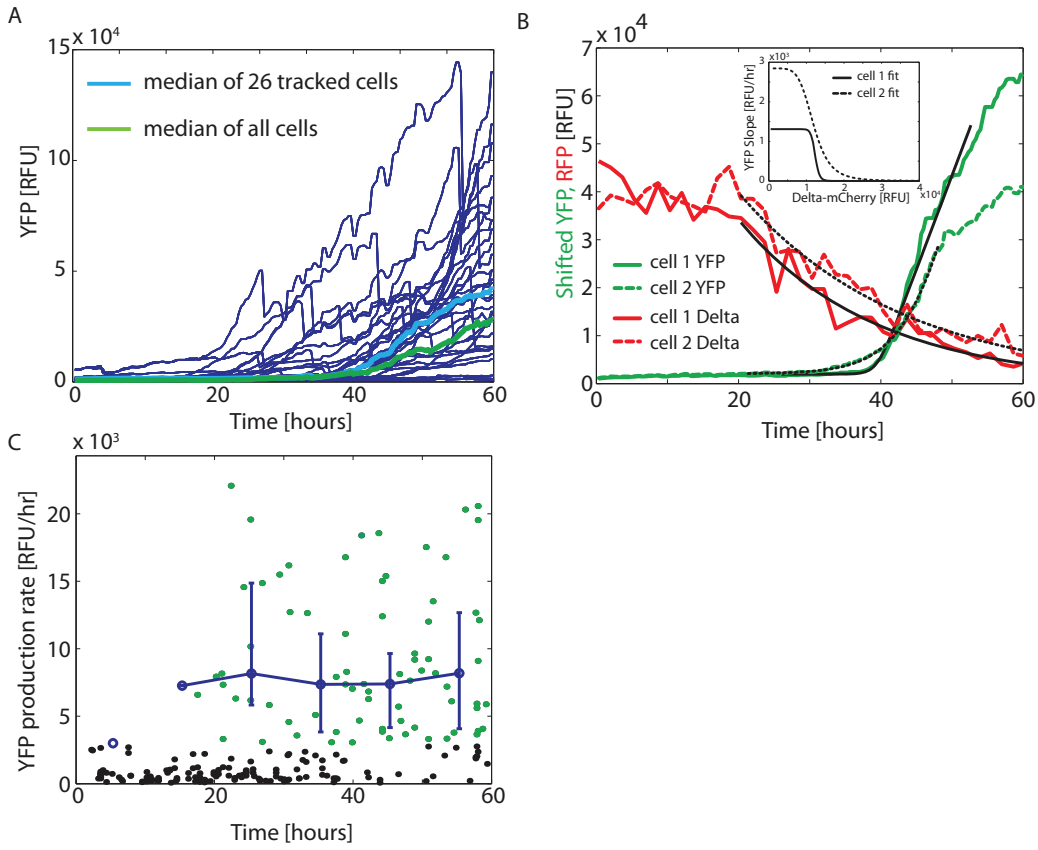

Figure : Figure S13: Relation of population average data (median over all segmented cells) and single cell data. (A) Plots of total cellular fluorescence versus time for each of 26 non-overlapping cell lineages from the movie shown in Figs. 3B, (blue lines). Sudden drops in total fluorescence are due to cell division events, as in Fig. 3D. We compare the median of these 26 responses (cyan) to the median over all cells (green). Note that this latter curve is identical to that shown in Fig. 3. For discussion see supplementary methods. (B) Analysis of sharp responses to *cis*-Delta in individual cells. The concentration of Delta-mCherry (red) and the shifted level of YFP (green, cf. Fig. 3e) are plotted as a function of time for two different cell lineages. Delta-mCherry concentrations were estimated from total Delta-mCherry fluorescence levels by assuming linear growth in cell volume during each cell cycle. The Delta-mCherry data were fit to exponential decays (superimposed black lines). The YFP response curves were fit to generate the turn-on function (superimposed black lines). The fit has four free parameters: a constant offset, a final slope, a turn-on time (t_{on}), and τ_{rise} (see supplementary methods). Inset: plots of resulting Hill function fits for the production rate of YFP as a function of the concentration of Delta-mCherry. These fits produced best fit Hill coefficients of $n = 22 \pm 10$ and $n = 5.5 \pm 0.8$ for cells 1 and 2, respectively. (C) Analysis of slope distributions of *cis*-Delta response shows a switch-like, rather than graded behavior. All 26 single cell traces were divided into short, 6 hour segments. The response on each segment was smoothed and its maximal slope was measured. Black and green points represent the values of individual slopes falling below or above a threshold, respectively. Note that the fraction of activated (green) points, but not their median value, increases over time, consistent with a switch-like model (Fig. 5e). The threshold value was determined from the early time points where cells are off. A few segments far from the switching point were filtered out, corresponding to saturating fluorescence levels or varying YFP expression at very late times (YFP curves in (b)). Similar filtering did not affect the distribution of trans-activation rates (Fig S5g). Blue circles represent the medians of the individual above-threshold (green) slopes in 30 hour bins. Error bars represent the 25th to 75th percentiles of each distribution. Comparison with trans-Delta distributions (Figs. S5e,f,g) shows that the response to *cis*-Delta agrees with a threshold-like model.

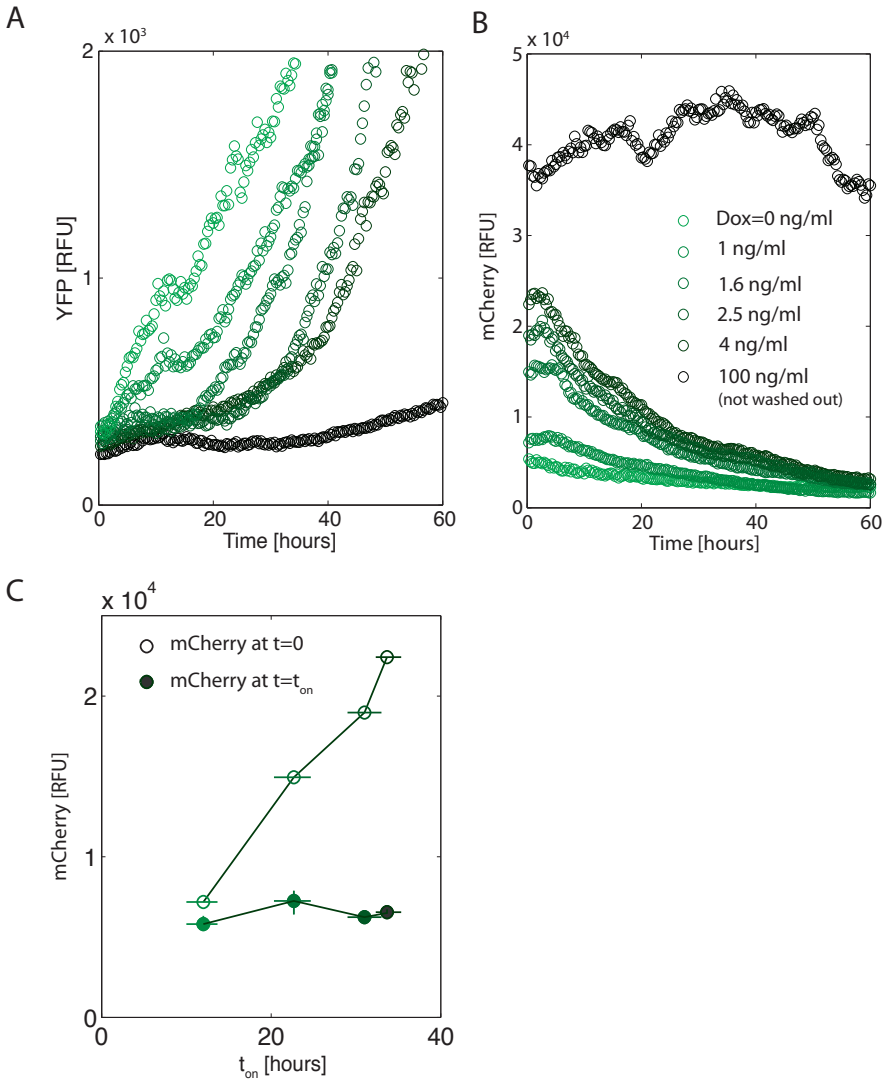

Figure : Figure S14: Initial Delta-mCherry levels correlate with turn-on time. (A) Notch signaling response was measured for varying Delta-mCherry induction levels. The experimental setup was similar to the scheme shown in Fig. 3A. Cells were grown on fixed D_{plate}=0.74 μg/ml and subjected to 12 hour pulses of varying doxycycline concentrations, as indicated in (B). Increased induction levels correspond to higher Delta-mCherry induction (B) and corresponding delays in the turn-on time (A). When doxycycline is not removed from the media (darkest green), cells show a negligible response to D_{plate}. (C) Here, t_{on} was calculated for the data in (A) and (B). For each Delta-mCherry induction level (same legend as in (B)), the Delta-mCherry fluorescence at the start of the movie (t=0) and att$_{on}$ are plotted. These data show that the time of Notch activation, t_{on}, varies with the initial level of Delta-mCherry expression, but occurs at an approximately constant Delta-mCherry concentration, as expected from the experimental scheme in Fig. 3A. Note that fluorescence levels differ in this figure from those in Fig. S13 due to variations in optical parameters (e.g. lamp intensity) between the two experiments.

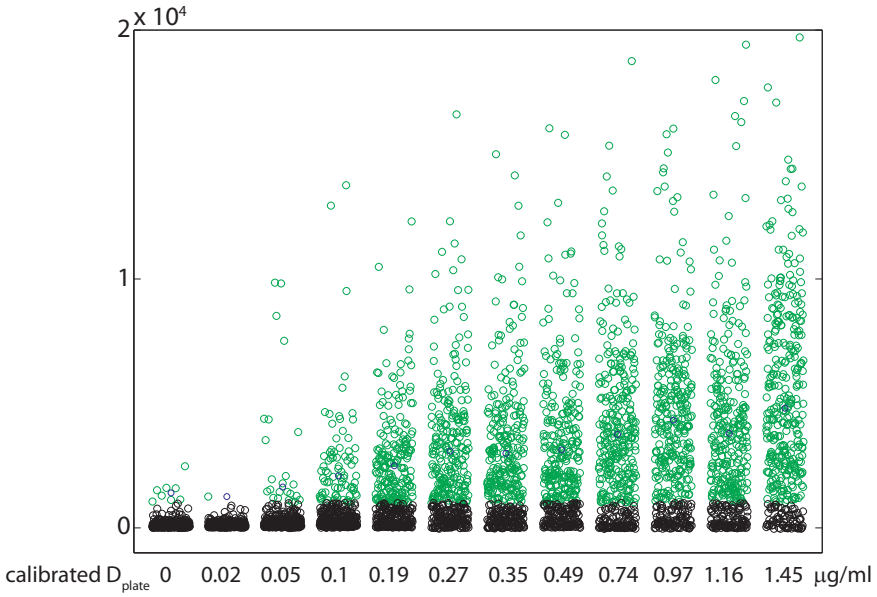

Figure : Figure S15: Distribution of activated cells at different D_{plate} shows graded response. Distributions of hN1G4^{esn} cells after onset of induction (t=50 hours) in Figure 3G. Activated cells (green circles) respond in a graded fashion to D_{plate} levels. Note that even at maximal activation there is a fraction of non-responding cells (black circles). Such variable behavior typically occurs due to silencing of viral promoters such as the CMV promoter used here. The blue circles represent the median of activated cells. Note that in Figure 2C we plot the median of all cells (green and black circles). The median of all cells exhibits a similar slope to the median of activated cells at longer times, but it shows an initial lag in the response. This lag occurs since the median of all cells remains unchanged until more than 50% of the cells respond to D_{plate}. See also discussion in Fig. S5.

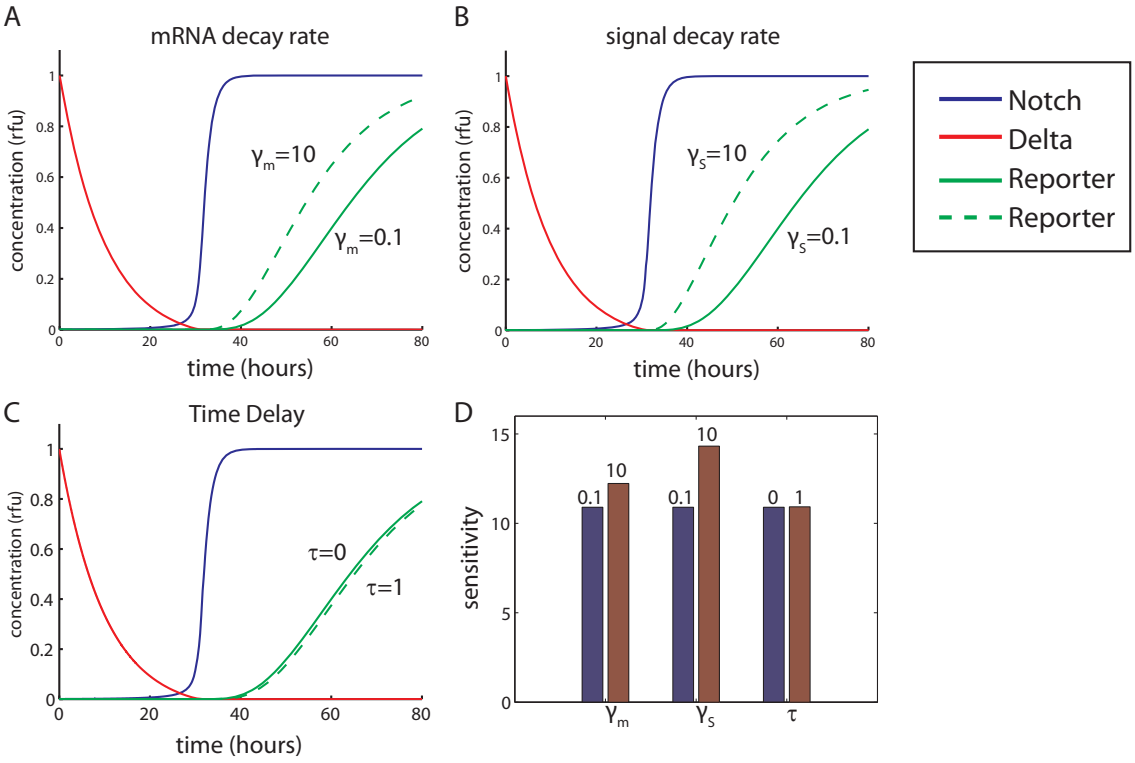

Figure : Figure S16: Effect of finite lifetimes and expression delays in the model. Time traces of Notch (blue), Delta (red), and the reporter (green) obtained from numerical simulations of the *cis*-inhibition model. Solid and dashed green lines are reporter traces for different parameter values, indicated on plot. (A) A 100x increase in the lifetime of the reporter mRNA leads to a delay of a few hours in the turn-on of reporter expression. (B) A similar effect is found for a 100x increase in the lifetime of the Signal. (C) A 1-hour delay in the expression of the reporter from the activating signal leads to a corresponding delay in reporter turn-on. (D) Despite these time shifts, the dynamic sensitivity of the system, defined as the logarithmic derivative of the Signal with respect to the total amount of Delta at any given time instant, is mostly unchanged. The sensitivity coefficient, shown in the bar plot for the different cases presented in plots A-C, increases at most 30% for the smallest lifetimes, and is effectively constant in the presence of delay in the reporter expression.

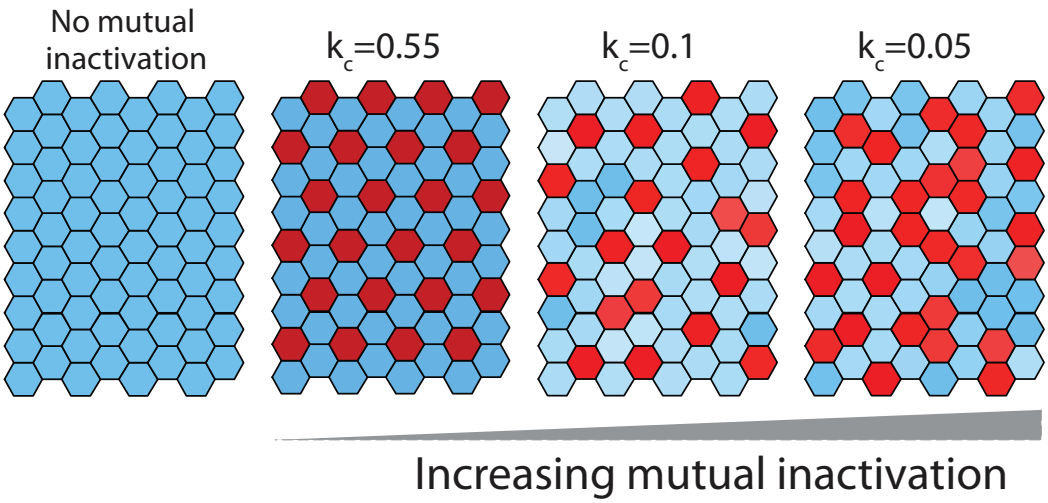

Figure : Figure S17: Lateral inhibition model with mutual inactivation (See theoretical supplementary section) facilitates broader range of patterns. Increasing the strength of mutual inactivation (reduced k_c) enables patterning (second panel), as well as the formation of alternative patterns in which cells with high Delta levels can stably co-exist next to each other (third and fourth panels). Such alternative patterns cannot be achieved using standard lateral inhibition model (even in the presence of cooperative feedback).

Supplementary Methods

Description of genetic constructs

All genetic constructs used in this paper were constructed using standard cloning and PCR techniques. All constructs were fully sequenced and the maps, sequences and construction details are available upon request. We provide below a description of the sources for vectors and DNA fragments used, as well as the main construction steps.

Reporter plasmids pEV-UAS-H2B-Citrine and pEV-12xCSL-H2B-Citrine were constructed as follows: The backbone vector pEV was constructed in the lab by amplifying pSecTagA without the secretion tag Murine Ig kappa-chain V-J2-C (Invitrogen, V900-20) and religating it with the SacII restriction site. The UAS-H2B-citrine and 12xCSL-H2B-Citrine were amplified or subcloned from earlier constructs and they contain the following DNA fragments: H2B-citrine originally obtained from pCS H2B citrine (a gift from Sean Megason and Scott Fraser[4]). UAS was obtained from ULyn-GFP (a gift from Scott Fraser[5]). 12xCSL was amplified from 12xCSL DsRedExpress (a gift from Urban Lendahl[6]).

pcDNA3-hN1-mod1 was constructed by first adding an NheI site to pcDNA3 hN1 (a gift from Jon Aster[7]). To add this NheI site we amplified the DNA fragment between the NotI to the XhoI site and included the NheI site in the reverse primer. The resulting amplicon was ligated into pcDNA3-hNI cut with the same restriction sites. This modified plasmid was then used to create pcDNA3-hN1-mCherry by inserting mCherry originally amplified from pFA6-link-mcherry-SpHis5 (a gift from Roger Tsien and Kurt Thorn[8,9]) into the NheI and XhoI sites.

pcDNA3-hNECD-Gal4^{esn} was constructed by cutting pcDNA3-hN1-mod1 with *Not*I and *Xho*I to remove hNICD. Gal4^{esn} was constructed by PCR amplification from *Saccharomyces cerevisiae* as described in Ptashne et al [10]. Gal4^{esn} amplified with *Not*I and *Sal*I restriction sites was inserted into the cut vector in the sites above. We note here that Gal4^{esn} was chosen over the more popular Gal4-VP16, since it does not use the viral activator VP16 which is extremely strong and generates high background signal.

pcDNA5/TO-hNICD-Gal4^{esn} was constructed using the pcDNA5/TO vector (Invitrogen , V1033-20) cut with *Bam*HI and *Not*I, and by amplifying hNICD-Gal4^{esn} with the same restriction sites from pcDNA3-hN1-Gal4^{esn} (a construct not used here but was constructed by introducing Gal4^{esn} into pcDNA3-hN1-mod1). pcDNA5/TO-Delta-mCherry was constructed by first modifying pcDNA5/TO (Invitrogen, V1033-20) to add a *Nhe*I restriction site by cutting with *Hind*III and *Bam*HI and then ligating in two annealed oligos, which contained the *Nhe*I site. The vector was then digested with *Nhe*I and *Bam*HI. Delta-mCherry was cut from a previously constructed vector with the same restriction sites as pcDNA5/TO. Delta originally came from pBOS-rDelta1[11] (a gift from Gerry Weinmaster) and was fused to mCherry using fusion PCR. The overlapping sequence between the two

fused proteins is: GTGTTATAGCGACTGAGGTTgtgagcaagggcgaggagga. pcDNA5/TO-Gal4^{esn} was constructed by removal of the mCherry from pcDNA5/TO-Gal4^{esn}-mCherry through BamHI and NotI digestion. A small DNA fragment (made from annealed oligos) containing a stop codon as well as the BamHI and NotI overhangs was ligated into the cut pcDNA5/TO-Gal4^{esn}-mCherry vector. The pcDNA5/TO-Gal4^{esn}-mCherry vector was originally created by first performing a fusion PCR of Gal4^{esn} and mCherry (sources for Gal4^{esn} and mCherry previously described). The PCR product was ligated into the pcDNA5/TO vector from Invitrogen. pCS-H2B-cerulean was a gift from Sean Megason and Scott Fraser[4].

pcDNA6-UAS-H2B-Citrine was constructed by subcloning UAS-H2B-citrine from pEV-UAS-H2B-Citrine into pcDNA6/ V5-HisA (Invitrogen, V220-01) using *Mfe*I and *Bst*BI restriction sites. pEV-12xCSL-H2B-mcherry was constructed by amplifying the 12xCSL promoter from 12xCSL DsRedExpress then fusing it to H2B-mCherry. The resulting amplicon was digested with *Mfe*I and *Bgl*II and inserted into pEV between *Mfe*I and *Bam*HI. H2B-mCherry was constructed by fusion PCR of H2B and mCherry fragments.

Generation of stable cell lines and cell-culture protocols

As a base cell line we used T-REx-CHO-K1 cells (Chinese Hamster Ovary cells supporting the T-REx inducible system, Invitrogen) which were grown in Alpha MEM Earle's Salts (Irvine Scientific) supplemented with 10% Tet System Approved FBS (Clontech), 100 U/ml penicillin -100 ug/ml streptomycin - 0.292 mg/ml L-glutamine (Gibco), and 10 ug/ml Blasticidin (InvivoGen) at 37°C in the presence of 5% CO2 under a humidified atmosphere. For construction of stable cell lines, cells were plated 24 h prior to transfection in 24-well tissue-culture-treated plates such that 80-95% confluency would be reached by the time of transfection. Cells were transfected using Lipofectamine 2000 (Invitrogen) as per the manufacturer's instructions. The amount of total DNA used was 800 ng/well: 100 ng of DNA containing the desired cassette + 700 ng empty plasmid (pOri).

Stable cell lines containing either the 12xCSL-H2B-Citrine or UAS-H2B-Citrine reporters were created by transfection of pEV-12xCSL-H2B-Citrine or pEV-UAS-H2B-Citrine into T-REx-CHO-K1 cells. A plasmid containing H2B-Cerulean under constitutive CMV promoter (pCS-H2B-Cerulean) was co-transfected together with the pEV-UAS-H2B-Citrine. Positive cells were selected by replating transfected cells into 6-well tissue-culture-treated plates with media containing 400 μg/ml Zeocin (Invitrogen) and 10 μg/ml Blasticidin 24 h post-transfection. Cells transfected with DNA lacking an antibiotic resistance gene were used as a control to monitor positive cell selection. After the control cells died, and after several passages of the selecting cells, positive cell populations were either sorted by FACS (FACSAria, Beckman Dickinson) or diluted in 96-well tissue-culture-treated plates in order to obtain single clones to test for reporter activity. For FACS, cells were transiently transfected with pEF-GV-ICD (a plasmid containing a fusion of Gal4-VP16 and Notch ICD) 24 h prior to cell analysis

and sorting. Individual cells expressing high levels of citrine were sorted into single wells in a 96-well tissue-culture-treated plates. Alternatively, positive cell populations were plated into 96-well tissue-culture-treated plates at 0.2 cells/well in order to increase the likelihood of obtaining a single cell/well. Individual cells were grown in selection media until enough cells were available to test reporter activity. Each clonal cell population was tested by transient transfection with pEF-GV-ICD, and clones with the best dynamic range of reporter induction were identified by microscopy and used for the next round of stable cell line creation. For the addition of Notch constructs into the two stable reporter cell lines constructed above, plasmids containing either hN1 fused to mCherry (pcDNA3-hN1-mCherry) or hN1G4^{esn} (pcDNA3-hNECD-Gal4^{esn}) were transfected into the 12xCSL-H2B-Citrine or UAS-H2B-Citrine reporter cell lines, respectively. Positive cell populations were selected as previously described with selection media that contained 400 μg/ml Zeocin, 10 μg/ml Blasticidin, and 600 μg/ml Geneticin (Invitrogen). Clonal cell populations were obtained by FACS or dilution as detailed above. Positive cell populations used for FACS were plated in wells treated with 2.5 μg/ml IgG-Delta^{ext} 48 hours before sorting. Individual cells expressing high levels of citrine were sorted. Clones were tested by plating cells in wells treated with or without 2.5 μg/ml IgG-Delta^{ext} and monitoring activation of the 12xCSL-H2B-Citrine or UAS-H2B-Citrine reporter by microscopy 48-72 hours post-Delta exposure. Single hN1 and hN1G4^{esn} clones with minimal H2B-Citrine background expression and high reporter activation when exposed to Delta were selected for further use.

To create the final cell lines hN1 and hN1G4^{esn} shown schematically in Figs. 1C, S1, a plasmid expressing Dl-mCherry under an inducible promoter (pcDNA-TO-Dl-mCherry) was transfected into each of these cell lines. A plasmid containing H2B-Cerulean under constitutive CMV promoter (pCS-H2B-Cerulean) was co-transfected with the Delta-mCherry into the hN1 cell line. Cells were grown in selection media containing 400 μg/ml Zeocin, 10 μg/ml Blasticidin, 600 μg/ml Geneticin, and 500 μg/ml Hygromycin (InvivoGen) for each of the hN1 cell lines. After selection, cells were either treated with 1 μg/ml doxycyclin and subjected to FACS or diluted into 96-well tissue-culture-treated plates as previously described. For FACS, single cells expressing high levels of mCherry were sorted. Clonal cell populations were grown and tested for low mCherry background expression in the absence of doxycycline and good inducibility of mCherry expression when exposed to 1 μg/ml doxycycline. Optimal clones for each of the above cell lines were identified by microscopy and used in further experiments. A separate cell line containing only inducible Delta-mCherry (used in co-culture experiments), was created by transfecting T-REx-CHO-K1 cells with pcDNA-TO-Dl-mCherry. Clones were generated in a similar process as above, albeit with a selection media containing only Blasticidin and Hygromycin. This cell line was used to generate the TO-DMC+hN1G4^{esn} used in Fig. S9 by stably transfecting into it the pcDNA3-hNECD-Gal4^{esn} construct (600 μg/ml Geneticin). *We note that the fusion to mCherry could in principle affect various activities of Delta. Therefore, we verified that Delta-mCherry can trans-activate Notch reporter cells efficiently (as shown in Fig. S3).*

This does not rule out the possibility that other activities or properties of Delta may be affected by the fusion.

For creation of the TO-Gal4^{esn} cell line, the UAS-H2B-Citrine + CMV-H2B-Cerulean cell line was transfected with the pcDNA5/TO-Gal4^{esn} plasmid. Cells were grown in selection media containing 400 μg/ml Zeocin, 10 μg/ml Blasticidin, and 500 μg/ml Hygromycin. After selection, cells were diluted into 96-well tissue-culture-treated plates to obtain single clones. Clones were tested for Gal4^{esn} inducibility by plating cells either with or without 1 μg/ml doxycycline. The clone with the lowest Citrine background expression in the absence of doxycycline and good inducible Citrine expression in the presence of doxycycline was chosen for further use in experiments.

For production of a double reporter cell line used in Figure S1, CHO-K1 cells (without T-REx, ATCC, CCL-61) were first transfected with pcDNA-UAS-H2B-Cit. A positive cell population was selected with media containing 10 μg/ml Blasticidin. After the initial selection, positive clones were obtained by FACS as previously described for the individual reporter stable cell lines. Each clone was then tested by transfection with pEF-GV-ICD, and a clone with the best reporter dynamic range was identified by microscopy and used to transfect in pEV-12xCSL-H2B-mCherry. Transfected cells were selected in media containing 10 μg/ml Blasticidin and 400 μg/ml Zeocin. A positive double reporter clone was identified by the method described above. In the clone chosen for further experiments, both reporters showed minimal background activation and high levels of Citrine and mCherry when transfected with pEF-GV-ICD.

Measurements of relative Notch expression levels in hN1G4^{esn} and hN1

To estimate the levels of ectopically expressed Notch receptors in the hN1G4^{esn} and hN1 we performed qRT-PCR on the two cell lines in which levels of Notch mRNA were compared to levels of endogenous β-actin mRNA. We found Notch levels 2.3 ± 0.15- and 4.5 ± 0.4-fold smaller than those of β-actin in the hN1G4^{esn} and hN1 cell lines, respectively. These results are within the physiological range of endogenous Notch receptors as observed in early T-cell progenitors where Notch is active[12]. See below for details of qRT-PCR analysis.

Description of experimental protocols and microscopy

Delta plating, preparation of cells for imaging, and calibration assay for IgG-Delta^{ext}. Protocol for setting up a time lapse movie: Cells were plated on a glass-bottom 24-well plate (Mattek). To bind IgG-Delta^{ext} to the plate, IgG-Delta^{ext} was serially diluted to different concentrations in cold 1xPBS (Invitrogen) containing 5μg/ml hamster fibronectin (Innovative Research). 500μl of diluted IgG-Delta^{ext} was incubated at 4°C for 1 hour on a rocker. Cells were trypsinized and diluted to 2×10^4 cells/ml (1×10^5 cells/ml for coculture experiments) in growth medium containing 100ng/ml doxycycline (Sigma Aldrich). The cells were plated immediately after the incubation onto

the 24 well plate containing IgG-Delta^{ext}. Prior to imaging, wells were washed twice with fresh medium and medium was replaced with low fluorescence imaging media αMEM without Phenol red, riboflavin, folic acid, and vitamin B12 (Invitrogen, custom made) and with 5% FBS and 1% L-glutamine+Penicilin-Streptomycin 100x mix (Invitrogen). Calibration of the IgG-Delta^{ext} bound to the plates is discussed in the captions of Fig. S4.

Microscopy details: Cells were imaged in an Olympus IX81-ZDC microscope equipped with an ASI 2000XY stage and a cooled back-thinned iKon-M CCD camera (Andor). All movies were taken with a 20x, 0.7NA objective. The microscope is also equipped with an incubator that maintains the temperature at 37C and with an environmental chamber with a humidified 5% CO2 flow (custom made). The microscopy setup is automatically controlled using commercial Metamorph (Molecular Devices) software. 48 stage positions (2 in each well) are set up manually and their coordinates are stored in the computer. In each position, the program first focuses using the Zero Drift Control module (Olympus Inc.), then takes a DIC image, and three fluorescent images (mCherry, citrine, CFP). Images are taken every 20 minutes for all positions. Typical total movie time is approximately 48 hours.

Western Blot: TO-Gal4^{esn} cells were plated in wells of a 6-well tissue-culture-treated plate at 5x105 cells/well. The cells were induced with 100 ng/ml of doxycycline. After 24 hr of induction, one well of cells was harvested (0 hr post-doxycycline removal) while the doxycycline was washed out of 4 additional wells. Those cells were harvested at 1 hr, 2hr, 4 hr and 6hr post-doxycycline removal (an uninduced sample was used as a control). The harvested cells were counted, and 4x106cells were pelleted and lysed with 200μl 1.5x complete SDS loading buffer (76.7 mM Tris-HCL, pH 6.8, 1.5% (w/v) SDS, 15% (v/v) Glycerol, 0.01% (w/v) Bromophenol blue, 30 mM Dithiothreitol (DTT), 213.8 mM 2-Mercaptoethanol, 1x protease inhibitors (Roche Applied Science), 6 mM ethylenediaminetetraacetic acid (EDTA)). Cellular extracts were boiled for 5 min at 95°C, vortexed, chilled on ice and centrifuged in a Beckman TLA-100.3 ultracentrifuge rotor at 55,000 rpm for 1 h at 4°C. For each sample, 10μl of supernatant was resolved in triplicate on a NuPAGE Novex 4-12% Bis-Tris Midi Gel (Invitrogen) and transferred to a 0.2 μm nitrocellulose membrane using the iBlot from Invitrogen (a standard curve made from serial dilutions of the 0 hr post-doxycycline sample was also included on the gel). The membrane was blocked with 5% (w/v) dry milk and 2% (w/v) BSA in 1xTBST (20 mM Tris base, 137 mM sodium chloride, 0.1% (v/v) Tween 20, pH 7.6), incubated with primary antibody in blocking buffer, followed by incubation with horseradish peroxidase-labeled secondary antibody in blocking buffer. SuperSignal West Femto chemiluminescent substrate kit was used for detection (Pierce). The following primary antibody was used: rabbit anti-Gal4 DBD (sc-577, Santa Cruz Biotechnology, 1:200). The secondary antibody used was horseradish peroxidase-linked anti-

rabbit IgG (Amersham, 1:2000). Protein bands were visualized on a VersaDoc gel imaging system (Bio-Rad Laboratories).

qRT-PCR: Notch mRNA levels in the hN1 and hN1G4^{esn} cells were compared to endogenous Notch mRNA observed in early T-cell progenitors. RNA was isolated from hN1 and hN1G4^{esn} cells using the RNeasy kit (Qiagen). cDNA was subsequently synthesized from 1μg of RNA using the iScript cDNA Synthesis kit (Bio-Rad). From a 20μl reaction, 2μl of cDNA was used to assess Notch and β-Actin mRNA levels using real-time qRT-PCR. Primer and probe sets used were as follows:

hNotch1		
	forward	5'–ATGAGTTCCAGTGCGAGT–3'
	reverse	5'–TGTAAGTGTTGGGTCCGT–3'
	probe	5'–FAM–AGATGCCCAGTGAAGCCCGT–Blk_FQ–3'
β-actin		
	forward	5'–ACTGGGACGATATGGAGAAG–3'
	reverse	5'–GGTCATCTTTTCACGGTTGG–3'
	probe	5'–HEX–ACCACACCTTCTACAACGAGCTGC–Blk_FQ-3'.

Flow cytometry: TO-DMC or TO-DMC+ hN1G4^{esn} "sending" cells were co-cultured with hN1G4^{esn} - No-Delta "receiving" cells in a transactivation assay. Co-cultures were plated at 10^5 cells/well in a 24-well plate at a ratio of 20% Delta cells to 80% Notch reporter cells. For each set of co-cultures, a 12 hr pulse of 1.6 ng/ml and 100 ng/ml doxycycline was performed (a well with no doxycycline served as a control). After doxycycline removal, the cells were washed 3x with 1xPBS (GIBCO) followed by addition of growth medium. Cells were incubated at 37°C, 5% CO_2 for an additional 24 hr before harvesting for flow cytometry analysis. Cells were trypsinized and diluted in 500μl analysis buffer (1x Hank's Balanced Salt Solution (GIBCO), 2.5 mg/ml BSA (w/v)). After filtering through a 40μm mesh, the co-cultured cells were analyzed for YFP fluorescence using a FACScalibur flow cytometer (Becton Dickinson).

Image and data analysis

Segmentation of images CFP images were used for automated segmentation of each frame of the movie. Segmentation was performed in a similar manner to previously described methods [2]. Briefly, each image was first subjected to an edge detection algorithm using Matlab. Closed edges were selected and several morphological and intensity criteria including total pixel area and mean fluorescence intensity level were used to identify the nuclei of the cells. The segmented image was used as a mask to calculate YFP and CFP fluorescence as well as centroid position for each nucleus. In some cases manual correction was applied to the segmented images. mCherry levels for the single

cell tracks in Fig. 3E were obtained by manual segmentation of the entire cell, in order to include total mCherry fluorescence.

Generating population-averaged response curves To generate the YFP response curve for each movie (such as the ones in Figs. 2C and 3C), the total YFP fluorescence of each cell was calculated and background fluorescence was subtracted. Each data point on Figs. 2C and 3C represent the median of this total fluorescence per cell over all cells of one frame in the movie. The median, rather than the mean, was used for two reasons: (1) the median is less sensitive to occasional bright outliers such as dead cells and multinucleated cells which may offset the mean. (2) median fluorescence taken in each frame roughly follows the response of the median cell lineage (see below), and thus better captures the sharp turn on feature shown in Fig. 3C-H. As shown in Fig. S13, the median curve essentially follows one of the single cell tracks for a while before switching to the next median curve. Hence, for such 'turn-on response' as in Fig. 3C, the median curve stays low until half the cells switch on. It then assumes a slope similar to that of the cells that have already responded. Thus, the rise time of the median curve provides a much better estimation of the median of the single cell lineage rise times than does the rise time of the mean curve (not shown).

The mean Delta-mCherry decay curve in Fig. 3C was calculated by taking the total mCherry level above background for each frame and dividing by the number of cells in that frame.

Single cell tracking was performed using a modified version of the Soft Assign algorithm 2,13 and was verified and corrected manually for each cell lineage tracked.

Data analysis Hill coefficients on Figs 2D, S1 were obtained by fitting the data to a Hill function of the form $y = A\frac{x^n}{K+x^n}$ where x is the D_{plate} value, y is the YFP production rate value, and A, K, and n are free fitting parameters. The fit was performed using a weighted non-linear least squares algorithm (Matlab). The weights vector was taken to be $\frac{1}{k+y_i}$, where y_i is the production rate value for the i^{th} data point and k is a minimal error parameter (typically 10% of $\max(y_i)$). This weighting takes into account both logarithmic errors (assuming a log-normal distribution of y_i's) and smaller fixed errors (i.e errors not proportional to y_i levels).We verified that the value obtained for the Hill coefficients, n, was not sensitive to the exact fitting procedure and parameters. The single cell rise times for the distribution obtained in Fig. 3F were calculated by fitting the shifted YFP curves (such as the ones in Fig. 3E) to the following functional form:

$$y(t) = S(t + \frac{1}{\gamma}\ln\left(\frac{1+\exp(-\gamma(t-t_c))}{1+\exp(\gamma t_c)}\right) + c. \quad (1)$$

Here, y represents the shifted YFP fluorescence level, t, represent time, t_c is the time at which the response turns on (i.e the 'knee'), γ quantifies the sharpness of turn-on, S is the maximal slope at $> t_c$, and $c = y(0)$ is a constant. This functional form is derived in the following way: We first

assume an effective Hill function response of the production rate of YFP (dy/dt) to the level of Delta-mCherry (DMC):

$$\frac{dy}{dt} = S\frac{k_d^m}{k_d^m + (DMC)^m}. \tag{2}$$

Here, m and k_d represent the effective Hill coefficient and the Delta-mCherry value that gives half-maximal expression, respectively. We assume an exponential decay of Delta-mCherry (i.e. $\mathrm{D_{cis}}$): $DMC = D_0 \exp(-\gamma_0 t)$ where D_0 and γ_0 are initial Delta-mCherry level and degradation rate, respectively. Hence the YFP production rate as a function of time is given by:

$$\frac{dy}{dt} = S\frac{1}{1 + \exp(-\gamma(t - t_c))}. \tag{3}$$

Here, $\gamma = m\gamma_0$ and $\exp(\gamma t_c) = \left(\frac{D_0}{k_d}\right)^m$, The functional form in Eq. (1) is obtained by integrating Eq. (2) over time. Fitting of the data to Eq. (1) was performed similarly to the Hill function fits described above. The rise time is then given by $\tau_{rise} = 2/\gamma$. We note that while eq. (1) is only an approximation to the actual response curve it fits the data well and enables estimation of rise times in simulated data.

Supplementary material — theory

Cells responding to *trans*-Delta ($\mathbf{D}_{plate}$) and *cis*-Delta ($\mathbf{D}_i$)

Model with mutual inactivation of Delta and Notch in *cis* Let us first consider the case where cells containing Notch (N_i), Delta (D_i), and a reporter of Notch signaling activity (R_i) are subjected to D_{plate} (D_p). The reactions we consider are the following:

$\mathrm{N}_i + \mathrm{D}_p \rightleftharpoons [\mathrm{N}_i\mathrm{D}_p] \rightarrow \mathrm{S}_i + \mathrm{D}_p$	*trans*–activation, with association/dissociation rates $k_D^{\pm}$ and cleavage rate k_S,
$\mathrm{N}_i + \mathrm{D}_i \rightleftharpoons [\mathrm{N}_i\mathrm{D}_i] \rightarrow \varnothing$	*cis*–inhibition, with association/dissociation rates $k_C^{\pm}$ and inactivation/dilution rate γ_{ND},
$\mathrm{S}_i \rightarrow \mathrm{R}_i$	Signal activation of reporter.

The first reaction represents the interaction of Notch with plate-bound Delta to form a complex that can then either dissociate or be cleaved to release the intracellular domain of Notch, denoted S_i. The dynamics of D_p are not relevant for the results presented below; thus we consider D_p not to be consumed in this binding reaction, so that its level is constant. The second reaction describes *cis*-inhibition with mutual inactivation of Notch and Delta. Note that we ignore the interaction between Delta in the cell and Notch in neighboring cells (*trans*-Notch), which is explicitly accounted for in the model presented in the Box. This interaction will be considered below. The third reaction represents

All simulations (Figs. 3H, 4 B,C,D,G, and S5) were performed using the ode15s ordinary differential equation solver of Matlab. The following equations and parameters were used in the simulations:

Figure	Equations	Parameters	Initial conditions and remarks
3H	Eqs. 8-10,12 in theoretical supplementary	γ = 0.1, γ_S = 0.1, γ_R = 0.1, k_t = 2, k_c = .2, k_{RS} = 1500, β_N = 1, β_D = 0, β_R = 1.8X10^8, p = 2, D_p = {0.063, 0.084, 0.11, 0.15, 0.20, 0.26, 0.35, 0.46, 0.62, 0.82, 1.1, 1.4}	Dimensional units*. D_0 = 200, $N_0 = \frac{\beta_N}{\gamma+\frac{D_0}{k_c}+\frac{D_p}{k_t}}$.
Box, S11	Eqs. 8-10, 12 in theoretical supplementary	γ = 0.1, γ_S = 1.0, D_p=0, k_t = 10, k_c = 1, β_N = 20, β_D = {various from 0 to 40}	Dimensional units*. Plot displays status of cell 1 (left column of equations) with D_2 and N_2 = 0.
4B	Eqs. 21-23 in theoretical supplementary	γ = 0.1, γ_S = 1.0, k_t = 10, k_c = {0.5, 1, 10}, β_N = 20, $\beta_D^{(1)}$ = {various from 0 to 34}, $\beta_D^{(2)}$ = 1.35$\beta_D^{(1)}$	Dimensional units*.
4C	Eqs. 24-27 in theoretical supplementary	γ = 0.1, γ_S = 1.0, γ_R = 0.05, k_t = 5, k_c = .25, k_{RS} = 1500, β_N = 10, β_D^0 = 17.5, β_R = 150, p = 2, n = 1, m = 1, x_0 = 7	Dimensional units*. Use periodic boundary conditions.
4F,S17	Eqs. 50-52 in theoretical supplementary	τ =1 , κ_C ={0.55,0.1,0.05} k_{RS} = 3e5, β_N =200 , β_D = 1000, β_R =3000, m = 1, p = 1	Dimensionless, as described in theoretical supplementary. Periodic boundary conditions. $D(0), N(0), R(0)$ were randomly distributed between 0 and $\beta_D, \beta_N, \beta_R$, respectively.
S8	Eqs. 17-20 in theoretical supplementary	γ = 0.1, γ_S = 0.1, γ_R = 0.1, k_t = 2, k_c = .2, k_{RS} = 1500, β_N = 1, β_D = 0, β_R = 1.8X10^8, p = 2, D_p = {3.16, 4.76, 7.15, 10.8, 16.2, 24.3, 36.6, 55.1, 82.8}	Dimensional units*. D_0 = 200, $N_0 = \frac{\beta_N}{\gamma+\frac{D_0}{k_c}+\frac{D_p}{k_t}}$.
S10A Top Left	blue: Eqs. 24-27 in theoretical supplementary red: Eqs. 32-35 in theoretical supplementary green: Eqs. 36-39 in theoretical supplementary magenta: Eqs. 40-43 in theoretical supplementary	blue: γ = 0.1, γ_S = 1.0, γ_R = 0.05, k_t = 5, k_c = .25, k_{RS} = 1500, β_N = 10, β_D^0 = 17.5, β_R = 75, p = 2, x_0 = 7	Dimensional units*
		red: γ = 0.1, γ_S = 1.0, γ_R = 0.05, k_t = 5, k_b = 1750, β_N = 10, β_D^0 = 17.5, β_R = 75, p = 8, q = 8, x_0 = 7	
		green: : γ = 0.1, γ_S = 1.0, γ_R = 0.05, k_t = 5, k_b = 1750, k_f = 600, β_N = 0.25, β_N' = 19.75, β_D^0 = 17.5, β_R = 75, p = 8, q = 8, n = 2, x_0 = 7	
		magenta : γ = 0.1, γ_S = 1.0, γ_R = 0.05, k_t = 5, k_b = 1750, k_{f2} = 1800, β_N = 10 , β_D^0 = 35, β_R = 75, p = 8, q = 8, m = 2, x_0 = 7	
S10A Top Right	Same as top left	red: same as top left except β_N = 5	Dimensional units*
		green: same as top left except β_N = 0.125, β_N' = 9.875	
		magenta: same as top left except β_N = 5	
S10A Bottom Left	Same as top left	red: same as top left except β_D^0 = 8.75	Dimensional units*
		green: same as top left except β_D^0 = 8.75	
		magenta: same as top left except β_D^0 = 17.5	
S10A Bottom Right	Same as top left	red: same as top left except β_N = 5, β_D^0 = 8.75	Dimensional units*
		green: same as top left except β_N = 0.125, β_N' = 9.875, β_D^0 = 8.75	
		magenta: same as top left except β_N = 5, β_D^0 = 17.5	
S10B	Eqs. 24-27	black: γ = 0.1, γ_S = 1.0, γ_R = 0.05, k_t = 25, k_c = .05, k_{RS} = 1500, β_N = 10, β_D^0 = 15, β_R = 75, p = 1, x_0 = 7	Dimensional units*
		orange: same as black except β_N =5	
		light blue: same as black except β_D^0 = 7.5	
		gray: same as black except β_N =5, β_D^0 = 7.5	
S10C	Eqs. 28-31	γ = 0.1, γ_S = 1.0, γ_R = 0.05, k_t = 5, k_c = .25, k_{RS} = 1500, β_N = 5, β_N^0 = 5, β_D^0 = 17.5, β_R = 75, p = 2, x_0 = 7, nn=1, k_{nn} as indicated in legend.	Dimensional units*
S16A	Eqs: 6-10	γ = 0.1, γ_S = 0.1, γ_R = 0.1, k_t = 2, k_c = .2, k_{RS} = 1500, β_N = 1, β_D = 0, β_R = 1.8X10^8, β_m = {0.1,10}, γ_m = {0.1,10}, p = 2, D_p =1	Dimensional units*
S16B	Eqs: 6-10	γ = 0.1, γ_S = {0.1, 10}, γ_R = 0.1, k_t = 2, k_c = .2, k_{RS} = {1500,1.5}, β_N = 1, β_D = 0, β_R = 1.8X10^8, β_m = 0.1, γ_m = 0.1, p = 2, D_p =1	Dimensional units*
S16B	Eqs: 6-10	γ = 0.1, γ_S = 0.1, γ_R = 0.1, k_t = 2, k_c = .2, k_{RS} = 1500, β_N = 1, β_D = 0, β_R = 1.8X10^8, β_m = 0.1, γ_m = 0.1, p = 2, D_p =1, τ={0,1}	Dimensional units*. Delay introduced in eq. 7 for the translation step. Used dde23 in Matlab.

* Dimensional units: decay rates, γ, γ_S, γ_R are in hours^{-1}, production rates β_N, β_D, $\beta_R$in RFU/hour, affinities k_{RS}, k_b, k_f, k_{f2}in RFU, $k_c$in RFU x hours, x_0 in cell diameters, $D_p$and k_t in effective plate bound concentrations. Here Relative Fluorescent Units [RFU] replace concentrations which are unknown.

Figure : Supplementary Table S3: Simulation parameters

the combined process in which the Notch intracellular domain translocates into the nucleus, binds with the CSL complex, and induces the expression of the reporter mRNA (m_R). This process is represented below phenomenologically by an increasing Hill function in the reporter production term.

These reactions are translated to the following set of ordinary differential equations:

$$\dot{N}_i = \beta_{\mathrm{N}} - \gamma_{\mathrm{N}} N_i - \left(k_{\mathrm{D}}^{+} N_i D_p - k_{\mathrm{D}}^{-} \left[N_i D_p\right]\right) - \left(k_{\mathrm{C}}^{+} N_i D_i - k_{\mathrm{C}}^{-} \left[N_i D_i\right]\right), \tag{1}$$

$$\dot{D}_i = \beta_{\mathrm{D}} - \gamma_{\mathrm{D}} D_i - \left(k_{\mathrm{C}}^{+} N_i D_i - k_{\mathrm{C}}^{-} \left[N_i D_i\right]\right), \tag{2}$$

$$\dot{[N_i D_p]} = k_{\mathrm{D}}^{+} N_i D_p - k_{\mathrm{D}}^{-} \left[N_i D_p\right] - k_{\mathrm{S}} \left[N_i D_p\right], \tag{3}$$

$$\dot{[N_i D_i]} = k_{\mathrm{C}}^{+} N_i D_i - k_{\mathrm{C}}^{-} \left[N_i D_i\right] - \gamma_{ND} \left[N_i D_i\right], \tag{4}$$

$$\dot{S}_i = k_{\mathrm{S}} \left[N_i D_p\right] - \gamma_{\mathrm{S}} S_i, \tag{5}$$

$$\dot{m}_{\mathrm{R}i} = f_A \left(S_i; \beta_{\mathrm{m}}, p, k_{\mathrm{RS}}\right) - \gamma_{\mathrm{m}} m_{\mathrm{R}i}, \tag{6}$$

$$\dot{R}_i = \alpha_R m_{\mathrm{R}i} - \gamma_{\mathrm{R}} R_i. \tag{7}$$

The function $f_A \left(S_i; \beta_{\mathrm{m}}, p, k_{\mathrm{RS}}\right)$ is an activating Hill function of the form $\beta_{\mathrm{m}} \frac{S_i^p}{k_{\mathrm{RS}}^p + S_i^p}$. We assume fast cleavage of the Notch-D_{plate} complex, which allows us to apply the quasi-steady-state approximation to its dynamics ($\dot{[N_i D_p]} \approx 0$). Furthermore, we assume that Notch binds to *cis*-Delta irreversibly ($k_{\mathrm{C}}^{-} = 0$), and in that way the dynamics of Notch no longer depend on the $[\mathrm{N}_i\mathrm{D}_i]$ complex. Finally, we consider that the relaxation time of the receptor mRNA is much shorter than the protein relaxation times. With these approximations, the model is reduced to

$$\dot{N}_i = \beta_{\mathrm{N}} - \gamma N_i - N_i \frac{D_p}{k_t} - N_i \frac{D_i}{k_c}, \tag{8}$$

$$\dot{D}_i = \beta_{\mathrm{D}} - \gamma D_i - N_i \frac{D_i}{k_c}, \tag{9}$$

$$\dot{S}_i = N_i \frac{D_p}{k_t} - \gamma_{\mathrm{S}} S_i, \tag{10}$$

$$\dot{R}_i = f_A \left(\frac{1}{\gamma_{\mathrm{S}}} N_i \frac{D_p}{k_t}; \beta_{\mathrm{R}}, p, k_{\mathrm{RS}}\right) - \gamma_{\mathrm{R}} R_i, \tag{11}$$

where we have defined $\beta_{\mathrm{R}} = \frac{\beta_{\mathrm{m}} \alpha_R}{\gamma_{\mathrm{m}}}$, $k_t^{-1} \equiv \frac{k_{\mathrm{D}}^{+} k_{\mathrm{S}}}{k_{\mathrm{D}}^{-} + k_{\mathrm{S}}}$ and $k_c^{-1} \equiv k_{\mathrm{C}}^{+}$. We also take the simplifying assumption that $\gamma_{\mathrm{N}} = \gamma_{\mathrm{D}} \equiv \gamma$ (solving with different degradation rates is straightforward). Additionally, and based on the simplifying assumption that the promoter of the reporter R is a far from saturation (i.e., that $k_{\mathrm{RS}} \gg \frac{1}{\gamma_{\mathrm{S}}} N_i \frac{D_p}{k_t}$), we approximate its expression as

$$\dot{R}_i = \beta_{\mathrm{R}} \left(\frac{1}{\gamma_{\mathrm{S}} k_{\mathrm{RS}}} N_i \frac{D_p}{k_t}\right)^p - \gamma_{\mathrm{R}} R_i. \tag{12}$$

We define the total concentration of Delta in the cell as $D_{\mathrm{tot}} = D_i + [N_i D_i]$. Using Eqs. (2) and

(4) and assuming $\gamma = \gamma_{ND}$, we find that $D_{\rm tot}$ follows a simple linear dynamics:

$$\dot{D}_{\rm tot} = \beta_{\rm D} - \gamma D_{\rm tot}. \tag{13}$$

This result holds even if the Notch-Delta binding is reversible ($k_{\rm C}^- \neq 0$), provided $\gamma = \gamma_{ND}$. The assumption of equal decay rates for both active Delta and the $[{\rm N}_i{\rm D}_i]$ complex is based on the experimental fact that adding Notch to our Delta-expressing cells does not lead to extra decrease of Delta levels beyond dilution. The trivial decay dynamics given by Eq. (13) are observed e.g. in the experiments of Fig. 3C, in which $\beta_{\rm D} = 0$. Equations (8)–(10) and (12) are the ones used in the simulations shown in Figs. 3H and Box.

Ultrasensitive response of the mutual inactivation switch Equations (8)–(9) and (12) can be readily solved in the steady state, leading to the following stationary levels of Notch and Delta:

$$N_{\rm st} = \frac{\beta_{\rm N} - \beta_{\rm D}}{2g} - \frac{\gamma k_c}{2} + \sqrt{\left(\frac{\beta_{\rm N} - \beta_{\rm D}}{2g} - \frac{\gamma k_c}{2}\right)^2 + \frac{k_c \gamma \beta_{\rm N}}{g}}, \tag{14}$$

$$D_{\rm st} = \frac{\beta_{\rm D}}{\gamma + \frac{N_{\rm st}}{k_c}}, \tag{15}$$

where $g = \gamma + D_p/k_t$. This solution is plotted in the Modeling box of the main text, for the parameter values given in the Supplementary Table S3. For $\beta_{\rm N} > \beta_{\rm D}$ the system reaches a steady state of high Notch and low Delta, in which the cell can send, but not receive, signals. Conversely, when $\beta_{\rm D} > \beta_{\rm N}$ the steady state corresponds to high Delta and low Notch, and the cell can receive, but not send, signals. In order to quantify how sensitive the cell is in the region around the switch, we define the sensitivity parameter as the logarithmic derivative of the steady-state signal $S_{\rm st}$ with respect to a control parameter [1], which here we take to be the production rate of Delta, $\beta_{\rm D}$:

$$\xi = \frac{d \log S_{\rm st}}{d \log \beta_{\rm D}},$$

According to Eq. (10), $S_{\rm st} = D_p N_{\rm st}/\gamma_S k_t$, so that using the result given in (14) at the switch location ($\beta_{\rm D} = \beta_{\rm N}$, where the sensitivity is maximal), and in the limit of large *cis*-inhibition, $\gamma k_c \ll \beta_{\rm N}/(\gamma + D_p/k_t)$, the sensitivity of the switch is approximately [2]

$$\xi \approx \sqrt{\frac{\beta_{\rm N}}{4 k_c \gamma (\gamma + D_p/k_t)}}, \tag{16}$$

For the parameters used in the Box figure, and given in the Supplementary Table S3, the switch is cleary ultrasensitive, with a sensitivity coefficient $\xi \approx 22.4$. This result does not change qualitatively when including reversibility in the binding of Notch and *cis*-Delta, since in the steady state a nonzero

value of $k_{\rm C}^-$ would simply lead to a renormalization of the *cis*-inhibition parameter in the steady-state calculation, equal to $k_c = \frac{\gamma + k_{\rm C}^-}{\gamma k_{\rm C}^+}$.

The sensitivity parameter has been defined above in terms of the signal, S_i, but the experimentally accesible quantity is the reporter's promoter activity, $\dot{R}_i$. The relationship between the reporter sensitivity and the signal sensitivity is given in a straightforward way by

$$\xi_R = \frac{d \log \dot{R}_{\rm st}}{d \log \beta_{\rm D}} = \frac{d \log \dot{R}_{\rm st}}{d \log S_{\rm st}} \frac{d \log S_{\rm st}}{d \log \beta_{\rm D}} \approx p\, \xi \,,$$

where we have assumed that the reporter promoter is far from saturation, as in Eq. (12). Thus the sensitivity measured in our experiments, ξ_R, is a combination of the switch sensitivity, ξ, and the cooperativity p of the reporter promoter.

Another difference between the steady-state calculation presented above and the experimental measurements presented in Fig. 3 is the fact that in the experiments Delta production rate, $\beta_{\rm D}$, is zero, and only the decay of an initial concentration of Delta is observed, as expressed by Eq. (13). Under these conditions, in our experiments we measure the *transient* sensitivity [1] of the reporter's promoter activity as a function of the instantaneous total concentration of Delta, $D_{\rm tot}$. Extensive numerical simulations of our model show that both parameters are similar to each other within 20% in our parameter range.

Alternative model without Delta inactivation by Notch An alternative model that fails to account for several distinctive features of this system (see text) proposes that the receptor-ligand interaction is catalytic in Delta (in which case Delta is said to be rapidly recycled). The corresponding reactions are the following:

$\mathrm{N}_i + \mathrm{D}_p \rightleftharpoons [\mathrm{N}_i\mathrm{D}_p] \rightarrow \mathrm{S}_i + \mathrm{D}_p$	*trans*–activation, with association/dissociation rates $k_D^{\pm}$ and cleavage rate k_S,
$\mathrm{N}_i + \mathrm{D}_i \rightleftharpoons [\mathrm{N}_i\mathrm{D}_i] \rightarrow \mathrm{D}_i$	*cis*–inhibition, with association/dissociation rates $k_C^{\pm}$ and inactivation rate k_E,
$\mathrm{S}_i \rightarrow \mathrm{R}_i$	Signal activation of reporter.

The *cis*-inhibition reaction now conserves Delta, unlike the mutual-inactivation model. Using the same assumptions as were made in the preceding case, we obtain the following ordinary differential

equations:

$$\dot{N}_i = \beta_{\mathrm{N}} - \gamma N_i - N_i \frac{D_p}{k_t} - N_i \frac{D_i}{k_c}, \tag{17}$$

$$\dot{D}_i = \beta_{\mathrm{D}} - \gamma D_i, \tag{18}$$

$$\dot{S}_i = N_i \frac{D_p}{k_t} - \gamma_{\mathrm{S}} S_i, \tag{19}$$

$$\dot{R}_i = f_A \left(\frac{1}{\gamma_{\mathrm{S}}} N_i \frac{D_p}{k_t}; \beta_{\mathrm{R}}, p, k_{\mathrm{RS}} \right) - \gamma_{\mathrm{R}} R_i, \tag{20}$$

which are the basis of the data in Fig. S8.

We note that in this case the steady-state solution of Eqs. (17)-(18) leads to the straightforward relation

$$N_{\mathrm{st}} = \frac{\gamma \beta_{\mathrm{N}}}{1 + \frac{D_p}{\gamma k_t} + \frac{\beta_{\mathrm{D}}}{k_c}},$$

which shows no sensitivity ($\xi = 1$) with respect to the control parameter β_{D}.

Effect of finite mRNA and signal lifetimes and reporter expression delay In the previous paragraphs we have assumed that the lifetimes of the signal, S_i, and of the reporter mRNA, $\mathrm{m}_{\mathrm{R}i}$, are very small in comparison with those of the proteins. We have also considered that the expression of the reporter is instantaneously determined by the level of signal. In order to ascertain that these approximations do not affect the qualitative behavior of our model as described above, we performed simulations of models (1)-(7), maintaining the assumptions of a fast cleavage of the Notch-D_{plate} complex and irreversible binding between Notch and *cis*-Delta. We also added a finite delay τ in the Hill function f_A describing the transcription of the reporter mRNA, Eq. (6), which is now made to depend on the signal S_i at an earlier time τ.

Figure S16 shows the effect of these three factors, namely γ_m, γ_S, and τ, independently of each other. As expected, slower decays of the reporter mRNA and signal (plots A and B) lead to a delay in the turn-on of the reporter. A similar effect is observed in the presence of a time delay in the expression of the reporter with respect to the signal (plot C). In spite of these time shifts, the ultrasensitivity of the switch is not substantially affected, with at most a 30% change in ξ for lifetime variations in the 100× range. We also note that in these simulations the reporter expression is assumed to depend cooperatively on the signal, with a Hill coefficient $p = 2$ that is on the order of the experimentally observed value. Other parameters used in Fig. S16 are given in the Supplementary Table S3.

Two cells with varying Delta expression

In Fig. 4B of the text we show the amplification of Notch signaling in a cell with some $\beta_{\mathrm{D}}^{(1)}$ with a neighbor identical except for a higher Delta production rate $\beta_{\mathrm{D}}^{(2)}$ such that $\beta_{\mathrm{D}}^{(2)} \gtrsim \beta_{\mathrm{N}} \gtrsim \beta_{\mathrm{D}}^{(1)}$. The

equations used to generate the figure are:

$$\dot{N}_1 = \beta_{\mathrm{N}} - \gamma N_1 - N_1 \tfrac{D_2}{k_t} - N_1 \tfrac{D_1}{k_c}, \qquad \dot{N}_2 = \beta_{\mathrm{N}} - \gamma N_2 - N_2 \tfrac{D_1}{k_t} - N_2 \tfrac{D_2}{k_c}, \tag{21}$$

$$\dot{D}_1 = \beta_{\mathrm{D}}^{(1)} - \gamma D_1 - N_2 \tfrac{D_1}{k_t} - N_1 \tfrac{D_1}{k_c}, \qquad \dot{D}_2 = \beta_{\mathrm{D}}^{(2)} - \gamma D_2 - N_1 \tfrac{D_2}{k_t} - N_2 \tfrac{D_2}{k_c}, \tag{22}$$

$$\dot{S}_1 = N_1 \tfrac{D_2}{k_t} - \gamma_{\mathrm{S}} S_1, \qquad \dot{S}_2 = N_2 \tfrac{D_1}{k_t} - \gamma_{\mathrm{S}} S_2, \tag{23}$$

Fig. 4B displays the numerical steady-state solution of these equations with parameter values as indicated in the Supplementary Table S3. Note that in Eq. (22) we have assumed that Delta is degraded due to its *trans* interaction with Notch. This is not, however, an essential feature of our model; ultrasensitivity is preserved even when Delta does not degrade in *trans*.

Spatially-varying Delta expression

Mutual inactivation model In Figure 4 C and D, we consider a field of cells in which Delta production is given by $\beta_{\mathrm{D}}(x) = \beta_{\mathrm{D}}^0 e^{-|x|/x_0}$ as a function of distance x from a central axis, yielding the axially-symmetric equations:

$$\dot{N}_i = \beta_{\mathrm{N}} - \gamma N_i - N_i \frac{D_i}{k_c} - N_i \frac{\langle D_j \rangle_i}{k_t}, \tag{24}$$

$$\dot{D}_i = \beta_{\mathrm{D}}(x) - \gamma D_i - N_i \frac{D_i}{k_c} - \langle N_j \rangle_i \frac{D_i}{k_t}, \tag{25}$$

$$\dot{S}_i = N_i \frac{\langle D_j \rangle_i}{k_t} - \gamma_{\mathrm{S}} S_i \approx 0 \quad \Longrightarrow \quad S_i \approx \frac{1}{\gamma_{\mathrm{S}}} N_i \frac{\langle D_j \rangle_i}{k_t}, \tag{26}$$

$$\dot{R}_i = f_A(S_i; \beta_{\mathrm{R}}, p, k_{\mathrm{RS}}) - \gamma_{\mathrm{R}} R_i. \tag{27}$$

The notation $\langle D_j \rangle_i$ refers to the average over Delta levels of all neighbors j of cell i. In particular, $\langle D_j \rangle_i \equiv \sum_j M_{ij} D_j$, where M is the connectivity matrix of a two-dimensional hexagonal lattice in which

$$M_{ij} = \begin{cases} 1/6 & \text{if } i \text{ and } j \text{ are neighbors} \\ 0 & \text{otherwise.} \end{cases}$$

This assumes that Delta and Notch are uniformly distributed over the boundary of the cell. The notation $\langle N_j \rangle_i$ is defined similarly. Note that we now assume that the signal decays sufficiently faster than Notch, Delta and the reporter, which allows us to adiabatically eliminate its dynamics [Eq. (26)]. Figure S10 indicates the ratiometric character of this model by demonstrating that a common rescaling of β_{N} and β_{D} leaves the pattern unchanged.

Band–pass filter model One could alternatively conceive of a model in which Delta expression still varies as $\beta_{\mathrm{D}}(x)$ above, but instead of mutual inactivation there is a process that restricts

expression of the reporter within a narrow band of signal values centered about some k_{b}. This band–pass model is governed by the following equations:

$$\dot{N}_i = \beta_{\mathrm{N}} - \gamma N_i, \tag{28}$$

$$\dot{D}_i = \beta_{\mathrm{D}}(x) - \gamma D_i, \tag{29}$$

$$\dot{S}_i = N_i \frac{\langle D_j \rangle_i}{k_t} - \gamma_{\mathrm{S}} S_i \approx 0 \quad \Longrightarrow \quad S_i \approx \frac{1}{\gamma_{\mathrm{S}}} N_i \frac{\langle D_j \rangle_i}{k_t}, \tag{30}$$

$$\dot{R}_i = \beta_{\mathrm{R}} \frac{S_i^p}{k_{\mathrm{b}}^p + S_i^p} \frac{k_{\mathrm{b}}^q}{k_{\mathrm{b}}^q + S_i^q} - \gamma_{\mathrm{R}} R_i. \tag{31}$$

Figure S10 shows that this model is not ratiometric.

Band–pass filter model with Signal activating Notch Adding a proposed mechanism by which Notch signaling induces Notch expression to the band–pass filter model, we have

$$\dot{N}_i = \beta_{\mathrm{N}} + \beta'_{\mathrm{N}} \frac{S_i^n}{k_{\mathrm{f}}^n + S_i^n} - \gamma N_i, \tag{32}$$

$$\dot{D}_i = \beta_{\mathrm{D}}(x) - \gamma D_i, \tag{33}$$

$$\dot{S}_i = N_i \frac{\langle D_j \rangle_i}{k_t} - \gamma_{\mathrm{S}} S_i \approx 0 \quad \Longrightarrow \quad S_i \approx \frac{1}{\gamma_{\mathrm{S}}} N_i \frac{\langle D_j \rangle_i}{k_t}, \tag{34}$$

$$\dot{R}_i = \beta_{\mathrm{R}} \frac{S_i^p}{k_{\mathrm{b}}^p + S_i^p} \frac{k_{\mathrm{b}}^q}{k_{\mathrm{b}}^q + S_i^q} - \gamma_{\mathrm{R}} R_i. \tag{35}$$

Figure S10 shows that the addition of the Notch induction term does not generate a ratiometric response.

Band–pass filter model with Signal repressing Delta Another potential feedback which we can include in the band–pass filter model is one in which Notch signaling represses Delta expression. In this case the model reads

$$\dot{N}_i = \beta_{\mathrm{N}} - \gamma N_i, \tag{36}$$

$$\dot{D}_i = \frac{\beta_{\mathrm{D}}(x)}{1 + (S/k_{f2})^m} - \gamma D_i, \tag{37}$$

$$\dot{S}_i = N_i \frac{\langle D_j \rangle_i}{k_t} - \gamma_{\mathrm{S}} S_i \approx 0 \quad \Longrightarrow \quad S_i \approx \frac{1}{\gamma_{\mathrm{S}}} N_i \frac{\langle D_j \rangle_i}{k_t}, \tag{38}$$

$$\dot{R}_i = \beta_{\mathrm{R}} \frac{S_i^p}{k_{\mathrm{b}}^p + S_i^p} \frac{k_{\mathrm{b}}^q}{k_{\mathrm{b}}^q + S_i^q} - \gamma_{\mathrm{R}} R_i. \tag{39}$$

Also for this feedback, Fig. S10 shows that the resulting response is not ratiometric.

Lateral inhibition patterning

In order to see the effect of Notch-Delta mutual inactivation on lateral inhibition patterning, let us first consider the classic lateral inhibition model studied by Collier *et al.* [3]:

$\mathrm{N}_i+\mathrm{D}_j \rightleftharpoons [\mathrm{N}_i\mathrm{D}_j] \rightarrow \mathrm{S}_i+\mathrm{N}_i+\mathrm{D}_j$	*trans*–activation, with association/dissociation rates $k_D^{\pm}$ and cleavage rate k_S,
$\mathrm{S}_i \rightarrow \mathrm{R}_i$	Signal activation of reporter/repressor as Hill function,
$\mathrm{R}_i \dashv \mathrm{D}_i$	Repression of Delta.

The *trans*-activation here does not entail the degradation or inactivation of either Notch or Delta. The third reaction introduces feedback of incoming signaling on Delta expression. Applied to a two-dimensional hexagonal lattice of cells (as shown in Fig. 4F), these become the following set of ordinary differential equations:

$$\dot{N}_i = \beta_{\mathrm{N}} - \gamma N_i, \tag{40}$$

$$\dot{D}_i = f_R\left(R_i; \beta_{\mathrm{D}}, m, k_{\mathrm{DR}}\right) - \gamma D_i, \tag{41}$$

$$\dot{S}_i = N_i \frac{\langle D_j \rangle_i}{k_t} - \gamma_{\mathrm{S}} S_i \approx 0 \quad \Longrightarrow \quad S_i \approx \frac{1}{\gamma_{\mathrm{S}}} N_i \frac{\langle D_j \rangle_i}{k_t}, \tag{42}$$

$$\dot{R}_i = f_A(S_i; \beta_{\mathrm{R}}, p, k_{\mathrm{RS}}) - \gamma_{\mathrm{R}} R_i. \tag{43}$$

The function $f_R\left(R_i; \beta_{\mathrm{D}}, m, k_{\mathrm{DR}}\right)$ is a repressive Hill function of the form $\beta_{\mathrm{D}} \frac{k_{\mathrm{DR}}^m}{k_{\mathrm{DR}}^m + R_i^m}$. It is now worth switching to dimensionless units by transforming variables as $t \equiv \mathrm{t}\gamma_{\mathrm{R}}$, $N \equiv \frac{N}{N_0}$, $D \equiv \frac{D}{D_0}$, and $R \equiv \frac{R}{k_{\mathrm{DR}}}$ where $N_0 \equiv \frac{\beta_{\mathrm{N}}}{\gamma}$ and $D_0 \equiv \frac{\gamma_{\mathrm{S}} k_{RS}}{k_t} \frac{1}{N_0}$ to give

$$\tau \dot{N}_i = 1 - N_i, \tag{44}$$

$$\tau \dot{D}_i = \beta_D \frac{1}{1 + R_i^m} - D_i, \tag{45}$$

$$\dot{R}_i = \beta_R \frac{\left(N_i \langle D_j \rangle_i\right)^p}{1 + \left(N_i \langle D_j \rangle_i\right)^p} - R_i. \tag{46}$$

where $\tau \equiv \frac{\gamma_{\mathrm{R}}}{\gamma}$, $\beta_D \equiv \frac{\beta_{\mathrm{D}}}{D_0 \gamma}$, and $\beta_R \equiv \frac{\beta_{\mathrm{R}}}{k_{\mathrm{DR}} \gamma_{\mathrm{R}}}$.

These equations can, under certain parameter ranges, generate lateral inhibition patterns as was shown by Collier *et al.* [3]. Recently, Plahte [4] has shown that the product of cooperativities $pm \equiv n$ must exceed 1 for a one-dimensional array of cells. Here we show that for a two-dimensional hexagonal lattice the condition on the product of cooperativities is more stringent, $n > 2$.

It is immediately clear that a necessary condition for patterning is the *in*stability of the homogeneous steady state (N^*, D^*, R^*) in which every cell has the same value of N_i, D_i, and R_i. Thus a linear stability analysis about the homogeneous steady state can provide necessary conditions for

patterning [4]. The stability analysis requires the computation of the Jacobian at the homogeneous steady state, which is in this case complicated by the large number of variables (three times the number of cells). This is made simpler by an observation originally from Othmer and Scriven [5] that the Jacobian can be expressed as the sum of two tensor products of matrices, one for the internal dynamics and the other for interactions with neighbors: $J = I_k \otimes H + M \otimes B$. The matrix tensor product is defined as $A \otimes B = \begin{pmatrix} a_{11}B & \cdots & a_{1k}B \\ \vdots & \ddots & \vdots \\ a_{k1}B & \cdots & a_{kk}B \end{pmatrix}$. Also, here I_k is the $k \times k$ identity matrix (k is the number of cells involved in the interactions in question), $H_{ij} = \frac{\partial \dot{q}_i}{\partial q_j}$ is the change in production of species i for a change in species j in the same cell, M is the connectivity matrix as defined above, and $B_{ij} = \frac{\partial \dot{q}_i}{\partial \langle q_j \rangle}$ is the change in production of species i for a change in species j in a neighboring cell. N, D, and R correspond to species $i = 1, 2, 3$ respectively. For the model described above, the matrices are:

$$H = \begin{pmatrix} -\frac{1}{\tau} & 0 & 0 \\ 0 & -\frac{1}{\tau} & -\frac{D^*}{\tau R^*} m g_0 \\ \frac{R^*}{N^*} p f_0 & 0 & -1 \end{pmatrix} \text{ and } B = \begin{pmatrix} 0 & 0 & 0 \\ 0 & 0 & 0 \\ 0 & \frac{R^*}{D^*} p f_0 & 0 \end{pmatrix}, \tag{47}$$

where $g_0 \equiv \frac{(R^*)^m}{1+(R^*)^m}$ and $f_0 \equiv \frac{1}{1+(N^* D^*)^p}$ are both ≤ 1. Othmer and Scriven [5] proved that the eigenvalues of the overall Jacobian are the eigenvalues of the various matrices $H + q_k B$ where q_k are the eigenvalues of the connectivity matrix M. Thus the eigenvalues λ of the Jacobian are set by the characteristic equation:

$$\begin{vmatrix} -\frac{1}{\tau} - \lambda & 0 & 0 \\ 0 & -\frac{1}{\tau} - \lambda & -\frac{D^*}{\tau R^*} m g_0 \\ \frac{R^*}{N^*} p f_0 & \frac{R^*}{D^*} p f_0 q_k & -1 - \lambda \end{vmatrix} = 0, \tag{48}$$

which aside from $\lambda = -\frac{1}{\tau}$ happens to be quadratic in λ, meaning that for every q_k there are two eigenvalues of the Jacobian

$$\lambda_\pm = \frac{-\left(1 + \frac{1}{\tau}\right) \pm \sqrt{\left(1 + \frac{1}{\tau}\right)^2 - \frac{4}{\tau}\left(pmg_0 f_0 q_k + 1\right)}}{2}. \tag{49}$$

For instability we need only a single λ to have a real part that is positive, which will be so if $pmg_0 f_0 q_k \leq -1$. An analysis of the matrix M in [5] tells us that $q \geq -0.5$, meaning that $pmg_0 f_0 > 2$ and, as $g_0, f_0 \leq 1$, $pm \equiv n > 2$ is a lower bound on the overall cooperativity of the system that must be satisfied for patterning to occur.

***cis*-Inhibition** To incorporate *cis*-inhibition we add an interaction $\mathrm{N}_i + \mathrm{D}_i \rightleftharpoons [\mathrm{N}_i \mathrm{D}_i] \rightarrow \varnothing$, and modify the *trans*-activation to annihilate Notch and Delta. Here it is more convenient to switch into a different set of dimensionless parameters in which Notch and Delta are normalized by the same

quantity: $t \equiv \gamma_R \mathrm{t}$, $N \equiv \frac{N}{N_0}$, $D \equiv \frac{D}{D_0}$, and $R \equiv \frac{R}{R_0}$ where $N_0 = D_0 \equiv \gamma k_t$, and $R_0 \equiv k_{\mathrm{DR}}$. The equations are then

$$\tau \dot{N}_i = \beta_N - N_i - N_i \langle D_j \rangle_i - N_i \frac{D_i}{\kappa_c}, \tag{50}$$

$$\tau \dot{D}_i = \beta_D \frac{1}{1 + R_i^m} - D_i - \langle N_j \rangle_i D_i - N_i \frac{D_i}{\kappa_c}, \tag{51}$$

$$\dot{R}_i = \beta_R \frac{\left(N_i \langle D_j \rangle_i\right)^p}{k_{RS}^p + \left(N_i \langle D_j \rangle_i\right)^p} - R_i. \tag{52}$$

where $\tau \equiv \frac{\gamma_{\mathrm{R}}}{\gamma}$, $\beta_N \equiv \frac{\beta_{\mathrm{N}}}{\gamma N_0}$, $\beta_D \equiv \frac{\beta_{\mathrm{D}}}{\gamma D_0}$, $\beta_R \equiv \frac{\beta_{\mathrm{R}}}{\gamma_{\mathrm{R}} R_0}$, $\kappa_c \equiv \frac{k_c}{k_t}$, and $k_{RS} \equiv \frac{k_{\mathrm{RS}} \gamma_{\mathrm{S}} k_t}{N_0 D_0}$. These were used in Figs. 4F (right panel) and S17, which demonstrate patterning even with $pm \equiv n = 1$.

References

1. N.E. Buchler and M. Louis. Molecular titration and ultrasensitivity in regulatory networks. *J. Mol. Biol.* **384**, 1106 (2008).

2. E. Levine, Z. Zhang, T. Kuhlman, T. Hwa. Quantitative characteristics of gene regulation by small RNA. *PLOS Biol.* **5**(9), e229 (2007).

3. J.R. Collier, N.A.M. Monk, P.K. Maini, J.H. Lewis. Pattern formation by lateral inhibition with feedback: A mathematical model of Delta-Notch intercellular signalling. *J. Theor. Biol.* **183**, 429 (1996).

4. E. Plahte. Pattern formation in discrete cell lattices. *J. Math. Biol.* **43**, 411 (2001).

5. H.G. Othmer, L.E. Scriven. Instability and dynamic pattern in cellular networks. *J. Theor. Biol.* **32**, 507 (1971).